| | |
|---|---|
| **Titre:** Title: | A Label Free CMOS-Based Smart Petri Dish for Cellular Analysis |
| **Auteur:** Author: | Ghazal Nabovati Khormazard |
| **Date:** | 2016 |
| **Type:** | Mémoire ou thèse / Dissertation or Thesis |
| **Référence:** Citation: | Nabovati Khormazard, G. (2016). A Label Free CMOS-Based Smart Petri Dish for Cellular Analysis [Thèse de doctorat, École Polytechnique de Montréal]. PolyPublie. https://publications.polymtl.ca/2372/ |



| | |
|---|---|
| **URL de PolyPublie:** PolyPublie URL: | https://publications.polymtl.ca/2372/ |
| **Directeurs de recherche:** Advisors: | Mohamad Sawan, & Ebrahim Ghafar-Zadeh |
| **Programme:** Program: | génie électrique |

UNIVERSITÉ DE MONTRÉAL

# A LABEL FREE CMOS-BASED SMART PETRI DISH FOR CELLULAR ANALYSIS

GHAZAL NABOVATI KHORMAZARD
DÉPARTEMENT DE GÉNIE ÉLECTRIQUE
ÉCOLE POLYTECHNIQUE DE MONTRÉAL

THÈSE PRÉSENTÉE EN VUE DE L'OBTENTION
DU DIPLÔME DE PHILOSOPHIÆ DOCTOR
(GÉNIE ÉLECTRIQUE)
DECEMBER 2016

UNIVERSITÉ DE MONTRÉAL

ÉCOLE POLYTECHNIQUE DE MONTRÉAL

Cette thèse intitulée :

A LABEL FREE CMOS-BASED SMART PETRI DISH FOR CELLULAR ANALYSIS

présentée par : NABOVATI KHORMAZARD Ghazal
en vue de l'obtention du diplôme de : Philosophiæ Doctor
a été dûment acceptée par le jury d'examen constitué de :

M. SAVARIA Yvon, Ph. D., président
M. SAWAN Mohamad, Ph. D., membre et directeur de recherche
M. GHAFAR-ZADEH Ebrahim, Ph. D., membre et codirecteur de recherche
M. MARTEL Sylvain, Ph. D., membre
M. IZQUIERDO Ricardo , Ph. D., membre externe

## DEDICATION

*To my Mother, in loving memory of my Father.*

## ACKNOWLEDGEMENTS

First and foremost I would like to express my sincere gratitude to my advisers Professor Mohamad Sawan and Professor Ebrahim Ghafar-Zadeh, for their understanding, encouragement, and mentoring throughout my PhD studies.

I also like to thank my committee members Professor Ricardo Izquierdo, Professor Sylvain Martel, and Professor Yvon Savaria for accepting to evaluate this thesis.

I would also like to thank Professor Michael Buschmann and Professor Mark Lavertu in Biomaterials and Cartilage Laboratory at Polytechnique Montreal for providing support and sharing their lab facilities.

Special thanks to all my friends in Polystim Neurotechnologies Laboratory, specially Bahareh Gholamzadeh, Sami Hached, Leila Montazeri, Mahya Dehbozorgi, Mohammad Honarparvar, and Elie Bou Assi, who were always there for me and made my study in Polytechnique one of the best experiences of my life.

I would like to gratefully acknowledge the help of two of my very special colleagues, Laurent Mouden for his technical support and training in LASEM and Biostim labs, and Antoine Letourneau for his hard work to contribute to my research project. This work would have not been possible without their help and support. I would like to thank Dr. Maryam Mirzaei for sharing her experience in biological and chemical experiments. Special thanks to Yuan Cheng for his technical support and suggestions for the biological experiments.

I am grateful to all the staff of Electrical engineering department of Polytechnique Montreal, specially Marie-Yannick Laplante, Jean Bouchard and Réjean Lepage for all their support. I am also grateful for the financial support from the Canada Research Chair on Smart Medical Devices, NSERC, ReSMiQ, and CMC Microsystems.

Last but not least, I am grateful to my family for their unconditional love and continued support.

# RÉSUMÉ

Le dépistage de culture cellulaire à haut débit est le principal défi pour une variété d'applications des sciences de la vie, y compris la découverte de nouveaux médicaments et le suivi de la cytotoxicité. L'analyse classique de culture cellulaire est généralement réalisée à l'aide de techniques microscopiques non-intégrées avec le système de culture cellulaire. Celles-ci sont laborieuses spécialement dans le cas des données recueillies en temps réel ou à des fins de surveillance continue.

Récemment, les micro-réseaux cellulaires in-vitro ont prouvé de nombreux avantages dans le domaine de surveillance des cellules en réduisant les coûts, le temps et la nécessité d'études sur des modèles animaux. Les microtechniques, y compris la microélectronique et la microfluidique, ont été récemment utilisé dans la biotechnologie pour la miniaturisation des systèmes biologiques et analytiques. Malgré les nombreux efforts consacrés au développement de dispositifs microfluidiques basés sur les techniques de microscopie optique, le développement de capteurs intégrés couplés à des micropuits pour le suivi des paramètres cellulaires tel que la viabilité, le taux de croissance et cytotoxicité a été limité. Parmi les différentes méthodes de détection disponibles, les techniques capacitives offrent une plateforme de faible complexité. Celles-ci ont été considérablement utilisées afin d'étudier l'interaction cellule-surface. Ce type d'interaction est le plus considéré dans la majorité des études biologiques.

L'objectif de cette thèse est de trouver des nouvelles approches pour le suivi de la croissance cellulaire et la surveillance de la cytotoxicité à l'aide d'un réseau de capteurs capacitifs entièrement intégré. Une plateforme hybride combinant un circuit microélectronique et une structure microfluidique est proposée pour des applications de détection de cellules et de découverte de nouveaux médicaments. Les techniques biologiques et chimiques nécessaires au fonctionnement de cette plateforme sont aussi proposées. La technologie submicroniques Standard complementary metal-oxide-Semiconductor (CMOS) (TSMC 0.35 $\mu m$) est utilisée pour la conception du circuit microélectronique de cette plateforme. En outre, les électrodes sont fabriquées selon le processus CMOS standard sans la nécessité d'étapes de post-traitement supplémentaires. Ceci rend la plateforme proposée unique par rapport aux plateformes de dépistage de culture cellulaire à haut débit existantes. Plusieurs défis ont été identifiés durant le développement de cette plateforme comme la sensibilité, la bio-compatibilité et la stabilité et les solutions correspondantes sont fournies. Plus précisément, un procédé de fonctionnalisation de surface à base d'un dépôt multicouche de polyélectrolytes est proposé afin d'améliorer l'adhérence cellule-électrode et d'augmenter la durée de vie des électrodes de dé-

tection. En outre, une nouvelle technique de fabrication de micropuits et d'intégration avec la puce CMOS est proposée permettant le dépistage parallèle des cellules.

Avec la possibilité d'effectuer des analyses de cellules de façon rapide, peu couteuse et en temps réel, la plateforme proposée permet la transition d'essais traditionnels passifs sur des cellules à un système de surveillance intelligent et en temps réel. Plusieurs applications d'analyse cellulaire pourraient tirer avantage de cette plateforme de suivi continu comme les études sur le cancer et la découverte de nouveaux médicaments.

# ABSTRACT

High throughput cell culture screening is a key challenge for a variety of life science applications, including drug discovery and cytotoxicity monitoring. Conventional cell culture analysis is widely performed using microscopic techniques that are not integrated into the target cell culture system. Additionally, these techniques are too laborious in particular to be used for real-time and continuous monitoring purposes. Recently, it has been proved that *in-vitro* cell microarrays offer great advantages for cell monitoring applications by reducing cost, time, and the need for animal model studies. Microtechnologies, including microelectronics and microfluidics, have been recently used in biotechnology for miniaturization of biological and analytical systems. Despite many efforts in developing microfluidic devices using optical microscopy techniques, less attention have been paid on developing fully integrated sensors for monitoring cell parameters such as viability, growth rate, and cytotoxicity. Among various available sensing methods, capacitive techniques offer low complexity platforms. This technique has significantly attracted attentions for the study of cell-surface interaction which is widely considered in biological studies.

This thesis focuses on new approaches for cell growth and cytotoxicity monitoring using a fully integrated capacitive sensor array. A hybrid platform combining microelectronic circuitry and microfluidic structure is proposed along with other required biological and chemical techniques for single cell detection and drug discovery applications. Standard submicron complementary metal–oxide–semiconductor (CMOS) technology (TSMC 0.35 $\mu m$) is used to develop the microelectronic part of this platform. Also, the sensing electrodes are fabricated in standard CMOS process without the need for any additional post processing step, which makes the proposed platform unique compared to other state of the art high throughput cell assays. Several challenges in implementing this platform such as sensitivity, bio-compatibility, and stability are discussed and corresponding solutions are provided. Specifically, a new surface functionalization method based on polyelectrolyte multilayers deposition is proposed to enhance cell-electrode adherence and to increase sensing electrodes' life time. In addition, a novel technique for microwell fabrication and its integration with the CMOS chip is proposed to allow parallel screening of cells.

With the potential to perform inexpensive, fast, and real-time cell analyses, the proposed platform opens up the possibility to transform from passive traditional cell assays to a smart on-line monitoring system. This continuous monitoring platform can be beneficial in a wide range of cell analyses applications such as cancer studies and drug discovery.

# TABLE OF CONTENTS

# LIST OF TABLES

# LIST OF FIGURES

# LIST OF ABBREVIATIONS

| | |
|---|---|
| ADC | Analog to Digital Converter |
| CBCM | Charge-Based Capacitive Measurement |
| CDC | Charge to Digital Converter |
| CMOS | Complementary Metal Oxide Semiconductor |
| DAC | Digital to Analog Converter |
| DC | Direct Current |
| DMA | Direct Memory Access |
| DNA | Deoxyribonucleic Acid |
| ECG | Electrocardiography |
| ECIS | Electric Cell–Substrate Impedance Sensing |
| EDTA | Ethylenediaminetetraacetic Acid |
| EMEM | Eagle's Minimal Essential Medium |
| ENOB | Effective Number Of Bits |
| FBS | Fetal Bovine Serum |
| FET | Field Effect Transistor |
| FFT | Fast Fourier Transform |
| FIFO | First In First Out |
| FPGA | Field Programmable Gate Array |
| IDE | Interdigitated Electrode |
| ISFET | Ion Sensitive Field Effect Transistor |
| LAPS | Light Addressable Potentiometric Sensor |
| LoC | Lab on Chip |
| MEA | Multi Electrode Array |
| MEMS | Micro Electro-Mechanical Systems |
| NMOS | N Channel Metal-Oxide-Semiconductor Field Effect Transistor |
| OSR | Oversampling Ratio |
| PBS | Phosphate-Buffered Saline |
| PCB | Printed Circuit Board |
| PDMS | Polydimethylsiloxane |
| PEM | Polyelectrolyte Multilayer |
| PMOS | P Channel Metal-Oxide-Semiconductor Field Effect Transistor |
| QCM | Quartz Crystal Microbalance |
| RPMI | Roswell Park Memorial Institute Medium |

| | |
|---|---|
| SNDR | Signal to Noise and Distortion Ratio |
| SPR | Surface Plasmon Resonance |
| UV | Ultra-Violet |
| VOC | Volatile Organic Compounds |

# LIST OF APPENDICES

# CHAPTER 1 INTRODUCTION

## 1.1 Motivation

Cells are fundamental unit of life and understanding the individual cell structure and behavior plays an important role in understanding more complex units such as tissues and organs. Cell culture monitoring and quantification of cellular phenotypes such as viability, growth rate, and metabolism, under controlled cell culture conditions, impact many different areas in biology and medicine. For instance, cell growth studies can be beneficial in many fields such as standardization of cell cultivation, tissue engineering, and most importantly in cancer research where the effect of certain anti-cancer drugs on the cells is of interest.

Conventionally, the cell studies and monitoring the response of populations of cells to drug candidates are performed in standard well-plates, Petri dishes, and microscopic slides. Microtitration (MTT) analysis and fluorescence microscopy are two of the well-established methods for monitoring cellular activities and metabolism rate [1–3]. Despite the fact that these techniques are widely used in biological laboratories, they are time-consuming because of the required labeling, incubation, and freezing processes. In addition, they require bulky optical setups including fluorescence microscope and spectrophotometer. Moreover, some of these labeling substances are toxic and not suitable for continuous monitoring of a sample in a long period of time. To address these issues, several alternative have been proposed including multi-electrode arrays (MEAs) [4], electric cell-substrate impedance sensing (ECIS) [5], light-addressable potentiometric sensing (LAPS) [6], and ion sensitive field effect transistors (ISFETs) [7]. Among them, integrated capacitance sensing technique have demonstrated interesting capability for developing miniaturized cell assays. Recent advances based on standard microelectronic technologies such as CMOS process have addressed the challenge of developing high throughput, low cost, label-free, and high precision impedometric and capacitive biosensors. In fact, low-cost mass production of CMOS provides the opportunity to implement scalable sensors as well as the array implementation for parallel cell detections.

Despite these great advances, still the development of a large number of capacitive microsensors for high throughput screening is under research and cell-based biosensors still suffer from some intrinsic shortcomings. The common problems in the design and integration of cell-based biosensor are choosing the optimum dimension and topology for the sensors and the design of an efficient readout interface. The detection sensitivity of readout circuits might be limited by noise resulted from large parasitic capacitances. Furthermore, employing CMOS technology in the applications where direct contact of the sensing electrodes with the chemical

and biological solutions is necessary, complicates the packaging and encapsulation process. The packages should protect the device against corrosive biological solutions while it should be robust enough against several cleaning procedures and long-term cell culture experiments.

Considering the tremendous future potential of lab-on-chip technologies, this thesis aims to demonstrate a new fully integrated platform that allows an efficient monitoring of cells and their physiological state in a high throughput mode while maintaining the system's simplicity and ease of implementation. Our proposed compact, low-cost and, re-usable cell-based biosensor can be employed as a versatile tool to transit Petri dish based experiments from the traditionally labor-intensive process to an automated and streamlined process which is significantly advantageous in different fields of biology and medicine.

## 1.2 Research hypothesis

The electrical properties of living cells and tissues have been of interest for many years. In fact all living cells, except viruses, have a similar structure including a cytoplasm surrounded by a membrane. The surface of most types of cells is negatively charged, which results in the attraction of positive ions in the growth medium to the cell surface and consequently the formation of a double layer [8]. The membrane is considered to be a highly highly non-conductive medium and its relative permittivity ranges from 2 to 10 [8]. It is reported that at low frequency fields there are two factors contributing to the dielectric properties of living cells [9].

— Reorientation of the dielectric dipoles of individual cells.
— The polarization of the surface charge accumulated on the cell membrane.

Also it has been shown that these electrical properties have a strong correlation with the morphology and health state of the cells. This means that any damage in the cell membrane can alter its dielectric properties. For this reason, the electrical properties can be used to differentiate between normal and abnormal cells and also to evaluate the cell physiological state.

When cells are placed on an electrode, there are two phenomenas that result in a change in the sensed capacitance (Figure 1.1). The electric fields give rise to an electric dipole in the cell surface ($C_{cell}$) [10] and also a capacitive coupling happens between the electrode and the cell's charged membrane, which varies with the distance ($C_{bond}$). The closer the cell is to the electrode and the stronger the cell-electrode attachment is, the value of coupling capacitance would be higher. Measuring this capacitance, can give valuable information regarding the cell-electrode interaction and the quality of cell-substrate adherence. Healthy cells have a well-formed membrane, thus sustaining a strong bond and electric dipole. However, if any

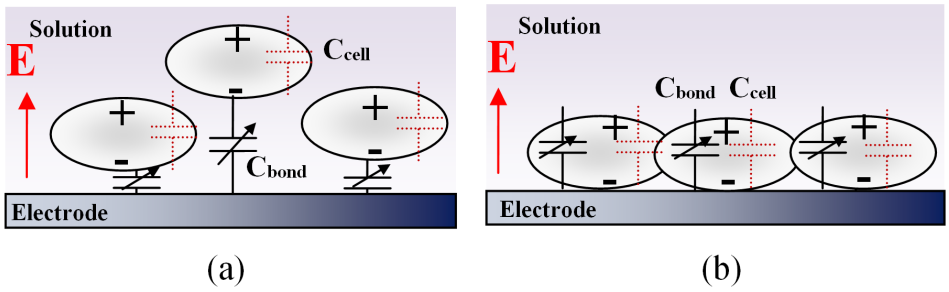


Figure 1.1: Cell-electrode capacitive model, (a) Cell suspension. (b) Adhered cells.

changes happens in the cells' morphology and health state, for example a damage in the membrane induced by toxic agents or drugs, the electric dipole in the cell membrane will change and the bonding gets weaker.

Our assumption is that with a very high-sensitivity capacitive readout interface implemented underneath the capacitive electrodes, one can exploit the minute changes in the dielectric properties of the cells. These changes can be measured to detect the presence of the cell on the substrate and to monitor their health state. Furthermore, by continuous monitoring of capacitance changes, we can detect the presence of toxic materials and assess the effect of certain drugs on the cells.

### 1.3 Research objectives

The objective of this thesis is to build a fully integrated, potentially high throughput, low cost, and easily scalable tool for real-time cell analyses. We aim to build a versatile device that allows the quantitative assessment of various cell types in terms of viability and growth rate as well as their response to cytotoxic drugs. The detailed objectives are as follows.

1. To design and fabricate a cell-based capacitive biosensor array for cell viability and growth monitoring.
2. To design high performance CMOS circuits for capacitive sensor data readout and analog to digital conversion.
3. To exploit a robust packaging technique for microfluidic/microelectronic hybrid cell-based microsystem in a biocompatible process.
4. To solve the biocompatibility and non-stability issues of CMOS-based fabricated electrodes and to improve the bio-interface interactions at cellular level using efficient biological and chemical methods.

5. To design and implement a computer interface for sensor data acquisition and automated array multiplexing and readout.
6. To explore new approaches for miniaturization of microsystems by integrating microfluidic structures and microelectronic building blocks in a single chip.
7. To validate the proposed microsystem through measuring cell viability, proliferation rate, and response to pharmacological stimuli/drugs.

# CHAPTER 2 LITERATURE REVIEW : ON-CHIP CELL MONITORING DEFINITIONS AND TECHNIQUES

## 2.1 Introduction

The basic *in-vitro* cell culture has become essential in understanding advanced cell biology and complex cellular systems such as tissues and human organs. The study of cells grown in laboratory can provide important information about cell-cell interactions, extra-cellular matrix and cell migration. In addition, these studies can be beneficial in drug toxicity screening and monitoring cellular responses to a variety of different stimuli and drugs. In this chapter we introduce the essential parameters to be measured in cell culture samples and conventional methods for acquiring them along with their limitations and shortcomings. In addition, we will review the recent advances in electrochemical and non-electrochemical biosensing technologies that can be integrated with a standard cell culture environment. The advantages and limitations of these methods will be discussed as well.

## 2.2 Key parameters in cell culture monitoring

Based on the nature of biological or medical applications, there are several parameters in a cell culture sample that are important to study. They can be classified as follows.

— **Metabolic activity**
  Living organisms require chemical energy to perform their daily activities and to maintain their viability and growing. In living cells, this chemical energy is derived from a molecule called Adenosine Triphosphate (ATP). Measuring the ATP levels in cells can give critical information about their health state. In addition, to find out more about the quality of cell metabolism and its health condition, the following parameters are of interest [11].
  — Extracellular oxygen ($O_2$) : indicates the cell respiration.
  — Extracellular carbon dioxide ($CO_2$) : reflects the cell overall viability.
  — Extracellular glucose : shows the cell's capacity to produce fuel.
  — Intracellular ATP : indicates how much fuel is available to the cell.
  — Extracellular pH : indicates cellular respiration and acidification rate.

— **Electro-physiological parameters**
  In electrophysiology, the study of ion channels has a great importance. Ion channels are transmembrane proteins that allow passage of ions through pores across a non-

permeable lipid layer. Studies of $Ca^+$, $K^+$, and $Na^+$ ion channels have shown their great importance in cell physiology. Defective ion channels are responsible for various health problems such as cardiac or neuronal diseases [12].

— **Cell signaling**

Communication and signaling between cells are crucial in understanding the cells and organs functions. Several types of cell signaling exist such as neurotransmitters, antigens triggering/ antibody responses, and cell response to specific hormones [13]. These parameters in cell signaling studies can be investigated using cell-based assays.

— **Cell adhesion**

Cell adhesion is the ability of a single cell to stick to another cells, substrates or extracellular matrix (ECM). Adhesion of cells is essential in inter-cellular communication and also in the development of tissues and body organs. Any changes in the quality of cell adhesion can be a sign of wide range of diseases such as arthritis, cancer, and osteoporosis. Since most mammalian cells are anchorage-dependent and stick firmly to suitable substrates, it is important to study the quality of this attachment in various fields of bio-material studies, implantable devices, tissue-on-a-chip, and organ-on-a-chip, cancer metastasis, and drug treatments [14–16].

— **Cell viability, proliferation, and cytotoxicity monitoring**

The viability levels and growth rate of cells in a sample are a good indicator of their health state. The proliferation and viability assessment is usually coupled with metabolism analyses which is essential in cell growth measurements. On the other hand, in pharmacological profiling of drugs, it is important to investigate the interactions between the cells and drugs quantitatively. Moreover, in cancer research, the study of chemical compounds that inhibit or promote the viability of cells and their proliferation has a great importance [17]. In order to perform drug screening test, it is important to have a high throughout platform in order to reduce the sample consumption and to improve the resolution and sensitivity.

Due to the importance of understanding cell-surface interactions and cell growth characteristics, our main focus in this thesis is measuring the cell adhesion, proliferation, and response to toxic drugs.

## 2.3 Conventional techniques for cell viability and growth monitoring

Among various techniques that exist for acquiring cell culture parameters, optical techniques and particularly fluorescence imaging has proven to be an inevitable tool for monitoring living cell samples. In optical assays, the cells are tagged with fluorescence dyes (fluorophores) and

based on the metabolic activity of cells, different colorimetric properties are observed [18]. This method requires special handling and treatment of cell cultures with fluorescent labels as well as the use of off-chip optics such as fluorescence microscopy and spectrophotometer.

Another convenient technique is microculture tetrazolium (MTT) assay which provides a good estimation of cell viability in a sample based on colorimetric principle. MTT is a yellow water-soluble tetrazolium dye that is reduced by live cells to produce a purple formazan product that is insoluble in aqueous solutions [19]. The use of this assay requires the cultivation of cells into multiwell plates and the addition of a drug or toxin at certain concentrations for a specified amount of time. This assay is an example of a lengthy procedure that employs conventional cell culturing techniques for cell studies.

As was mentioned earlier, the cells require ATP to maintain their viability and health. During the cell death, the ATP levels falls to the points where cells can no longer maintain their metabolic activity. Therefore, a low ATP level is used as an important indicator of cell death. In contrast, any increase in the ATP levels is a direct indicator of cell proliferation and growing. In ATP assays, the bioluminescent detection of the ATP is performed for viability monitoring [20]. In this technique, a reagent called Luciferase is used to catalyze the formation of light from ATP and Luciferin that generates photons. Studies show that ATP assays have a better sensitivity, particularly for viability measurement of very low cell numbers compared to MTT assay [21].

Another technique to measure cell viability and proliferation is the use of Alamarblue reagent. The active ingredients in Alamarblue is Resazurin which is a cell-permeable blue component that is naturally non-fluorescent. Upon entering the cell membrane, it is converted to Resorufin, which is a bright red fluorescent compound. To perform viability tests, a certain concentration of Alamarblue is added to the cell culture wells and at certain time intervals, the reduction of Alamarblue is measured by fluorescence readings [22].

The reported assays are widely used in biological laboratories and have been very successful in cell culture monitoring. However, they all require external optical setups. Moreover, most of these methods do not provide a continuous monitoring and the measurement needs to be taken at certain time intervals after following several preparation steps. On the contrary, cell-based microsystems can provide efficient solutions to these problems by integrating and automating the sensing, readout and analyses processes in one single device. These features result in a noticeable reduction in infrastructure requirements, and measurement complexity.

## 2.4 Integrated approaches for cell adhesion, proliferation, and cytotoxicity monitoring

In last recent years, biosensors have rapidly expanded and evolved in many fields of biology, medicine, environmental monitoring, and nanotechnologies. These devices, by utilizing biologically driven sensing elements, detect the presence of specific target analytes such as DNA, proteins, hormones, bacterias or living cells. The interaction of these analytes with the sensor interface brings about some physiochemical changes. These changes that correlate with the presence of a target analyte, can be further detected and measured by a transducer for which a transduction scheme is normally chosen based on the type of parameters to be measured such as electrochemical, mass, optical, pH, etc (Figure 2.1).

Among various types of biosensors, cell-based biosensors that measure electrochemical signals such as voltage, current or impedance, resulting from cell activity and metabolism, have become a focus of research in recent years. The living cells can be seen as an electrochemical dynamic system in which several reduction-oxidation (redox) reactions and changes of ionic composition and concentration happen. These changes which are direct indicator of cell growth and development, result in the electron generation and charge transfer which can be detected using electrochemical methods. In this regard, several biochemical parameters such as ion concentrations ($H^+$, $K^+$, $Na^+$, $Ca^+$, $Cl^-$, etc.), membrane potential, adhesion, and morphology can be detected by electrochemical biosensors.

In the remaining of this chapter we will briefly introduce various types of integrated cell-based biosensors aimed for cell adhesion, proliferation, and drug cytotoxicity monitoring.

### 2.4.1 Electric cell-substrate impedance sensing (ECIS)

ECIS is one the most efficient techniques for monitoring cell adhesion, spreading, and morphology in real-time. The measurement principle is based on the fact that as mammalian cells attach and spread on the surface of a gold electrode, they hinder the current flow and charge transfer between the electrodes which results in an increase in the overall electrode output impedance [23]. Impedometric biosensors are divided into two categories of faraidic and non-faraidic sensors. Faraidic detection involves the charge transfer detection in the electrode-cell interface. On the contrary, in non-faraidic schemes there is no charge transfer between the electrode and test samples and instead the transient current that is charging the capacitive electrodes is measured. Thus non-faraidic impedometric sensors are usually referred as capacitive sensors [24] which will be discussed later in details in chapter 3.

Figure 2.2 shows a schematic overview of the impedance measurement setup pioneered by

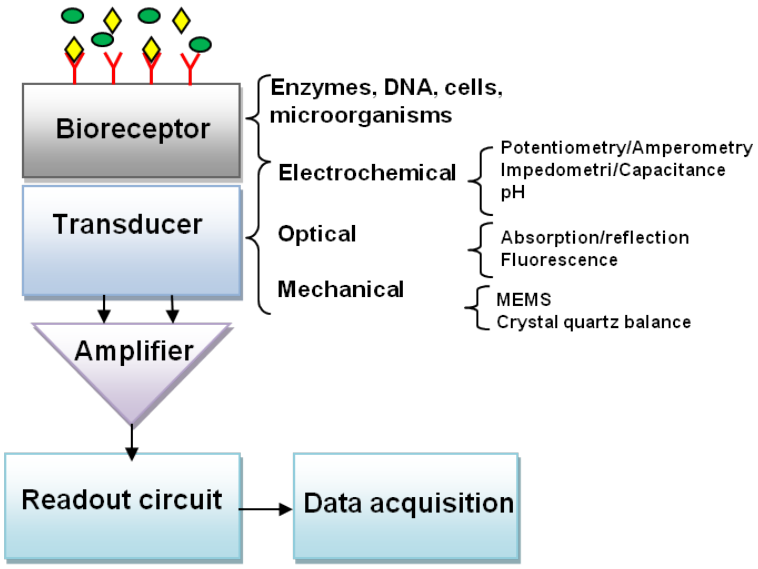


Figure 2.1: Simplified block diagram of a biosensor and its conversion schemes.

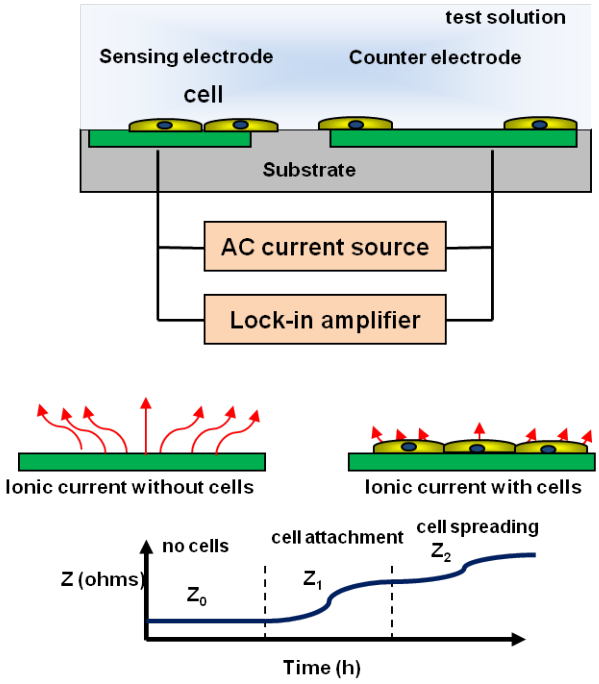


Figure 2.2: Schematic overview of ECIS technique for cell adhesion detection.

Giaever and Keese [25]. In this sensing scheme, an alternating current is applied to the electrodes and the voltage is recorded using a lock-in amplifier. When there is no cell, the current flows freely on the electrodes, however as the cell, which are insulator in nature, attach

to the electrode, they hinder the current flow and as a result giving rise to the impedance. Conventionally, two electrode structures are used to realize impedometric systems, planar (monoploar electrodes) or interdigitated electrodes (IDEs). In planar architecture, usually a large counter electrode should be used for precise impedance measurements resulting in a large sensing area and a reduced sensitivity. In addition, the use of large counter electrodes makes the integration and array implementation of the ECIS difficult ; thus it is not suitable for high throughput cell-based measurements. On the contrary, in interdigitated electrodes, current flows in close proximity of the electrode surface, resulting in a higher sensing sensitivity and improved performance.

The fabrication process of ECIS consists of a metallic layer deposition on the substrate, followed by lithography and etching process. Despite the great advantage of this technique in comparison with optical techniques, it requires off-chip readout system that limits the number of input channels and consequently the number of sensing sites. Consequently, ECIS is not the best solution for high throughput applications that require a large number of multiplexed sensors. To overcome this problem, recent advances in standard microelectronic technologies such as CMOS have addressed the challenge by developing high throughput low cost label-free and high precision impedometric and capacitive biosensors [26], [27].

### 2.4.2 Capacitive sensing

Capacitive sensors operation principle is based on the modulation of capacitance value by physical or chemical parameters' variation. Due to their high resolution, reliability, and low temperature dependence, these types of sensors are widely used in various applications such as pressure sensing [28], accelerometers [29], humidity measurements [30], and molecular/cellular biology [31]. Since capacitive sensors have no static power consumption, they are suitable for use in energy-constrained applications, such as low-power battery-operated systems, point of care devices, and wireless sensor networks. Among different implementation of capacitive sensors, the development of miniaturized integrated capacitive arrays has a crucial importance for the successful employment of these microsystems in practical chemical and biological applications such as DNA hybridization detection [31], cellular studies [32], and protein interactions quantification [33]. There are two technical advantages in using fully integrated capacitive sensors ; the use of fully electronic circuitries allows the signal processing in close proximity of the sensors which results in a very high sensitivity and noise immunity. Moreover, using CMOS technology allows the integration of large number of electrodes on a single die which allows high throughput mode measurements. In addition, by using digital addressing and multiplexing techniques, integrated arrays of capacitive sensors require only

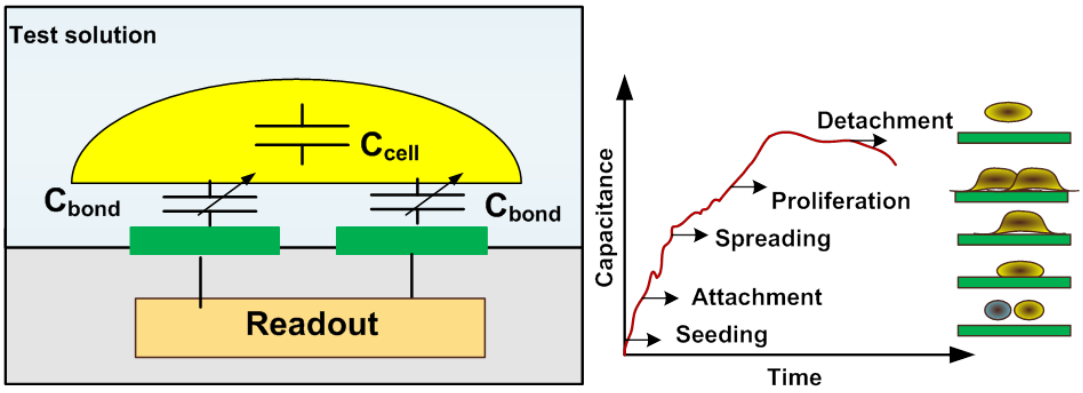


Figure 2.3: Schematic overview of capacitive technique for cell adhesion and growth monitoring.

a few electrical wirings to off-chip interfaces that can notably reduce the number of pins and packaging costs as well.

In cell monitoring, when cells are placed above the capacitive electrodes, they start attaching and spreading over the electrodes and increasing the total capacitance (Figure 2.3). As they start spreading and growing above the electrodes, the value of sensed capacitance increases. Any changes in the cells health state induced by addition of certain drugs or chemicals that lead to detachment of the cells, results in a decrease in the capacitance value.

### 2.4.3 Light-addressable potentiometric sensor (LAPS)

LAPS is a newly developed semiconductor device which was first proposed by Hafeman et al. in 1988 [34]. The device is used to monitor extracellular potentials in electrogenic cells and cell metabolism rate. The simplified overview of a typical LAPS device is shown in Figure 2.4. Based on electrolyte- insulator-semiconductor (EIS) or electrolyte-metal-insulator-semiconductor (EMIS) structure, a modulated external light source can be used to generate a photocurrent corresponding to the potential on $Si_3N_4$ surface. An external DC bias voltage is applied to form a depletion layer at the interface of insulator ($SiO_2$) and semiconductor. Upon a change in the chemical or biological properties of electrolyte, the surface potential that reflects electrical charge at the electrolyte-solid interface is altered.When a light source is applied to the substrate, the light induced charge carriers contribute to the generation of a photocurrent. The current amplitude depends on the surface potential and can be detected by an external readout circuitry.

In cell culture application, if cells are appropriately positioned on the insulated semicon-

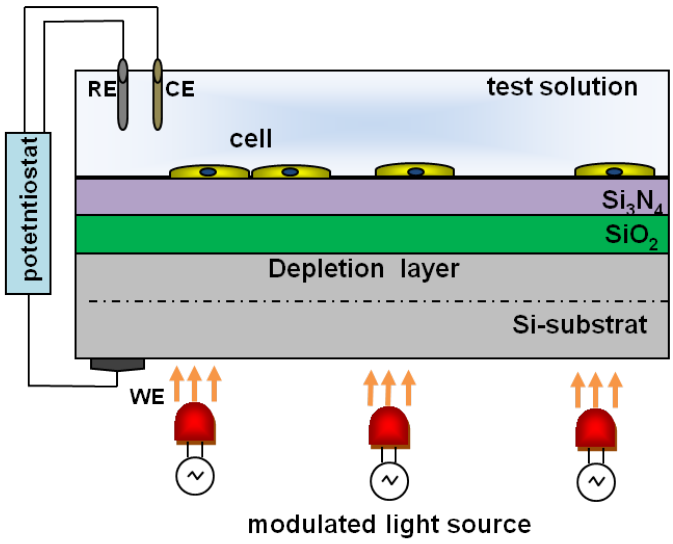


Figure 2.4: Schematic diagram of a LAPS measurement setup.

ductor surface, the extracellular potentials of electrogenic cells coupled to the LAPS can be monitored by surface potential alteration, which allows measuring the extracellular potentials at different positions on the sensor's surface. Based on this theory, various LAPS devices have been constructed for different cell-based applications including cellular metabolism detection, cytotoxicity evaluation, and detection of various electrogenic cells such as cardiac, neural, and olfactory cells [35–37].

For its simple structure, the fabrication and encapsulation of LAPS is easier than other electrochemical biosensors, especially for extracellular measurements. Moreover due to the extremely flat surface, the integration of microfluidic channels with the electrode is less critical [38]. Despite the excellent integration properties of LAPS, the signal-to-noise ratio of the measured signals is low and the range of baseline drift is wide, especially in the detection of signals fired by neurons. These factors limit the application of LAPS in neural studies. To improve the performance, certain signal processing techniques such as wavelet transform denoising are proposed. They can partially cancel out the background noise [39].

### 2.4.4 Ion-sensitive field effect transistor (ISFET)

The ISFET invented by Bergveld in 1970 [40], is a chemically sensitive field effect transistor. As shown in Figure 2.5 it can be described as a MOSFET with the gate connection separated from the chip and inserted in an aqueous solution referred as reference electrode. Due to its small size, rapid pH response, repeatability, low process variation, and low cost construction,

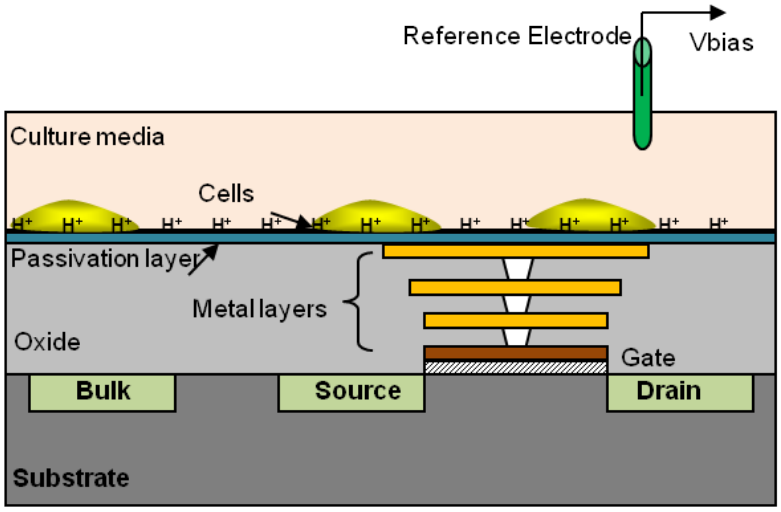


Figure 2.5: Schematic diagram of ISFET pH-sensor, the gate is connected to the pH-sensitive membrane by stacking metal layers.

the ISFET is widely used for electrochemical detections.

The standard ISFET structure has an insulating membrane which is sensitive to hydrogen ions in the test solution. As a result, any charge build-up on the membrane, which varies with pH solution, causes a modulation of the ISFETs threshold voltage.

ISFETs can be fabricated in standard CMOS process following the exact steps for MOSFET fabrication, which is referred as ISFETs in unmodified CMOS process [41]. This process employs a floating-electrode design. All the metal layers in the process are connected together with vias, allowing the silicon nitride passivation layer to act as the pH-sensitive membrane. Silicon nitride is well known for ISFET fabrication and gives a linear response, with sensitivity in the range of 45-56 mV/pH [42]. If ISFET is used as a pH sensor only, no extra processing step for membrane modification is required. However making the ISFET sensitive and selective to other ions such as $Na^+$, $K^+$ and $Ca^+$, requires extra steps for the deposition of membranes [43, 44].

The fabrication of floating gate ISFETs in standard CMOS process leads to some non-idealities including the accumulation of trapped charge on the gate and passivation layer during the fabrication process. The presence of trapped charge can result in a large and unpredictable variation in ISFET threshold voltage. However the excess charges can be removed by UV radiation and hot electron injection techniques [45, 46].

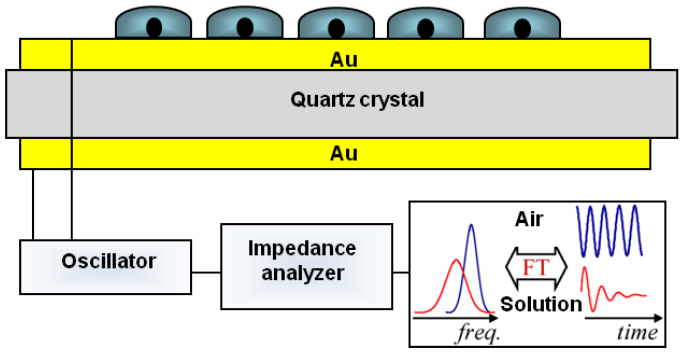


Figure 2.6: Schematic diagram showing the mechanism of cell-based assays employing QCM devices [47].

### 2.4.5 Quartz crystal microbalance (QCM)

QCM is a type of label-free acoustic sensor that is used in various physical, chemical and biological applications. By measuring the mass and energy dissipation of the materials on the sensor surface, it has been applied in various cell-based assays for studying the cell-cell and cell-surface interactions [48, 49]. The simplified schematic of a QCM sensor is shown in Figure 2.6. The main component of the device is a quartz crystal which is placed between two metal electrodes. The signal transduction mechanism of the QCM devices is based on converse piezoelectric principle in which electrical charges are generated on opposite sides of a crystalline substance upon its mechanical deformation [49]. By applying an alternating current (AC) to the pair of metal electrodes which are sandwiching the crystal, an oscillation in the quartz crystal happens which its frequency is linearly proportional to the mass above the electrodes [50]. By employing QCMs and measuring the changes in the oscillation frequency, the attachment and spreading of the cells above the gold electrodes can be monitored. In addition, this type of biosensor can be potentially useful in identifying active drug compounds that affect cell attachment and proliferation specially in cancer cell studies when the sensitivity of the cells to anticancer drugs is of interest [51].

### 2.4.6 Surface plasmon resonance (SPR)

Surface plasmon resonance (SPR) is an optical biosensor that is used to detect the changes in physio-chemical properties of the solution-sensor interface. By using the refractive index of the analyte on the sensor's surface, this method allows the quantification of several bio-moelcular and cellular interactions. Although it is mostly used for molecular research and analysis of the bio-molecules, it can be employed to study the interactions between the living

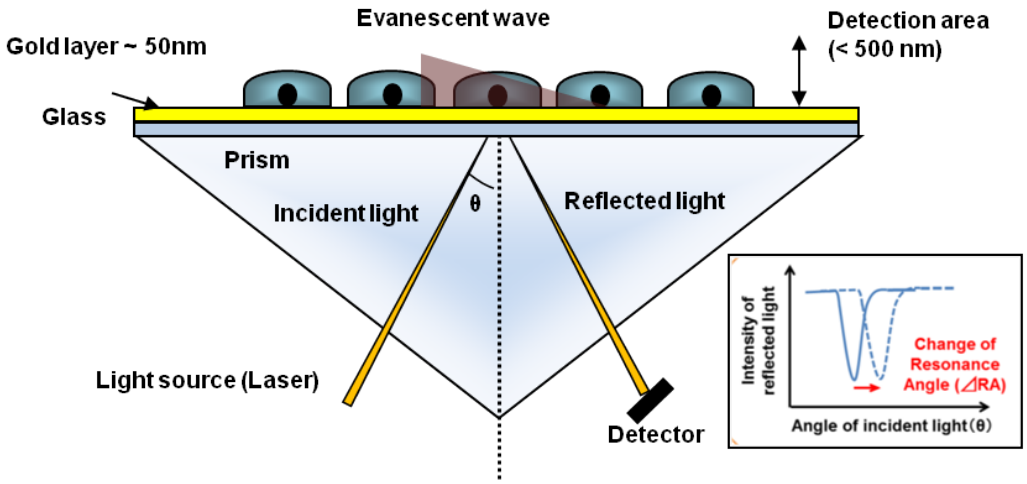


Figure 2.7: Schematic overview of Surface plasmon resonance (SPR) sensors which detect a refractive index change within a detection area (<500 nm) as a change of resonance angle caused by the cell attachment.

cells and to analyze the molecules that induce any reactions from cells [52].

The principle of operation is based on the fact that when a light beam hits an interface of two transparent medias (e.g. a glass prism and a solution), the light is partly reflected from the media with the highest refractive index (glass prism) [53]. In SPR devices one side of the glass prism is coated with thin Au layer (Figure 2.7). The light excites the free electrons at the metal surface (known as surface plasmons) and makes them oscillate. Some of these plasmon particles are confined on the metal surface, creating an electric field that extends a few tenth of nanometer into the buffer, Au film, and the prism and is called evanescent wave. If any changes happens in the metal surface property, such as interaction of target and probe molecule, the momentum of the plasmons and their evanescent fields will alter and a shift in the incidence light reflection angle will happen. The shift in the resonance angle is directly proportional to the density of biological molecules in the evanescent field thus it can detect the association and dissociation of biological molecules on a gold surface with no labelling process needed.

Despite the other types of biosensors, SPR can also reveal valuable information about sub-cellular structures with high temporal and spatial resolutions and can be used as a powerful tool for intracellular studies [54].

### 2.4.7 Comparison of different cell-based sensing schemes

In previous section we briefly reviewed some of the most widely used techniques in cell studies. It is worth mentioning that great progress in biology and medicine relies on convenient and traditional techniques such as MTT analysis, viability reagents (such as Alamarblue or Trypan blue) and fluorescence microscopy. These techniques are employed as the most standard assays for monitoring cellular activities and metabolism rate. Despite their great performance, they have some drawbacks such as processing time, bulky instrumentation, and discontinuous measurements.

As an alternative to traditional methods several techniques have been proposed including ECIS, capacitive, ISFETs, LAPS, QCM, and SPR sensors which were briefly reported above. The advantage of standard microelectronic technologies, particularly CMOS, is the fact that they allow a monolithic integration of large numbers of micro-sensors along with their associated electronic circuitry for creating a single device capable of performing several cell-based experiments. The comparison between these methods is summarized in Table. 2.1. It is worth mentioning that each of these techniques has its own advantages in specific cell-based application and selecting among them strongly depends on the type of parameters to be measured. For example, for extracellular pH and cell metabolism monitoring ISFETs and LAPS are the best candidates, although they might require external reference electrodes for the former and external light sources for the latter. For the applications that rely on the quality of cell-substrate adhesion, ECIS and capacitive measurements are suitable alternatives while these two techniques cannot be used for non-adherent cells measurements. Since most mammalian cells are anchorage dependent which means that they need to attach to the substrate in order to growth and maintain their life cycle. Understanding cell-substrate interaction has a great importance in medical and bioengineering applications. In this regard, capacitive and impedometric cell culture platforms are capable of analyzing several cell events including cell adherence, spreading, proliferation, and death quantitatively.

## 2.5 Integrated biosensors for cell viability, growth, and cytotoxicity monitoring : A review.

In previous section we introduced the most well-known electrochemical, optical, and mechanical techniques for cell analyses. We finish this chapter by reviewing the state of the art of these technologies with the focus on cell viability, growth, and cytotoxicity monitoring. Various advanced technologies and techniques including microelectronic, microfluidic, surface functionalization, and packaging are required to realize an efficient cell-based microsystem.

Table 2.1: Comparison of electrochemical and non-electrochemical cell analyses techniques

| Technique | Basic of operation | Advantages | Limitations |
|---|---|---|---|
| **Fluorescence** | Measuring fluorescence of cells based on the concentrations of ions or protein expressions | -High throughput<br>-High selectivity | -Optical setup required<br>-High cost<br>-Long sample preparation |
| **MTT** | Measuring cell metabolic activity using chemical assays | -High throughput | -Limited detection range<br>-Off-chip optics<br>-Toxic in long term |
| **Alamarblue** | Fluorometric/colorimetric growth indicator based on detection of metabolic activity | -Quantitative<br>-Easy sample preparation<br>-Non-toxic | -Requires incubation<br>-Off-chip optics |
| **LAPS** | Photocurrent modulated by the surface potential | -Simple<br>-Microfluidic integration<br>-Low-cost | -External light source |
| **QCM** | Measuring frequency shift happens by mass change on the crystal surface | -Non-invasive<br>-Label-free<br>-Long term | -Low specificity |
| **SPR** | Measuring the excitation of surface plasmons (Au or Ag surfaces) by ultraviolet or visible | -Non-invasive<br>-Label-free<br>-Continuous | -Limited detection range<br>-External light source<br>-External detector |
| **ISFET** | Measuring pH changes using a pH sensitive MOS device | -Ease of fabrication<br>-High sensitivity , | -Ref. electrode required<br>-Drift variation<br>-Trapped charge |
| **ECIS** | Measuring the current between the electrodes by applying a sinusoidal voltages at different frequencies | -High sensitivity<br>-Label-free<br>-Fast response | -Complex data analyses<br>-Power hungry<br>-Ref. electrode required |
| **Capacitive** | Measuring capacitance changes due to the variations in dielectric constant of the analyte | -Simple readout<br>-Low cost<br>-Ease of fabrication | -Bio-compatibility<br>-electrode lifetime<br>-Parasitics |

We will also review the pros and cons of these platforms in terms of CMOS integration capability, ease of implementation, and accuracy.

### 2.5.1 Case study 1 : Multichannel lens-free CMOS sensors for real-time monitoring of cell growth

In [55] a platform for real-time monitoring of cells is proposed that is realized by integration of a three-layer poly-methyl methacrylate (PMMA) cell culture microchip and a multichannel lens-free CMOS/ Light-emitting diode (LED) imaging system.

Figure 2.8 shows the schematic illustration of this platform for real-time cell growth imaging. The PMMA microchip consists of three layers in which the top layer contains a circular hole for the installation of the cell culture medium tube and the two other layers are used to ba-

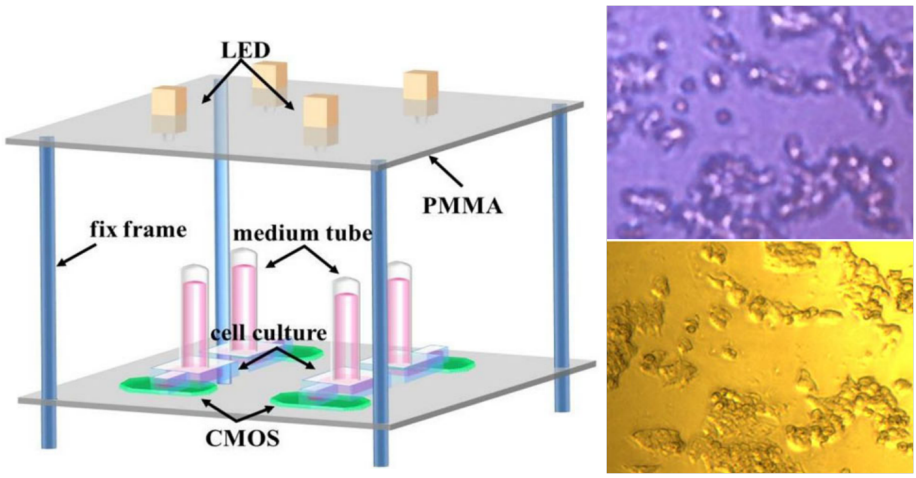


(a) (b)

Figure 2.8: (a) Schematic illustration of lens free CMOS-based imaging system. (b) Comparison of images acquired by CMOS-based imaging system (top) and traditional microscope with 40x magnification (bottom) [55].

lance the air pressure. The monitoring system consists of four CMOS image sensors arranged in a rectangular array on a lower PMMA substrate and four LED white light sources placed on the upper PMMA substrate above the corresponding CMOS image sensors. The LED light sources and CMOS sensors are controlled using a program in LabVIEW. Using a custom-designed interface, the light sources and sensors are turned on at predetermined 30 min intervals and at the end of image acquisition they are tuned off. For imaging, commercially-available CMOS image sensors are used. The feasibility of the imaging system is investigated by using various concentrations of HepG2 cell lines. For each samples, the cells are cultivated for a period of 48 h and a series of images is acquired at 8 h intervals. Cytotoxicity tests were also performed in which the HepG2 samples were seeded in the microfluidic cell culture chip for 24 h and were treated with cyclophosphamide and then monitored for a further 24 h. The results show that while the untreated cells grow steadily over time, the treated cells exhibit a decreased growth rate as a result of cytotoxic drug.

This work shows a good example of real-time cell growth monitoring using CMOS-based optical techniques. The results obtained from the lens-less CMOS imaging system are in good agreement with a conventional microscope under 40x magnification. Despite the good performance of the system as a low throughput array, because of the passive substrate used for integration, the device is not applicable in high throughput applications where a higher number of sensors is required. The alignment of LEDs on the top PMMA layer with the image sensors on the bottom plate can be difficult especially when integrating a large number of

sensors on a limited substrate space.

### 2.5.2 Case study 2 : High density CMOS electrode array for high throughput and automated cell counting

In another effort in [56], a high-density biosensor array based on electrical-impedance spectroscopy (EIS) is developed for real-time cell counting. This biosensor, aimed to detect breast tumor MCF-7 cells, consists of an array of 96 x 96 densely placed electrodes fabricated in 0.18 $\mu m$ CMOS technology. Each single electrode is addressable by using an underneath multiplexing circuitry. The exposed Al electrodes (22 $\mu m$ x 22 $\mu m$) are post processed and 100 nm of titanium (Ti) and 1 $\mu m$ of gold (Au) are deposited on the electrodes by standard photolitography process. The addressing and impedance readout circuitry are used off-chip (Figure 2.9) and are controlled by LabVIEW. To encapsulate the chip and to provide a chamber for containing the solution, a glop top bio-compatible silicone encapsulants is used. To realize the counter electrode for impedance measurement, an indium-tin-oxide (ITO) coated glass is positioned on top of the chamber to act as a counter electrode. In the proposed chip, the impedance readings are based on the binary "on" and "off" response and the presence/ absence of the cells is detected by the recorded impedance value.

Although this platform has the advantage of high-density electrodes, it suffers from a couple of limitations ; first, due to the use of off-chip LCR meter, the sensitivity and resolution of the impedance readings is low, thus only a binary signal showing the presence or absence of the cells is obtained. Second, the need for ITO glass electrode, makes the integration of the proposed platform difficult and its not very suitable for portable and point of care diagnostics. However, due to the simplicity in the design and high-density of electrodes, the device is a suitable candidate for short term cell counting applications where only the number of cells in a sample is of interest.

### 2.5.3 Case study 3 : CMOS capacitive sensor for viability and proliferation monitoring

As was discussed earlier, label-free capacitive sensors are one of the most efficient alternatives for cell viability monitoring. In this regards Prakash *et al.* developed a CMOS capacitive sensor for cell viability and proliferation monitoring [32, 57]. In this platform, the working principle is based on measuring the changes in capacitive coupling between the sensing electrodes and cultured cells resulted from the adhesion of cells. As mentioned in this paper, when cells are placed in low frequency electric fields, the ionic cloud surrounding the cells membrane is polarized giving rise to electric dipoles. For healthier cells, the value of this

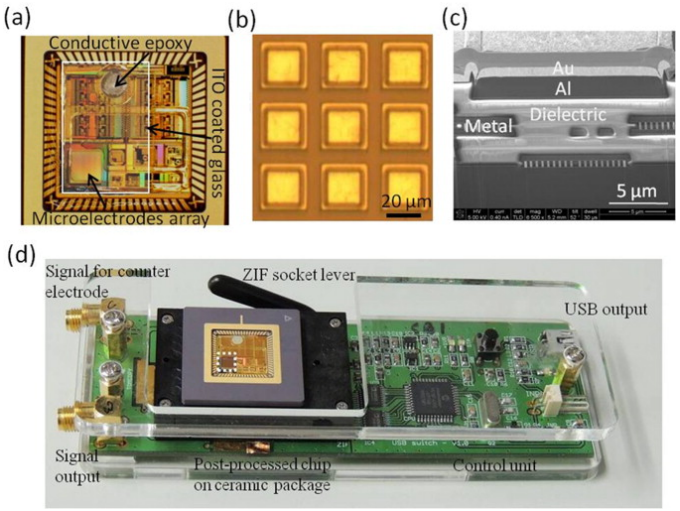


Figure 2.9: Electrical-impedance spectroscopy (EIS) platform for tumor cell counting. (a) micro-photograph of the fabricated chip.(b) Image of post-processed micro-electrode. (c) SEM micrograph of microelectrode with 6 stacks of metal layers. (d) CMOS chip in a PGA carrier mounted on the PCB [56].

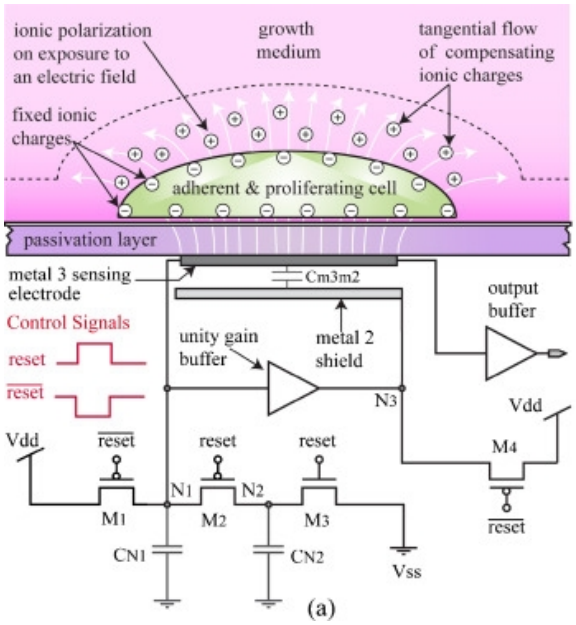


Figure 2.10: CMOS cell-based biosensor for cell viability and proliferation monitoring [57].

capacitance is higher [10]. The capacitance measurement is based on the charge sharing principle. The sensor chip is mounted on a DIP40 ceramic package and encapsulated using biocompatible polymer. A typical well (diameter = 1.5 cm, height = 0.5 cm) is attached on top of the packaged chip for containing the cell culture medium. The platform is used for on-line tracking of human MDA-MB-231 breast cancer cell proliferation, with a sensor chip

that is fabricated in a 0.5 $\mu m$ CMOS technology. During the cell adhesion and forthcoming proliferation the sensor recorded capacitance variations in a range of a few fF.

Despite the other presented LoC devices, this platform is fully integrated employing CMOS technology and thanks to its high sensitivity, it is a good example of a continuous measurement setup for cell proliferation monitoring. The work can be further optimized by increasing the array size and adding microfluidics for high throughput measurements.

### 2.5.4 Case study 4 : Label-free monitoring of cell-based assays : Combining impedance analysis with SPR for multiparametric cell profiling

In another effort in [58], a two-parameter cell-based sensor is developed monitoring the electrical and optical changes in cell sample, simultaneously. The dual sensor platform is implemented by integrating both techniques, ECIS and SPR, on a single sensor chip. The proposed system is based on the commercially available SPR substrate with high refractive index glass slides that is covered with a gold layer on top. The gold layer is structured by standard photolithography and wet etching (Figure 2.11). After realizing electrodes on the SPR chip, a biocompatible flow chamber is glued on the top which is made of PDMS with the fluid volume of approximately 500 $\mu m$. The sensor surface features two addressable circular working electrodes and one shared large counter electrodes which used for SPR measurement as well. The SPR measurements are performed with an off-chip device and the impedance measurements are conducted via a commercially available impedance analyzer. In described work, the proof of concept experiments are mostly focused on MDCK II (Madin-Darby canine kidney, strain II) cell attachment and spreading as well as cytotoxicity monitoring of actin cytoskeleton disrupting drug [58].

The combination of SPR with ECIS technique is a powerful tool to obtain complementary parameters from a cell sample while requiring no reagent preparation and labelling process.

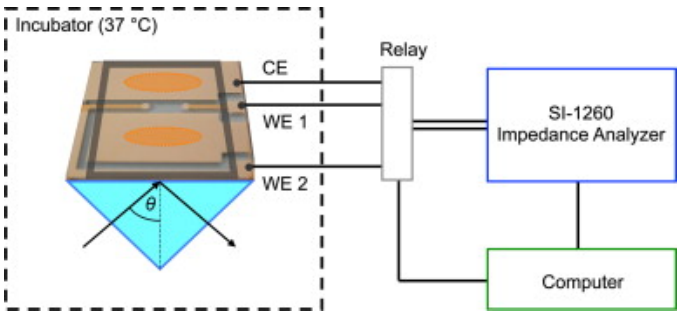


Figure 2.11: Simultaneous SPR and ECIS measurements setup. [58].

However the proposed device has a very low spatial resolution and in order to analzye a larger population of the cells, multi-electrode array is required. In addition the size of working electrode is around 1 mm which compared to the cell size (10-20 $\mu m$) is large, thus the offset impedance caused by the electrode itself can decrease the sensor sensitivity, specially when monitoring low cell concentrations.

### 2.5.5 Case study 5 : An integrated label-free cell-based biosensor for simultaneously monitoring of cellular physiology multiparameter in vitro

In [59] a cell-based biosensor is proposed in which the LAPS and ECIS sensors are fabricated on a single silicon wafer. The schematic of sensor chip and its fabrication process are shown in Figure 2.12. To fabricate LAPS and ECIS, an n-type silicon wafer is used which is insulated with $SiO_2$ and $Si_3N4$ through low pressure chemical vapor deposition (LPCVD) process. In order to form the LAPS regions, the $SiO_2$ and $Si_3N4$ are partially etched following a photolitography process. ECIS electrodes are patterned on a gold layer through etching process.

The sensor chip consists of three parts : culture chamber , LED system for LAPS detection, and ECIS/LAPS sensor (Figure 2.12). The input and output ports of of LAPS and ECIS are connected to a PCB for control and readout. The AC signal generator and the detection module is shared between two sensors including potentiostat, lock-in amplifier and ADC. To validate the system performance, neonatal SD rat cells were used for growth monitoring. ECIS measurement results show a significant increase in the impedance of the electrode with cells compared to ones without cells. LAPS was used for pH monitoring and to measure extracellular acidification rate. the acidic wastes in the extracellular environment, resulted in a pH drop. A cytotoxicity test is also performed in which the addition of an anti-cancer drug resulted in a decrease in the impedance values and extracellular acidification rate.

The major limitation of this work is the use of lock in amplifier and potentiostate which makes the system complicated and bulky [60]. In addition, the impedance of LAPS chip is high resulting in a decreased sensitivity in the LAPS device.

## 2.6 Conclusion

In all aforementioned research work using CMOS for monitoring cellular activities in particular cytotoxicity monitoring and drug screening, the researchers aim to develop a fully automated high throughput CMOS system or so called smart Petri-dish. Despite great efforts, smart Petri-dish technology is in early stage of development and there are several challenges

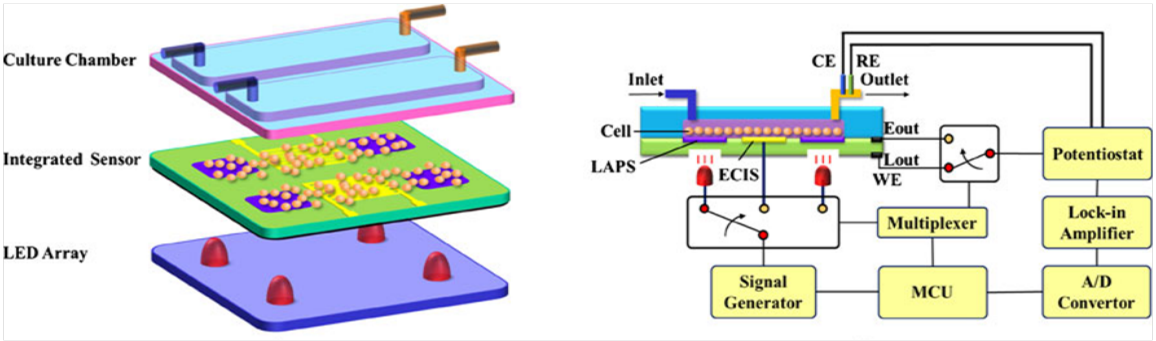


(a)

Figure 2.12: Schematic of integrated sensor including the LAPS and ECIS [59].

that should be investigated. Among various techniques that was discussed, impedometric and capacitive sensors show a better potential for high throughput cell-based platforms. This is mainly because of their ease of implementation and the possibility to integrate sensors and readout interfaces in one single chip. A brief comparison of reviewed sensing schemes is made in Table 2.2. Due to the superior performance of capacitive sensors in terms of miniaturization, scalability, sensitivity and hardware complexity, they can be very efficient in performing cell-based experiments. In next chapter we will review the principle operation of capacitive

Table 2.2: Comparison of different cell-based sensing schemes

| Sensor type | Off-chip optics | Ref. Electrode | Need for post-processing | Integrated sensor/readout | CMOS compatibility | High throughput |
|---|---|---|---|---|---|---|
| LAPS | YES | YES | YES | NO | NO | NO |
| ISFET | NO | YES | NO | YES | YES | YES |
| QCM | NO | NO | YES | NO | NO | NO |
| SPR | YES | NO | YES | NO | NO | NO |
| ECIS | NO | YES | YES | YES | YES | YES |
| **Capacitive** | NO | NO | NO | YES | YES | YES |

sensors in more details and we will discuss about various types of sensing electrodes and readout circuit implementation.

# CHAPTER 3 PROCESS FOR THE RESEARCH PROJECT AS A WHOLE AND GENERAL ORGANIZATION OF THE DOCUMENT INDICATING THE COHERENCE OF THE ARTICLES IN RELATION TO THE RESEARCH GOALS

In last two chapters we discussed the current challenges in cell assays and we also reviewed some of the state-of-the art of cell-based biosensors. Among various techniques that are employed to implement cell based assays, capacitive and impedometric techniques have shown a great potential for high throughput instrumentation. Despite the great advancement in the field of biosensors still the design and fabrication of a fully integrated biosensor is challenging. In this thesis we aim to address these challenges by proposing a fully integrated capacitive sensor array that can be used as a means for quantitative cell-substrate interaction studies.

This thesis is based on three journal articles. In first article the implementation of a capacitive sensor working based on charge based capacitive measurement is presented. The proposed design is extended into an array of capacitive sensors and the second article includes the implementation of this capacitive sensor array as well as biological and chemical characterisations. Article 3 focuses on proposing a novel bio functionalization technique as well as a rapid prototyping method for microfluidic packaging of the CMOS chips. In this article we also propose a new solution for cytotoxicity monitoring of drug candidates.

In addition to the introduction and literature review chapters, six other chapters are forming the presented thesis.

In chapter 4 we describe the fundamentals of capacitive sensing as well as common techniques adapted for capacitive electrode fabrication and data acquisition platforms.

We focus in chapter 5 on the design and implementation of a first proof of concept smart Petri dish device including an integrated capacitive sensor based on charge measurement. Electrical characterizations and chemical test results are presented in this chapter.

In chapter 6 the implementation of proposed capacitive sensors as an 8x8 sensor array is discussed and characterization results using organic solvents, polystyrene beads, and living cell samples are presented.

In chapter 7 the achieved chip is further optimized for cell concentration and cytotoxicity monitoring. Moreover, a new technique based on polyelectrolyte multilayers (PEMs) deposition is proposed to enhance the cell-electrode adhesion. A low-complexity microwell array is proposed that is integrated with the proposed smart Petri dish to allow high throughput

screening of cell samples.

Chapter 8 provides general discussions. Final conclusion, summary of thesis contributions, and recommendations for future work are outlined in chapter 9.

# CHAPTER 4 CAPACITIVE SENSING : DESIGN AND IMPLEMENTATION

## 4.1 Capacitive sensors operation principle

A simple yet convenient configuration of a capacitive sensor is made of two parallel plates separated by a certain distance (d) with a non-conducting medium which is known as dielectric, and overlapping area of A (Figure 4.1).

The capacitance value is determined by

$$C = \frac{\epsilon_0 \epsilon_r A}{d} \tag{4.1}$$

where $\epsilon_0$ is the vacuum permittivity and $\epsilon_r$ is the relative permittivity of the material in-between the capacitor's plates. When two plates of capacitor have a voltage difference ($\Delta V$), the equal and opposite amount of charge (Q) will be accumulated on two plates which its value is calculated by

$$Q = C\Delta V \tag{4.2}$$

If more than one material is placed between the electrodes, an effective value of $\epsilon_r$ should be used which depends on the permittivity of each individual material and its volume. For example, if only two materials are present between the plates, they can be considered as a series combination of two capacitors and the effective value of $\epsilon_r$ is determined by :

$$\frac{1}{\epsilon_{eff}} = \frac{vol_1}{\epsilon_1 vol_{tot}} + \frac{vol_2}{\epsilon_2 vol_{tot}} \tag{4.3}$$

where $\epsilon_1$ and $\epsilon_2$ are the relative permittivity of the material 1 and material 2, respectively, $vol_1$ and $vol_2$ represent their volumes, and $vol_{tot}$ is the total volume of dielectric material between the plates. This equation can be further extended when there are more than two materials between the capacitor's plates. From Eq. (4.1) it is clear that the changes in capacitance value can be initiated by three ways : 1) the changes in the two plates distance (e.g. pressure sensors), 2) changes in the permittivity of the material between the plates (e.g. humidity sensors), and 3) changes in the overlapping area of the capacitance plates (e.g. displacement sensors). Based on the application, changes in any of these three parameters leads to capacitance variation. Herein we mostly focus on the fixed plate planar capacitive sensors that operate mainly based on the dielectric changes of materials in proximity of the

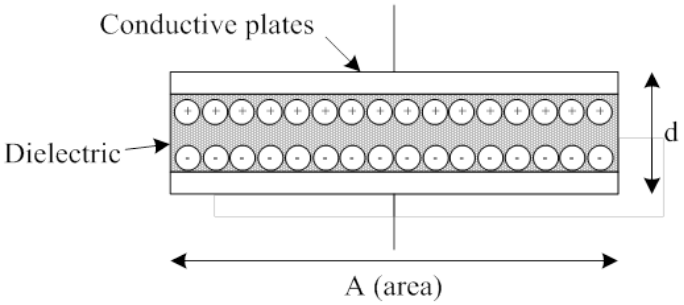


Figure 4.1: Basic parallel plate capacitor structure.

sensor.

## 4.2 Capacitive sensing electrodes : fabrication and post-processing

The sensing electrodes of a capacitive sensor can be fabricated into various forms and structures. The shape and dimension of electrodes are very important in the overall performance of the capacitive sensor. Different types of sensing electrodes, such as cylindrical rods, rectangular plates, helixical wires, and tubular shaped capacitors exist which are usually used as discrete devices and are not suitable for array implementation. Among various implementations, the use of of interdigitated electrodes (IDEs) in biosensor systems has shown promising features in terms of low ohmic drop, increased signal to noise ratio, fast establishment of steady state, and high sensitivity [61]. Moreover, the IDEs eliminate the need for a reference electrodes which facilitates the implementation and integration of these electrodes in a limited chip area.

IDEs consist of two separate interlocking metal arranged in a comb-like structure. Two important parameter in the design of IDEs are fingers width and fingers spacing. Normally, choosing the smaller finger spacing results in a higher detection sensitivity. For cell detection application usually the finger width and spacing in the range of several micrometers is effective, however for molecular applications, such as DNA detection, sub-micron dimensions is required [62]. For this reason, the proper sizing and optimization of IDEs is necessary for high sensitivity cellular/molecular applications. Herein we focus on the integrated design of IDEs in CMOS technology. Several techniques for implementation of sensing electrodes on CMOS chip have been reported so far and we will briefly review some of the existing techniques for chemical and biological applications.

### 4.2.1 Electrode fabrication in standard CMOS technology

The capacitive sensing electrodes, fabricated on top of a CMOS chip play the important role of interfacing between readout circuitry and test solution. Although the CMOS process has several advantages such as possibility to integrate the readout circuitry and sensing electrode and substantial increase in the electrodes density, it suffers from a main drawback which is the use of aluminum alloys as the metal layers. The metal layers in CMOS process are basically made of aluminum as well as some silicon impurities (e.g. 0.18 $\mu m$ CMOS, Al with 1% silicon) [63].

In order to make a direct contact with analyte solutions, the passivation layer in CMOS technology can be removed in foundry using etching techniques. After passivation removal, the topmost metal layer in the technology can be used as a sensing membrane (Figure 4.2). Due to its limited stability and poor biocompatibility, the aluminum electrodes are not suitable for biological and chemical applications [64]. Considering mentioned disadvantages, the use of aluminum as the sensing layer can be challenging due to its poor stability and fast corrosion.

To overcome these limits, Prakash *et al.* employed the CMOS chip passivation layer to monitor the cancer cell proliferation rate [57], however due to the high parasitic capacitance introduced by passivation layer, the sensitivity decreases in this method. Moreover, for applications where the immobilization of specific bio-particles is required, the use of passivation layer is not very practical. Ghafarzadeh *et al.* removed the passivation layers between the electrodes to increase the sensitivity for bacteria growth application [65]. In another effort in [66] an $Al_2O_3$ layer was deposited on the aluminum electrodes for a better stability and improved biocompatibility for single bacteria detection. The application of $Al_2O_3$ covered electrodes has been shown for biosensing purposes such as DNA detection [67], bacteria growth monitoring [66] and relative humidity measurement [68]. Some works also showed the use of $SiO_2$ insulating layer on the aluminum electrodes which can be functionalized for molecular and cellular detection [69]. However, the use of this protective layer requires a careful etching of $Si_3N_4$ layer while keeping the $SiO_2$ unchanged. In the remaining of this section we review some of the well-known approaches for CMOS-based electrode fabrication.

### 4.2.2 Gold electrode fabrication by CMOS post-processing techniques

In some applications, especially those who deal with chemical and physiological solutions, a durable and inert electrode should be adapted. Among different materials available for electrode implementation, gold is proven to be a suitable choice due to its bio-compatibility and inertness. Furthermore, as a result of its surface properties, self-assemble monolayers can be

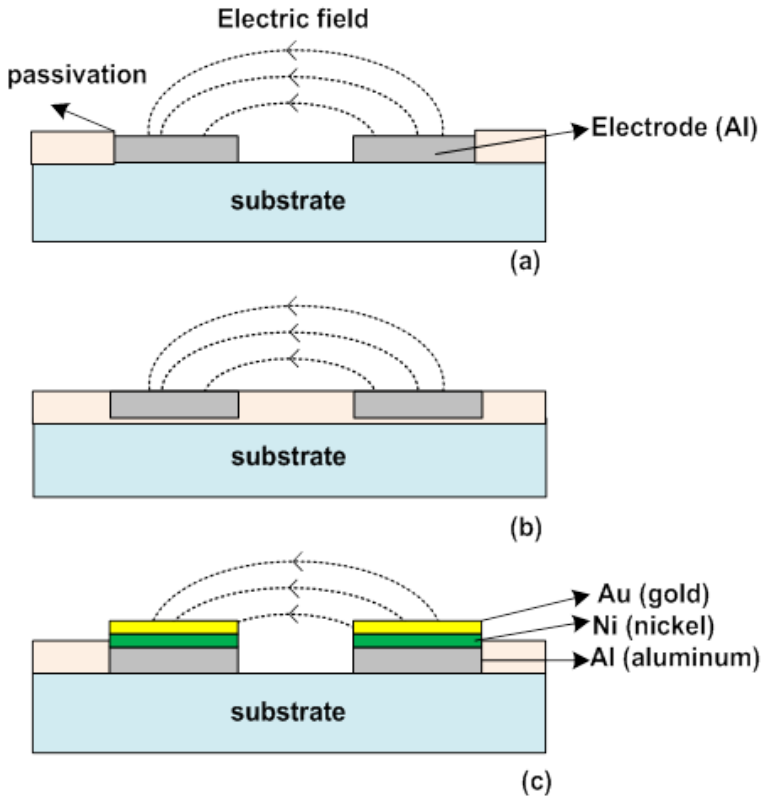


Figure 4.2: Sensing electrodes implemented using standard CMOS process. (a) Topmost metal layer with removed passivation. (b) Passivated topmost metal layer. (c) Top most metal layer with gold deposition as a biocompatible and stable material.

formed on the surface of gold which work as a linker between gold electrodes and recognition elements (probe molecules) [70]. To deposit gold on aluminum electrodes several techniques have been reported including evaporation/sputtering [71], and electroless deposition [72]. Herein we briefly review these two techniques.

### Photolithographic deposition

In this method the gold deposition is done using standard photolithography steps. Initially, samples are spin coated with a negative or positive photo-resist material as a sacrificial layer, and then they are exposed to UV light to define the electrode positions where gold should be deposited. This step is done using a mask aligner and the mask is typically a glass plate with patterned opaque layers ; for lower resolutions and large pattern shapes simple transparent sheets may be used as a mask to reduce the process costs and complexity. Depending on the photo-resist type and whether it is negative or positive, the exposed/ non-exposed areas are

removed by chemical resist development procedure. In next step, by using thermal or e-beam evaporation a thin layer of Nickel (Ni) or Chromium (Cr) is deposited to enhance the gold adhesion. Thereafter using e-beam or sputtering machines gold layer is deposited on top of the electrodes. At the end, the excess gold on unwanted area is removed by chemical lift-off process [73].

**Electroless deposition**

The electroless deposition is one the most convenient methods for metal deposition since it requires no photolithography process and mask design. This type of coating has been widely used in variety of applications including flip-chip bonding of CMOS chips on PCB boards and protective coating [74]. Although gold can be deposited on several materials such as Ni, Pd, Pt and Cu [75], for deposition on aluminum, it is mandatory to use inter-layers such as Ni and Zn. Therefore this technique is usually know as electroless nickel immersion gold deposition process (ENIG). In this technique the CMOS chip is first completely cleaned and rinsed using acetone, methanol, isopropanol, and deionized water. The next step is alkanline double zincation in which Al ions are replaced by Zn ions by placing the samples in a Zn-plating solution. In third step the chip is immersed in a Ni plating solution in which Zn layer is replaced by Ni later. In the final step, by immersing in gold, the gold atoms will adhere to the nickel plated areas.

As an alternative to the described standard process, in [76] a method is proposed for gold deposition without using any inter-layer materials. In this method gold deposition is performed following two steps : initially aluminum surface treatment is done by galvanic displacing in atomex solution (a commercial solution) which produces a gold seed layer and prepared the surface for electroless deposition process. In next step, the electroless deposition is done in the Catagold 2A solution. Since this method can be done by using a small droplet of electroless solution on the packages chip it would be very practical in biosensor applications where reproducible and clean electrode surfaces is required.

### 4.2.3 Platinum electrode fabrication by CMOS post-processing techniques

Platinum is a metal which is widely used as electrode material in biomedical applications due to its unique chemical, physical and mechanical properties. Similar to gold, it is inert and does not corrode in biological solutions. The platinum deposition techniques follow the same steps as gold and it usually involves the photolithography techniques for platinum deposition patterning, the use of titanium/tungsten layers as an adhesion layer, and diffusion barrier between aluminum and platinum.

### 4.2.4 MEMS electrode fabricated in standard CMOS technology

Microelectromechanical systems (MEMS) are widely applied for various physical/mechanical application. One of the most common applications of MEMS capacitive sensors is pressure sensing which is realized by measuring the amount of membrane displacement. Among different fabrication methods, the monolithic integration of MEMS structures with CMOS sensing circuitries results in a noticeable reduction in parasitic elements and an increased signal-to-noise ratio. The MEMS membrane which can be fabricated on a CMOS chip with no lithography or film deposition steps is usually consists of a deformable loading membrane and one stationary sensing electrode (Figure 4.3). A polymer layer, such as PDMS, is also used between two plates which controls the stiffness of the tactile sensor [77]. The implementation of these electrodes can be done via etching of layers between two metal layers of CMOS technology to form top and bottom electrodes. Unlike CMOS electrodes, the passivation layer in this method is usually remains of top of the membrane for protection and electrical insulation of layers [78].

## 4.3 Design and modelling of the capacitive electrodes for cell monitoring

In order to properly design the electrodes for cell detection, it is important to study the dielectric changes caused by the living cells in details. This helps to obtain a proper estimation of capacitance changes and required sensitivity and capacitance detection limit thus designing the appropriate electrode dimensions. It is proven that all living cells have some positive or negative charges in the membrane (based on the cell type). When the cells are placed on a metal sensing electrode and are exposed to low frequency electrical fields, this charge becomes polarized, creating an electric dipole surrounding the cell membrane. This phenomena leads to creation of a insulation layer above the electrodes and a dielectric change in their surrounding media (Figure 4.4). Although these changes are very small, by using a very high sensitivity and accurate readout interface, the minute capacitance changes can be converted into a readable electronic signal. The quality and quantity of these changes depend on the cell morphology and their health state. By continuously measuring these minute changes, quantitative data about the number of cells, their viability and growth rate as well as their interactions with the substrate can be obtained. The most important concern in the design of capacitive electrodes is the optimal arrangement and configuration of sensors in a limited design space and constrained mask resolution while reaching the optimum sensitivity. To study the effect of living cells on capacitive electrodes, the electrode and cell modeling as well as numerical simulations can be done using multiphysics software such as COMSOL package. As well as allowing geometry definitions, the software helps to see the end results

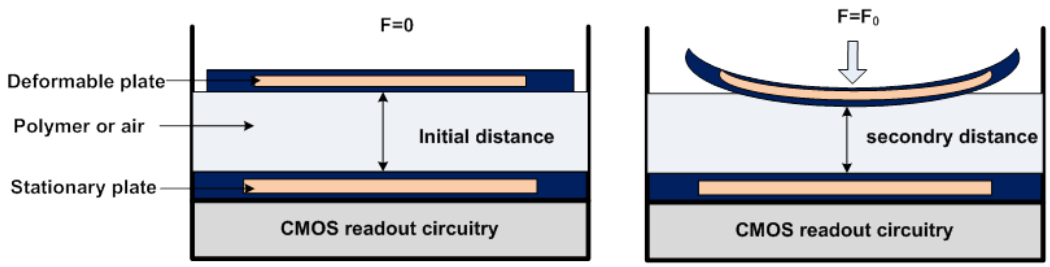


Figure 4.3: CMOS-MEMS capacitive sensor with deformable and polymer-filled membrane.

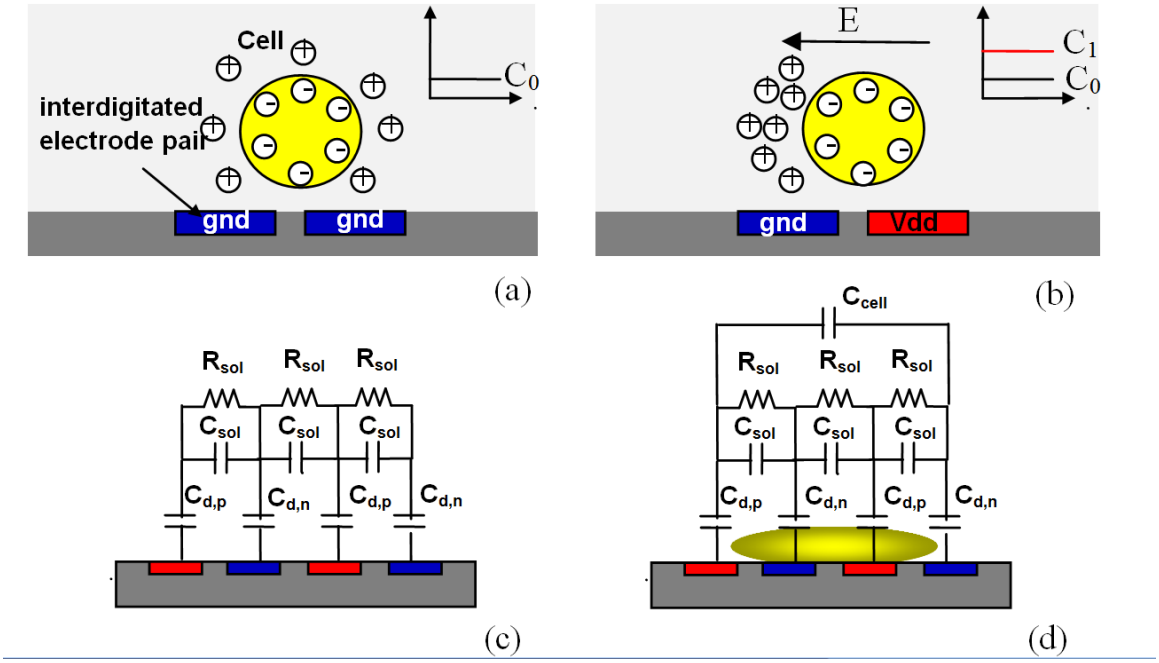


Figure 4.4: Cell-electrode interface (a) T=0 , no voltage applied to the sensing electrodes,( b) T=T1 , voltage applied to the electrodes, (c) Electrode-electrolyte equivalent circuit model when there is no cells, (d) Electrode –electrolyte model in the presence of cells.

to find the best dimensions and capacitance values for the desired application.

## 4.4 Surface modification techniques for capacitive electrodes

As was discussed earlier, in capacitive and impedometric biosensors, the adherence of the cells on the electrodes and formation of extra-cellular matrix have a great impact on sensor's performance. In order to enhance the coupling between the cells and the sensors, complementary surface modifications techniques are required. In micro-fabricated biosensors such as MEA, FET, LAPS, and patch clamps, the sensing unit is usually made of glass or silicon.

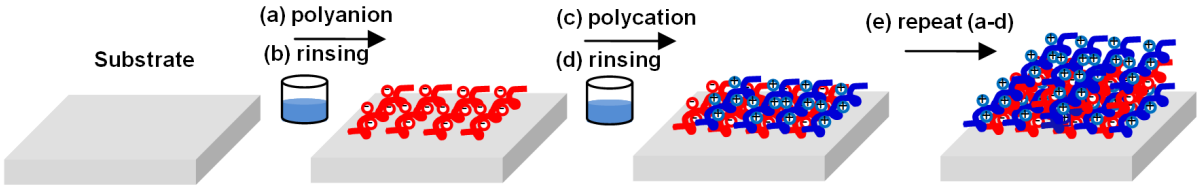


Figure 4.5: Schematic diagram of layer-by-layer deposition of polyelectrolyte multilayers [79].

For these types of membranes, several chemical coating techniques exist that use peptides or ECM components which can greatly improve cell-sensor adhesion. In this regard, several ECM components such as polylysine, laminin, fibronectin, and collagen are used which can notably improve the growth of cells on the sensing sites. Although these techniques are applied in various types of biosensors, employing them in capacitive sensors requires several factors to be considered such as physical properties of coating material that includes the thickness, roughness, and stability of the material. On the other hand, the chemical and electrical properties of these layers can drastically change the sensor performance and deteriorate the signal to noise performance. Additionally, it is very difficult to control the thickness of deposited layers, which results in a decreased sensitivity.

Among many electrode coating techniques, layer by layer (LBL) deposition of complementary polyelectrolyte membranes (PEMs) has been recognized as an efficient technique with precisely controlled thickness. In this technique, the self-assembly of PEMs occurs on sensor substrates through consecutive exposures of a substrate to polycation and polyanion solutions, followed by rinsing steps to remove unadsorbed polymers through deposition steps (Figure 4.5). The first polyelectrolyte layer is chosen to have the opposite charge of the substrate, resulting in a strong electrostatic interaction. Polyelectrolytes of opposite charges are subsequently deposited in an alternate fashion with water or buffer solution rinses between each layer [80]. Since this method is based on electrostatic forces it provides a very stable and durable coating. Moreover, the thickness of the layers can be precisely controlled with nanometer accuracy. Although this method has been applied in various types of substrates in biosensor applications but it is not employed in CMOS-based aluminium electrodes. In chapter 6 of this thesis we will propose a novel method based on the PEM deposition for surface modification of CMOS capacitive sensors.

## 4.5 Capacitive readout interfaces

So far, different methods have been reported to deal with the conversion of measured capacitance values to readable voltage outputs which some of them allow the detection of minute capacitance changes with a very high sensitivity. Herein we briefly review some of the most popular and efficient capacitive readout interfaces.

### 4.5.1 AC-bridge

AC-bridge is a classic configuration for measuring small changes in capacitive electrodes. The basic of operation is similar to the resistive wheatstone bridge where any changes in the impedance results in an imbalance in the bridge which appears as a current change at the output. In capacitive configuration, a bridge consisting of the sensing and reference capacitors is made which is driven by AC signals. Depending on the single-ended or differential configuration of sensors ; half-bridge or full-bridge structures are formed. An example of half-bridge readout interface is shown in Figure 4.6. The output voltage amplitude is proportional to the capacitance changes [81, 82].

$$V_{out} = AV_{in}\frac{\Delta C}{2C_{sens} + C_P} \tag{4.4}$$

where $\Delta C$ is the capacitance variation, $C_P$ is parasitic capacitance, A is amplifier gain, and $V_{in}$ is the input voltage amplitude. The sensitivity and minimum detectable capacitance value is limited by the parasitic capacitances that exist at the input nodes of amplifier. By using the differential full bridge, the effect of these parasitic can be partially mitigated.

Despite its simple structure, the drawback of this circuit is its sensitivity to interference and noise. Another potential problem arises from the stray capcacitances at the circuit nodes which results in a current path to the ground and can imbalance the circuit. Due to these limitations, this circuit not suitable for applications when very small capacitance changes needs to be detected.

### 4.5.2 Switched capacitors

Switched capacitors are the most common circuits for capacitive electrode interfaces. In [83] a differential switched capacitor circuit is proposed for capacitive gas detection in which the difference between sensing an reference capacitors in applied to the inputs of a second order switched capacitor circuit. Figure 4.7 shows a simplified block diagram of a differential switched capacitor interface which operates as a $2^{nd}$ order $\Sigma\Delta$ modulator. The circuit detects

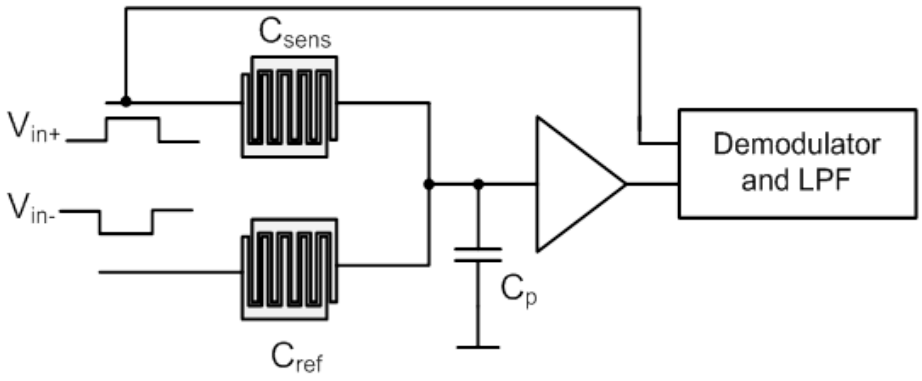


Figure 4.6: Simplified diagram of half-bridge capacitive sensor.

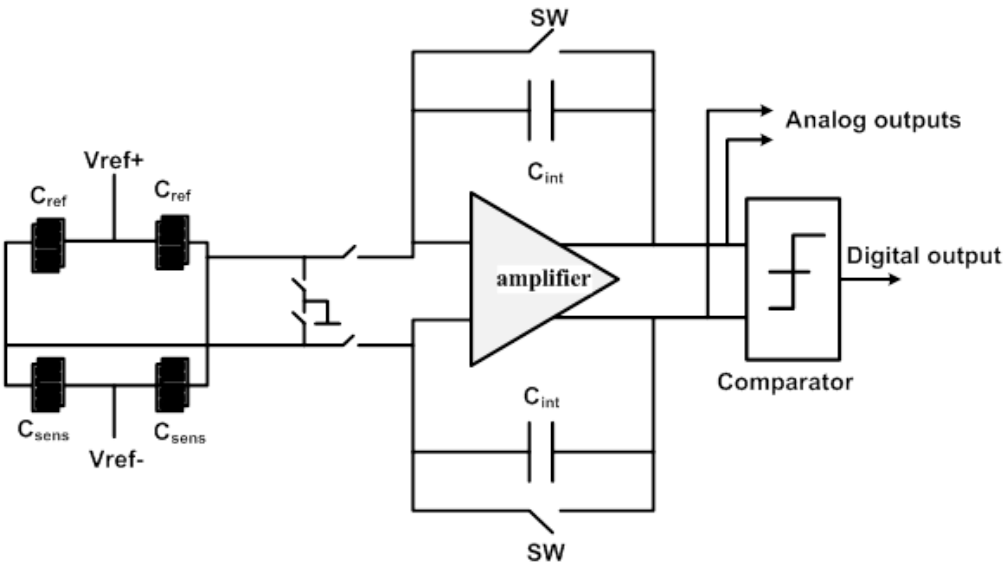


Figure 4.7: Simplified block diagram of a switched capacitor circuit.

the sensor capacitance changes and produces an output voltage proportional to these changes. The differential mode readout allows the switching error reduction and noise cancellation, and reduces the effect of parasitic capacitances effectively [84]. The advantage of switch capacitor readout is the temperature insensitivity of the capacitors compared to resistors. However switched capacitors suffer from speed limitation and also the need for non-overlapping clocks. In addition, the charge injection of the MOS switches and clock feed-through, result in gain error, offset and distortion. Certain circuit techniques such as correlated double sampling can be employed to reduce the effect of these non-idealities [85].

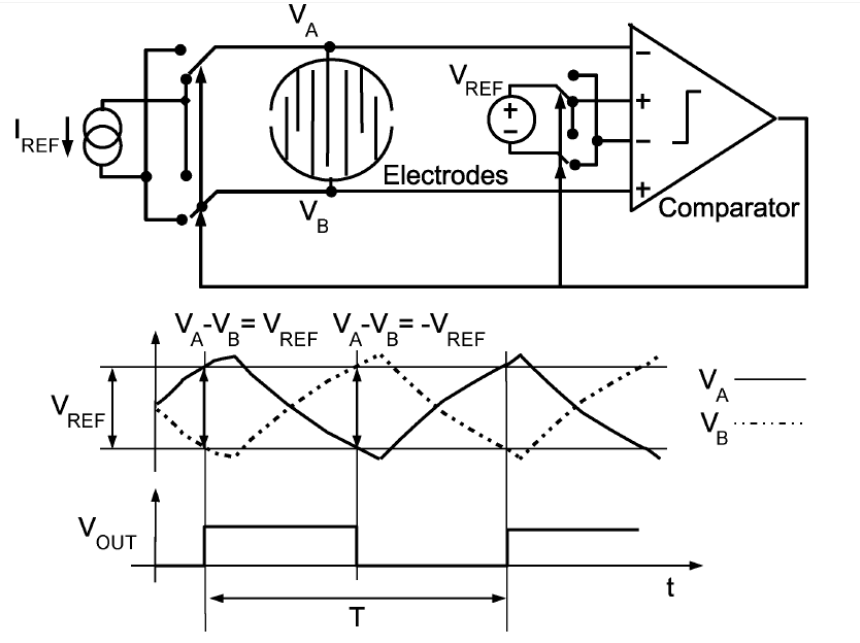


Figure 4.8: The capacitance to frequency converter : the comparator produces a digital bit stream whose frequency is inversely proportional to sensed capacitance [31].

### 4.5.3 Capacitance to frequency converter

Another common technique for measuring capacitance changes is the conversion of capacitance value to the frequency. In this circuits, a self-oscillating readout circuit is employed that produces digital bit streams with the frequency proportional to the capacitance changes (see Figure 4.8). As an example, in [31] a capacitance to frequency converter is proposed for DNA hybridization detection. As shown in Figure 4.8 the electrodes are excited with a periodic current ($I_{REF}$). The time constant of transient waveform generated at the electrode outputs is dominated by the capacitive component of the electrodes. The output voltage is compared with two reference voltages ($V_{REF+}$ and $V_{REF-}$) and the results form a digital bit-stream at the comparator's output. The frequency of this bit-stream is proportional to the rate of change in electrodes voltage and hence the capacitance value. The frequency of comparator's output is determined as

$$\frac{1}{f} = 2RCln\frac{1}{1-\frac{V_{REF}}{I_{REF}R}} \tag{4.5}$$

where R and C are electrode-electrolyte interface resistance and capacitance, respectively. The important advantage of this readout interface is the elimination of ADC converter. In fact, the frequency value is easily measured by counting the number of reference crossings at certain time intervals. This method is used extensively in various applications such as

measuring single bacteria detection [86] and displacement sensing [87].

### 4.5.4 Capacitance to pulse width converter

Figure 4.9 shows a capacitance to pulse-width converter topology with the pulse width directly proportional to the sensing electrode capacitance [69]. In this work an 5x5 array of CMOS-based capacitive sensor is fabricated for neurotransmitter dopamine detection. The readout interface produces a digital bitstream with the pulse width proportional to the dopamine concentration. The electrode-electrolyte capacitor is charged with a fixed DC current and the resulted voltage which is a ramp with positive slope is compared with a reference voltage in the comparator block. When the voltage reaches the switching voltage of the comparator, the output gets high and a pulse is generated which consequently turns-on the reset switch and discharges the sensing electrode. The important advantage of this type of readout interface is that it does not require any additional analog to digital conversion, resulting in a smaller sensor footprint. However, the offset resulting from the initial sensing electrode capacitor can reduce the detection limit and resolution.

### 4.5.5 Charge sharing capacitive sensor

Charge-sharing circuits are another type of capacitive interfaces which provide a linear high-sensitive dependence between the output voltage and the input capacitance [66] and depending on the switching frequency they can be applied in various applications. A good example of charge-sharing circuit is proposed in [57] for cell proliferation monitoring application. As shown in Figure 4.10, the circuit has two nodes N1 and N2 with stray capacitances CN1 and CN2. Three switches (M1-M3) are used to control the charging and discharging of these capacitors in reset and evaluation phase. The output voltage (VN) which is the function of input capacitor is described by

$$VN = \frac{(CN1 + C_{sensed}).V_{DD} + CN2.V_{SS}}{CN1 + CN2 + C_{sensed}} \tag{4.6}$$

where $C_{sensed}$ refers to the effective capacitance value seen by sensing electrodes. By minimizing the nodal parasitic capacitances, the dynamic range and the sensitivity of the circuit can be improved. To shield the capacitive coupling between the sensing metal (Metal 3) and substrate, a larger area metal plate (Metal 2) in the lower layer is used.

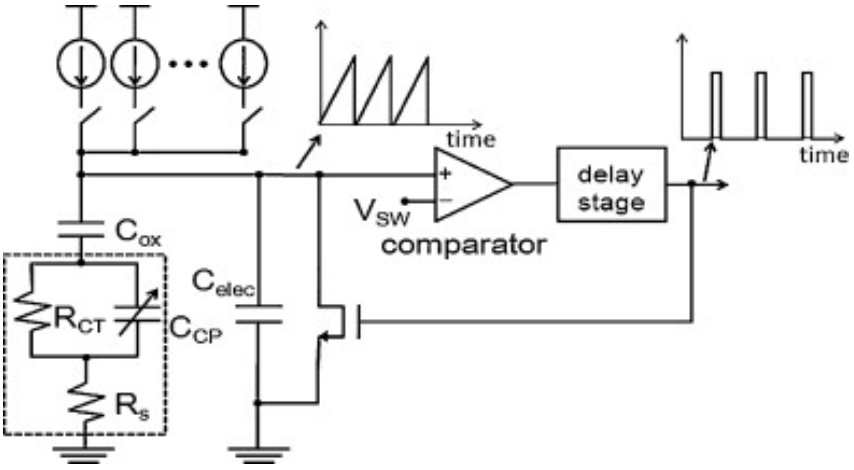


Figure 4.9: Capacitance to pulse-width converter for neurotransmitter dopamine detection.

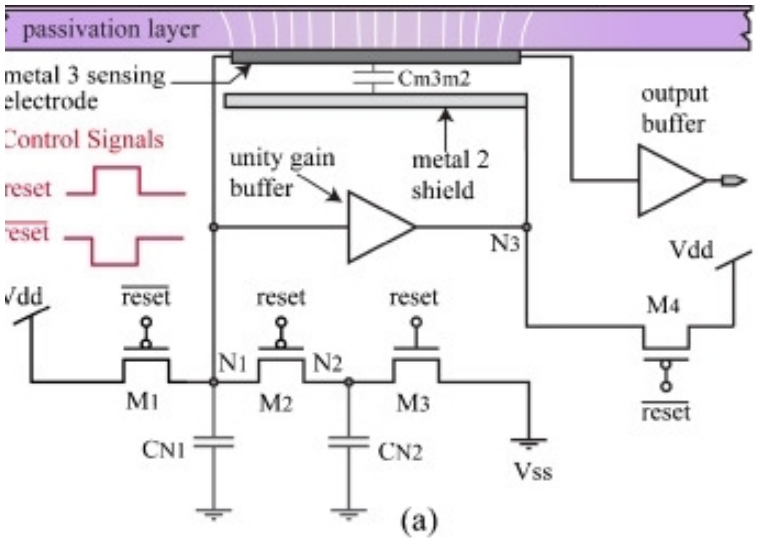


Figure 4.10: Capacitance readout based on charge-sharing principle.

### 4.5.6 Charge-based capacitive measurement

The Charge based capacitive measurement (CBCM) was first proposed by Sylvester *et al.* [88] for measuring the parasitic interconnect capacitance with a very high sensitivity and accuracy. In contrast to the other capacitive readout approaches, the CBCM does not require signal conditioning modules thus offering the minimal on-chip footprint. This features leads to potential use of the CBCM-based capacitive sensor in high throughput applications where multiple sensing sites with the minimum on-chip area is required. The basic structure consists of two transistors (Figure 4.11) in which the sensing capacitor is connected in between the drains of PMOS and NMOS pairs. The sensing capacitor is charged and discharged by two

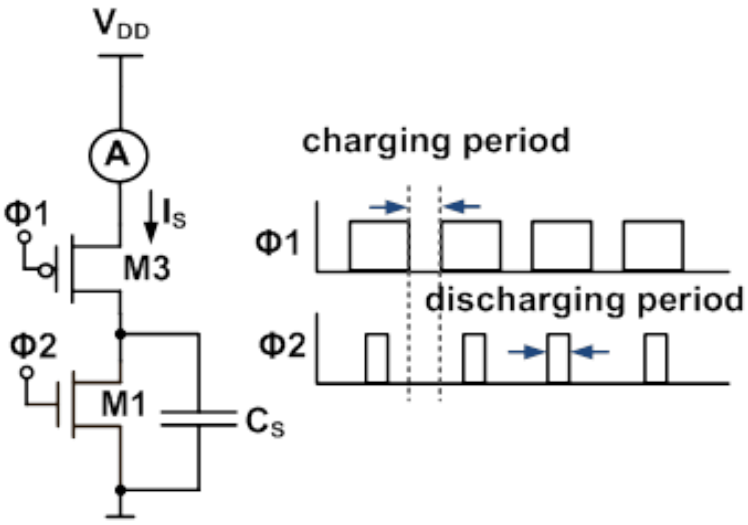


Figure 4.11: Charge based capacitive sensor structure.

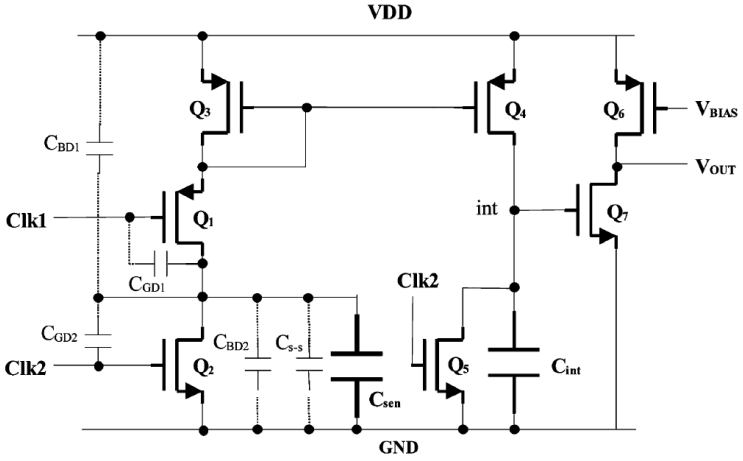


Figure 4.12: Charge based capacitive sensor for particle detection [89].

transistors during $\Phi_1$ and $\Phi 2$ clock periods. The current that is required to charge the sensing capacitor can be measured using an external ammeter and is obtained as

$$I_S = C_s \frac{dv}{dt} = C_S V_{DD} f \tag{4.7}$$

where f is the frequency of $\Phi_1$ and $\Phi_2$ clocks. This circuit was first proposed to characterize interconnect capacitances and accurately estimate their effect on the circuit speed and noise performance. Later Evans *et al.* developed the design for detecting the particles in oil and replaced the off-chip ammeter with CMOS transistors working as current mirrors while

reaching the sensitivity of 42 mv/fF [89] (Figure 4.12). Ghafarzadeh *et al.* further extended the design by improving the sensitivity (reaching to 200 mv/fF) and employing it for bacteria growth monitoring applications [65]. In this platform, microfluidic channels were also implemented on-chip for directing the chemicals and biological solutions to the electrodes.

Despite its simplicity, the circuit can be optimized to reach unprecedented levels of accuracy in atto-farad ranges. In next chapter we will present a novel fully differential circuit based on the CBCM structure for biosensor applications. More details about circuit performance and optimizations will be discussed as well.

## 4.6 Conclusion

In this section we discussed various design aspects of capacitive sensors including the sensing electrode implementation, cell-electrode interface and capacitive readout circuits. There are several advantages in using capacitive biosensors compared to their other integrated counterparts which is discussed as follows.

- By employing advanced microfabrication technologies, a large array of sensors can be easily fabricated on a single chip providing parallel and high throughput measurements.
- The electrical measurement techniques are usually non-invasive and more compatible with the cell natural state. This means that there is no need to extra processing and sample preparation steps and the cells can be analyzed as they naturally are.
- The provided results by the capacitive sensors are quantitative and the readout data which is usually a current or voltage can be easily translated to meaningful biological data.
- The integration of signal amplifiers and analog to digital converter blocks on close proximity of sensing sites allows very accurate and noise-free measurements.
- All measurements are performed in real-time mode, eliminating the need for any sample preparation steps while notably decreasing the labor work and processing time.

Due to the above facts, the cell-based capacitive have been widely applied in many fields such as cellular physiological analysis, medical diagnosis and pharmaceutical applications. Despite their excellent features, the design of capacitive sensors for cell-based applications is challenging and there are several parameters that needs to be considered including : sensitivity, shelf life, cost per assay, throughput, linear range, detection limit, and biocompatibility. In this thesis we will discuss about these challenges and propose new solutions to overcome these limitations. A detailed literature review was also presented in this chapter introducing various readout interfaces for capacitance measurement. Due to the inherent features of CBCM

circuits in terms of low complexity, ease of integration, and high accuracy, this scheme is chosen in this thesis as the core circuitry.

# CHAPTER 5 A HIGH-SENSITIVITY CAPACITIVE SENSOR INTERFACE CIRCUIT FOR CHEMICAL AND BIOLOGICAL APPLICATIONS

## 5.1 Overview

Among various capacitive interfaces that were introduced in last chapter, core-CBCM circuitries have recently shown a great promise for various chemical and biological applications. The low complexity and high sensitivity of this readout interface makes it a suitable candidate for biological applications where a minute capacitance change happens at the interface between the sensing electrodes and test solutions. Herein we propose a high precision integrated CMOS capacitive sensor featuring a DC-input $\Sigma\Delta$ modulator interconnected to capacitive interface circuit. We also show the electrical and chemical characterization results of the fabricated chip. The following sections are the reproduction of a published article in IEEE Transactions on Biomedical Circuit and systems.

— G. Nabovati, E. Ghafar-Zadeh, M. Mirzaei, G. Ayala-Charca, F. Awwad, and M. Sawan, "A new fully differential CMOS capacitance to digital converter for lab-on-chip applications", IEEE Transactions on Biomedical Circuits and Systems, vol. 9, no. 3, pp. 353–361, 2015.

## 5.2 Article 1 : A new fully differential CMOS capacitance to digital converter for lab-on-chip applications

### 5.2.1 Abstract

In this paper, we present a new differential CMOS capacitive sensor for Lab-on-Chip applications. The proposed integrated sensor features a DC-input $\Sigma\Delta$ capacitance to digital converter (CDC) and two reference and sensing microelectrodes integrated on the top most metal layer in 0.35 $\mu m$ CMOS process. Herein, we describe a readout circuitry with a programmable clocking strategy using a Charge Based Capacitance Measurement technique. The simulation and experimental results demonstrate a high capacitive dynamic range of 100 fF-110 fF, the sensitivity of 350 mV/fF, and the minimum detectable capacitance variation of as low as 10 aF. We also demonstrate and discuss the use of this device for environmental applications through various chemical solvents.

*Index Terms : CMOS, Capacitive Sensor, $\Sigma\Delta$ Modulator, Lab-on-Chip, Chemical Sensor.*

### 5.2.2 Introduction

CMOS capacitive sensors have successfully been employed for a variety of applications including DNA analysis [31, 90], chemical gas detection [83, 91], virus detection [92], and bacteria growth monitoring [65]. To date various integrated circuit techniques have been reported for the detection of minute capacitance changes in microelectrodes realized on top of CMOS chips. Among these techniques, Charge Based Capacitance Measurement (CBCM) method by offering a highly accurate circuitry has attracted the attentions for large capacitive sensor arrays suitable for high throughput screening. Sylvester *et al.* initially proposed CBCM for the assessment of undesired cross-talk phenomenon, caused by parasitic capacitance, in deep CMOS chips [88]. This method was originally implemented using off-chip measuring instruments. Ghafar-Zadeh *et al.* took the technique to a whole new level by implementing signal buffering techniques to achieve unprecedented levels of precision [93]. The idea of measuring the small capacitance changes, between co-planar micro- electrodes built on the topmost metal layer of a CMOS IC promoted the technique to be a good candidate for use in bio-sensing applications such as bacteria growth monitoring and chemical solvent detection.

A CMOS capacitive sensor (Figure 5.1) consists of sensing electrodes, interface readout circuit and microfluidic package. A microfluidic package is developed to direct the biological/chemical fluid toward the sensing site and prevent the direct contact between the fluid and the remaining parts of the chip. The sensing electrodes detect the dielectric changes of fluid in close proximity of the sensing sites. Finally a readout circuit measures the capacitance changes of sensing electrodes. It is noteworthy that the selective detection of biological components requires a bio-recognition element formed above electrodes. For example, antibodies, DNA probes or enzymes (e.g. glucokinase) can be coated on electrodes as such an element for the detection of related antigens, complementary DNA sequences, and glucose, respectively [94].

The focus of this paper is placed on the design and implementation of a new readout circuitry. For this purpose, we employ the top most metal layer in CMOS to realize sensing electrodes without any additional post-CMOS processes. We also develop a low complexity fluidic package to test the functionality of CMOS capacitive sensor and to characterize the sensor using chemical solvents. These polar solvents (e.g. Dichloromethane, Acetone, Methanol, Ethanol and etc.) can change the output of capacitive sensors due to their dielectric properties. We demonstrate the capability of our proposed device as a chemical sensor which produces a different response upon exposure to different solvents. The accurate concentration measurement of chemical solvents can be used for various environmental monitoring applications, such as detection of toxic particles in water [95, 96]. The high sensitivity of sensor however,

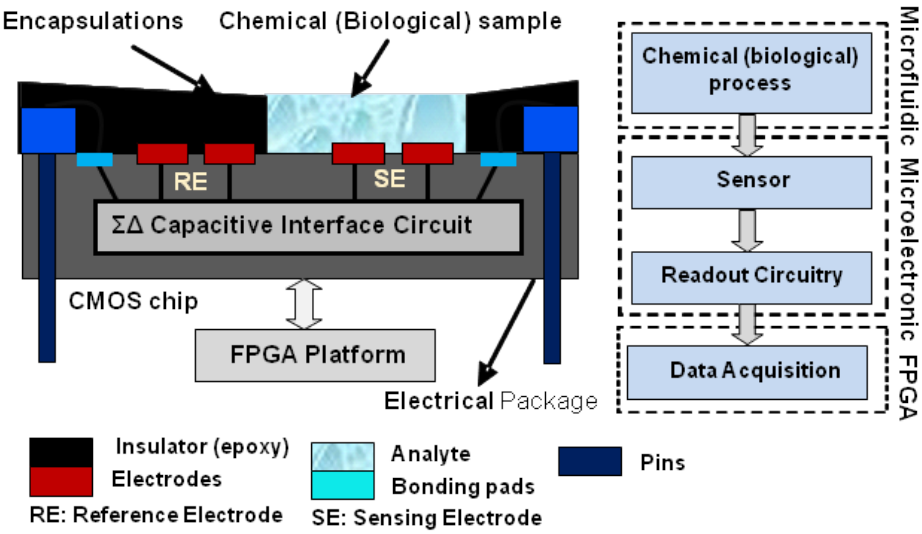


Figure 5.1: Illustration of CMOS capacitive sensor for Lab-on-Chip applications.

can extend the use of this device to biological applications such as cell growth monitoring. The proposed new ΣΔ capacitive sensor demonstrates the concentration measurement of chemical solvents that shows a significant improvement on the sensitivity in comparison to previously reported core-CBCM capacitive sensors.

### 5.2.3 Related work

The CBCM circuitry which consists of four transistors (Figures 5.2a and b) was reported as an accurate technique for the measurement of parasitic capacitances generated in between the electrodes in deep CMOS technology using external DC ammeters [88]. Our team took the first step toward the fully integrated CMOS capacitive sensor by developing the circuitry shown in Figures 5.2c. This current mode single-ended differential capacitive circuit, consisting of a CBCM structure, three current mirrors (Mi1-Mi6), and an integrating capacitor ($C_{int}$), demonstrated a high linear relationship between the input capacitance to output voltage. As a continuation of this work, our team also developed a core-CBCM DC input ΣΔ analog to digital converter (ADC) to convert the sensing capacitance into 1-bit stream (Figures 5.2d and e) [97]. In another effort, Prakash and Abshire built up a full differential capacitive to voltage converter (CVC) on the proposed circuitry in order to increase the sensitivity for the measurement of minute capacitance changes occurred during the proliferation of cancerous cells [57]. In this paper we propose a new fully differential current-mode capacitive to digital converter. The proposed sensor offers a higher sensitivity and wider dynamic

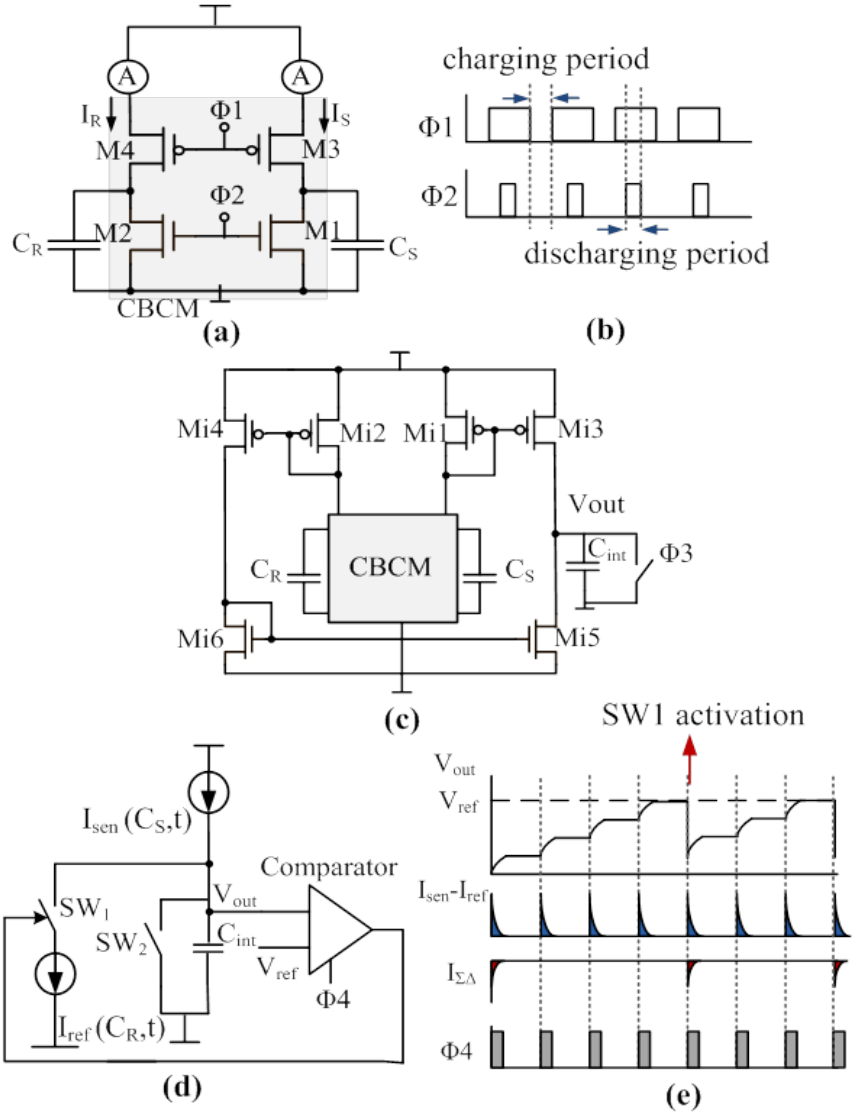


Figure 5.2: CBCM circuitry : (a) Basic CBCM circuit with off-chip ammeter, (b) Associated clock pulses for basic CBCM, (c)-(d) Our previously proposed CBCM circuitry and ΣΔmodulator, (e) Input and output signals associated with ΣΔmodulator.

range in comparison with previously reported core-CBCM capacitive sensors.

### 5.2.4 Proposed core-CBCM capacitive sensor

Figure 5.3 shows the block diagram of the proposed CMOS sensor featuring a core-CBCM capacitive sensor and an FPGA pulse generator. The CMOS chip includes two sensing and reference interdigitated microelectrodes along with differential core-CBCM ΣΔ readout system. The FPGA module is used as a programmable unit to generate various clock pulses and

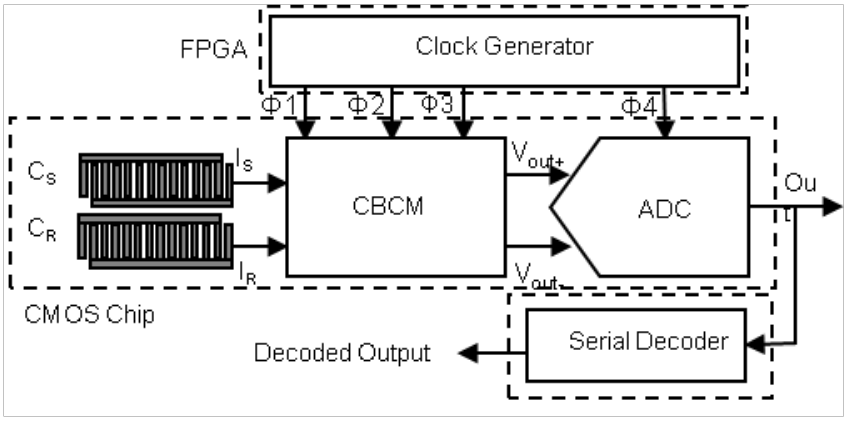


Figure 5.3: Proposed capacitive sensing system consisting of on chip readout interface (interdigitated electrodes, differential core-CBCM CVC and ADC), and off-chip FPGA system (pulse generator and decoder).

to decode the 1-bit stream generated by dedicated $\Sigma\Delta$ modulator.

**Fully differential CVC**

As shown in Figure 5.2a the operation principle of CBCM is based on charging and discharging the sensing capacitance by two switches. When $\Phi 1$ and $\Phi 2$ clocks are low, $C_S$ and $C_R$ capacitors are charged via PMOS transistors (M3 and M4) and when these two signals are high, they are discharged via NMOS transistors (M1 and M2). The resulted current, which is an indication of capacitance change, is amplified using current mirrors in the circuit. To implement the capacitive sensor, we propose a fully differential CBCM architecture shown in Figure 5.4. The sensing capacitor changes is defined by measuring the charging current. Since it is a differential structure, $I_S$ and $I_R$ currents are amplified by the gain of current mirrors and the difference will enter the next stage of the circuit. The next stage can be a current to voltage converter such as an integrating capacitor. The current, which is charging $C_{int+}$ capacitor, is described by :

$$I_{x1} = I_1 - I_2 = K_1 I_S - K_2 K_3 I_R = K_1 C_S \frac{dV}{dt} - K_2 K_3 C_R \frac{dV}{dt} \tag{5.1}$$

where $C_S$ and $C_R$ are sensing and reference capacitances respectively. Also, $K_1$, $K_2$ and $K_3$ can be described as follows

$$K_1 = \frac{(W/L)_{Mi3}}{(W/L)_{Mi1}}, K_2 = \frac{(W/L)_{Mi4}}{(W/L)_{Mi2}}, K_3 = \frac{(W/L)_{Mi5}}{(W/L)_{Mi6}} \tag{5.2}$$

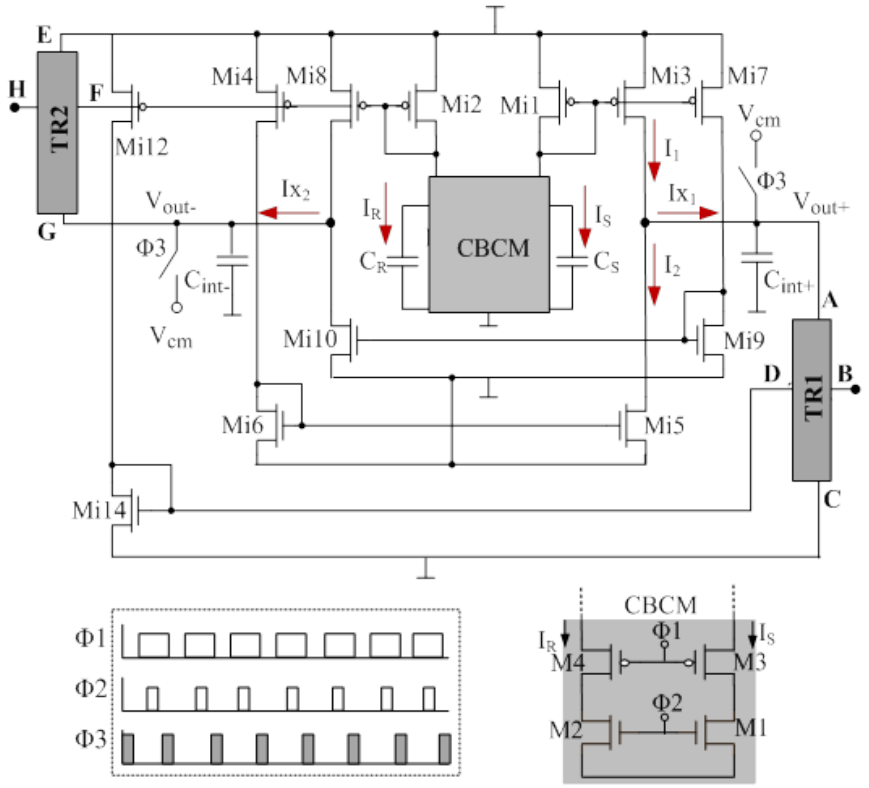


Figure 5.4: Proposed fully differential CBCM architecture and input clock pulses.

We assume that in each Φ2 clock pulse's period the capacitances are fully charged to approximately $V_{DD}$ and we also assume that $K_1 = K_2.K_3 = K$. Therefore, the output current can be obtained as

$$I_{x1} = K\frac{\Delta V}{\Delta t} = K\Delta C V_{DD} f_s \tag{5.3}$$

where $\Delta C = C_S - C_R$ and $f_s$ is the frequency of Φ2. The output voltage can be calculated as

$$V_{out+} = \frac{K\Delta C V_{DD} f_s}{C_{int} f_{int}} \tag{5.4}$$

where $C_{int}$ is the value of integrating capacitances ($C_{int+}$ and $C_{int-}$) and $f_{int}$ is the frequency of Φ3. It should be mentioned that in each period of Φ3, the value of the output voltage is set to a common mode voltage ($V_{cm}$). In this design, since dual supply voltages, $\pm V_{DD}$, are used, the common mode voltage is set to zero. Due to the circuit symmetry, the same equations exist for both voltages developed across $C_{int+}$ and $C_{int-}$ but with a negative sign for the latter. It is noteworthy that $TR1$ and $TR2$ in Figure 5.4 show the extra devices that

we added to develop a $\Sigma\Delta$ modulator (see section 4.2.5).

**Sensing Capacitors**

Two interdigitated electrodes were realized on the topmost metal layer (Metal 4) in CMOS 0.35 $\mu m$ technology. The passivation layer ($Si_3N_4$) was removed for $C_S$ capacitor using "pad" mask in CMOS. The COMSOL simulation results are used to estimate $C_S$ and $C_R$ values (Table 5.1). Since $C_R$ is covered with passivation layer, it has a higher dielectric constant which results in a larger value of capacitance. Based on these results, we simulate the readout circuitry in Cadence environment. In order to evaluate the designed electrode response to dielectric changes, the interdigitated electrode are simulated in COMSOL multiphysics environment based on the Cadence layout. To investigate the variation of sensing capacitance based on the proximity of a dielectric material, a set of simulations using COMSOL multiphysics are done when distance of the material from electrode surface is changed in 1 $\mu m$ steps. The resulted curve is shown in Figure 5.5a.

Figure 5.5b shows the electrodes and electrical field distribution where no material is placed on the electrode. Figure 5.5c shows the presence of a dielectric close to the electrodes (1 $\mu m$ distance) and Figure 5.5d shows the attachment of dielectric material on top of electrode where it has completely covered the surface. These three different states are modeled and simulated and electrical field distribution is shown in the above mentioned figures. In fact if the dielectric constant of the material covering the electrodes increases, the distribution of electrical field has to change. This change results in the change of the capacitance in between the electrodes. In these simulations, the electrode length (l), width (w), and thickness (t) are 250 $\mu m$, 100 $\mu m$, and 0.8 $\mu m$, respectively. The dielectric material used for changing the dielectric constant of the medium is epoxy resin (dielectric constant : 3.6). These simulation results are compared with similar experimental results using probe station to verify the functionality of capacitive sensor which is discussed in next sections.

### 5.2.5 Core-CBCM $\Sigma\Delta$ modulator

The proposed sensor acts similar to a first order $\Sigma\Delta$ modulator consisting of a voltage comparator, a quantizer and a digital to analog converter (DAC) as shown in Figure 5.6. In each quantizer's sampling period (TQ) the voltage of the integrating capacitor ($C_{int}$) is compared with a reference voltage. If the difference between $V_{out+}$ and $V_{out-}$ is larger than $V_{ref+} - V_{ref-}$, the comparator output signal will be activated and subsequently turns-on $SW_1$ and $SW_2$ switches. By activating $SW_1$ and $SW_2$, $I_{\Sigma\Delta-}$ current will be subtracted from the positive current ($I_{x1}$) and $I_{\Sigma\Delta+}$ will be added to the negative current ($I_{x2}$) (Figure 5.6c). The

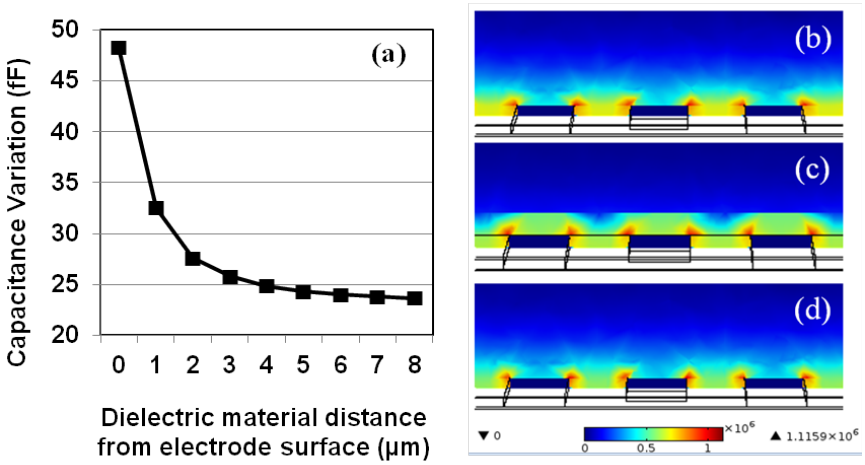


Figure 5.5: COMSOL simulation results : (a) Capacitance variation versus dielectric material distance from electrodes, (b-d) : Electrical field distribution over electrodes where (b) No material is near electrodes, (c) A material exist in 1 $\mu m$ proximity of electrodes, and (d) A material is attached to the electrodes. (Dimensions are mentioned in Table 5.1).

$I_{\Sigma\Delta+}$ depends on $C_R$. Comparing the architecture shown in Figure 5.6a with Figure 5.6b, it is seen that $C_{int+}$ and $C_{int-}$ act as a summing node and low pass filter in the first order $\Sigma\Delta$ modulator.

The $SW_1$ and $SW_2$ switches and $I_{\Sigma\Delta+}$ and $I_{\Sigma\Delta-}$ current sources realize the DAC block in the first order $\Sigma\Delta$ modulator. The circuit implementation of differential $\Sigma\Delta$ modulator for the proposed readout interface is achieved by integrating the circuitries of $TR1$, $TR2$ and a comparator as shown in Figure 5.7. Transistors $M_{S1}$, $M_{S2}$ realize the $I_{\Sigma\Delta+}$ current and $SW_1$ switch and $M_{S3}$ and $M_{S4}$ realize the $I_{\Sigma\Delta-}$ current source and $SW_2$ switch. For comparator implementation, we adapted the architecture proposed in [98] which is a differential pair comparator with 4 inputs (two for input voltages and two for reference voltages). In order to hold the output voltage of comparator after each $\Phi 4$ period, we have added a RS latch which is used for saving the logic state of the output for one clock pulse period.

To demonstrate the circuit performance, the proposed circuit is simulated in Cadence software using TSMC 0.35 $\mu m$ CMOS technology. The value of $C_R$ capacitance is kept constant at 100 fF and the value of $C_S$ is varied between 100 fF and 110 fF. The output waveforms for the $C_S$ values between 100 fF and 103 fF are plotted in Figure 5.8. In each reset signal cycle, the output voltage is set to the common mode value and in sampling cycle, as the value of sensing capacitor increases the output voltage also increases. Figure 5.8 demonstrates the output voltage, which is the difference between Vout+ and Vout-, for two different frequencies of $\Phi 3$ (4 MHz and 2 MHz). Based on Eq. (5.4) and as seen in this figure, the output voltage

Table 5.1: CMOS core-CBCM capacitive sensor facts

| **Parameter.** | **Value** |
|---|---|
| Technology | 0.35 $\mu m$ |
| $C_R$ , $C_S$ | 100 fF |
| W (electrode width) | 100 $\mu m$ |
| L (electrode length) | 250 $\mu m$ |
| Power Consumption | 580 $\mu W$ |
| Sensitivity (N=10) | 350 mV/fF |
| Sampling frequency | 150 kHz |
| Resolution | 10 aF |

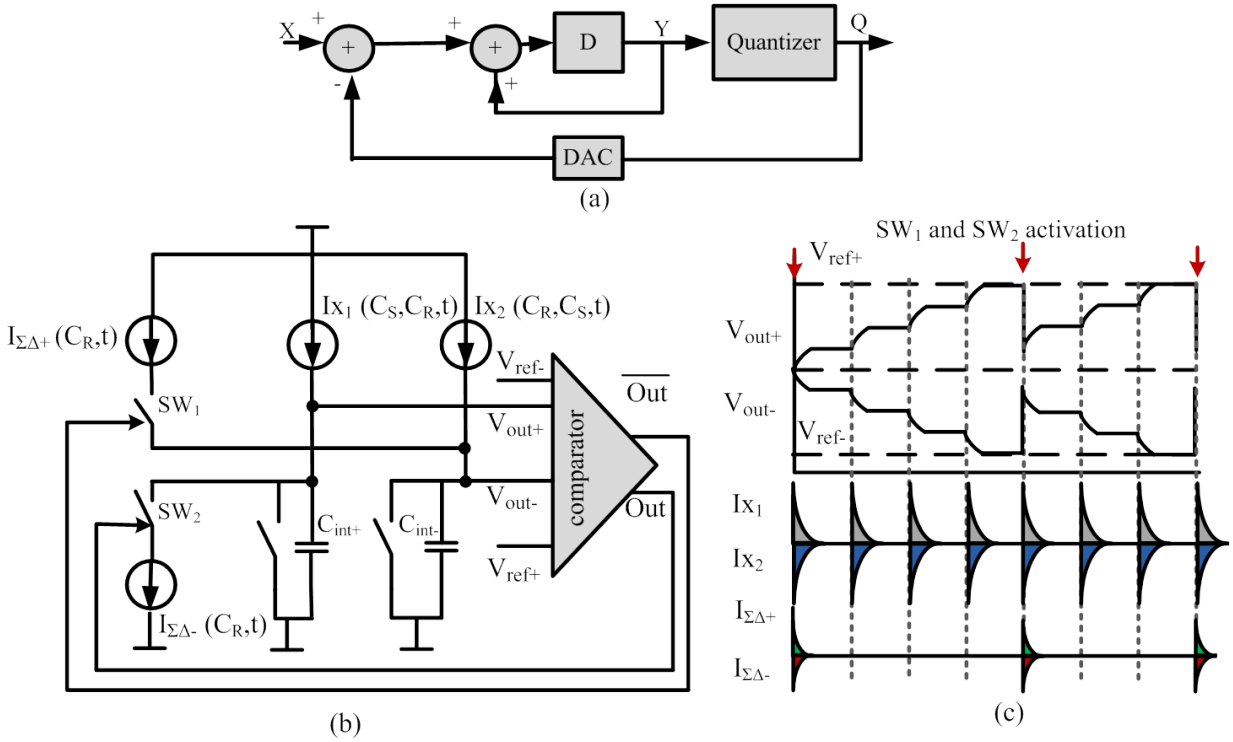


Figure 5.6: ΣΔ modulator (a) Ideal $1^{st}$ order, (b) proposed modulator, (c) signal diagrams.

(Vout) value depends on the frequency of Φ3 . The proposed ΣΔ modulator is also simulated in Cadence and the results are shown in Figure 5.9.

This figure shows the generated 1-bit-stream by the modulator for three different capacitance

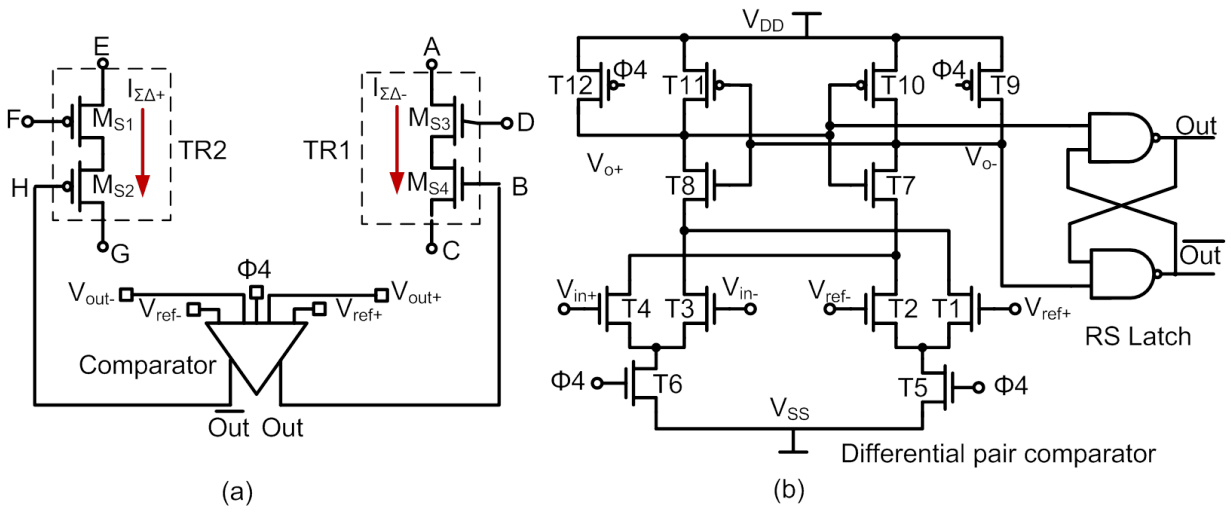


Figure 5.7: Proposed ΣΔ Modulator circuit implementation : (a) TR1, TR2 and comparator shown in Figure 5.6, (b) differential comparator implementation.

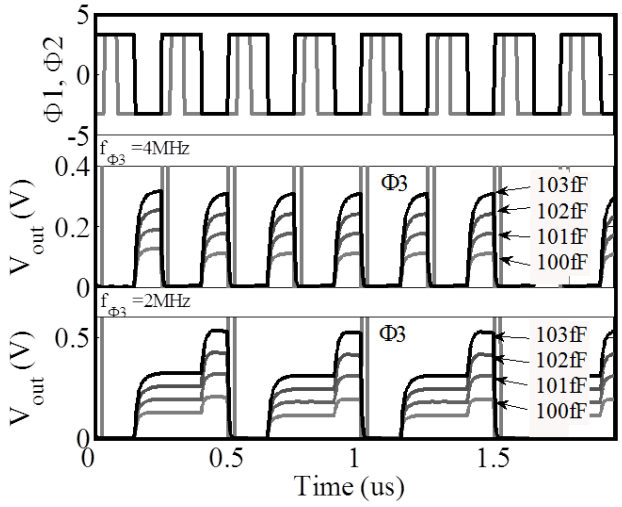


Figure 5.8: CBCM clock pulses and generated waveforms for Cs values between 100 fF and 103 fF, the output voltage is plotted for two Φ3 frequencies (4 MHz and 2 MHz).

values with 10 aF difference. In order to decode this bit stream we apply a simple averaging technique. Based on this technique, the produced output bit stream is used to trigger a serial counter to which each '1' in this bit stream, increments the counter and subsequently results in a number that is proportional to the average of bit steam. To simulate the decoder operation, a code is developed in Matlab software, which takes the data, generated by Cadence simulations, and calculates the average of output for a 50-bit sequence. The averaging

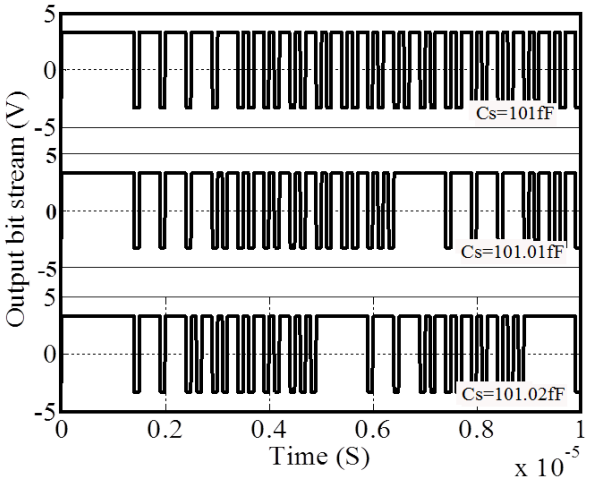


Figure 5.9: Generated bit stream by proposed ΣΔ modulator for $C_S$ values of 101 fF, 101.01 fF and 101.02 fF.

procedure is repeated for 10 consecutive sequences. The data for 10000 different values of $C_S$ ranging from 100 fF and 110 fF with 1 aF resolution is imported in Matlab. This procedure helps us to evaluate the ΣΔ modulator linearity and sensitivity for a wide range of sensing capacitance. The decoded bit stream (average of bit stream) is shown in Figure 5.10 for the sensing capacitances between 100 fF and 100.5 fF. This curve shows that ΣΔ modulator has generated 50 different values for 50 different values of capacitance with 10 aF resolution.

### FPGA System

In this work, the main role of FPGA system (Spartan3, Xilinx) is to generate $\Phi 1, \Phi 2, \Phi 3$ and $\Phi 4$ clocks and decode the received bit stream from ΣΔ modulator. After calculating the average, it is sent to the computer via USB port. Moreover, in order to implement a configurable clocking strategy, the FPGA platform allows selecting a set of signals with specific delays, pulse widths and periods through 8 switches. This enables the user to choose the best sampling scheme based on the desired circuit performance.

### Circuit non-idealities

In order to investigate the effect of circuit non-idealities such as transistors mismatch, parametric simulations are done in Cadence environment where the aspect ratios of current mirror transistors are changed by 20%. As shown in Figure 5.11, the mismatch error of current mirrors has changed the offset voltage however it has not affected the dynamic range or sensitivity considerably, except for transistor $Mi10$, $Mi7$ and $Mi12$, where sensitivity is

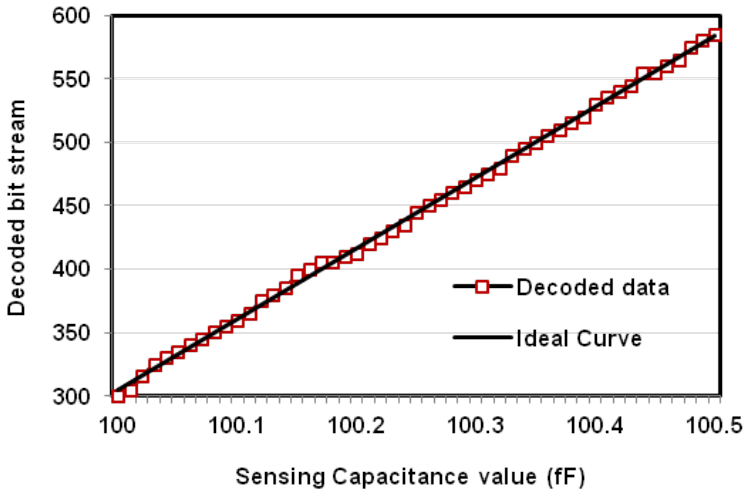


Figure 5.10: Novel ΣΔ modulator's main result : Decoded bit-stream generated by Cadence simulation and imported in Matlab, $C_S$ varies between 100 fF and 100.5 fF in 10 aF steps. This curve shows a linear relation between the decoded output bit stream and input capacitances.

changed to some extents. The non ideal effect of mismatch can be cancelled by calibration technique proposed in [8]. The comparator's non-idealities such as kick back noise and offset which is caused by transistors mismatch can also affect the ΣΔ modulator performance. Figure 5.12 shows the effect of mismatch in comparator's input transistors on output curve of ΣΔ modulator. As it is seen, the mismatch has deteriorated the linearity of modulator to some extent but it has not affected the resolution.

### Clocking strategy

In this section we discuss the development of an optimal clocking scheme for the best circuit performance (e.g. power consumption, linearity, and sensitivity). Based on Eq. (5.4), $f_s$ and $f_{int}$ frequencies can significantly affect the sensor performance in terms of linearity, sensitivity and power consumption. $f_s$ is the sampling clock pulse while $f_{int} = \frac{1}{N} f_s$, where N is the number of clock pulses. As shown in Figure 5.8, for a higher number of charging time per reset cycle, a higher output voltage for a specific value of $C_S$ is expected. This results in the improvement of sensitivity of capacitive sensor. The sensitivity can be formulated as follows.

$$\frac{dVout}{dC_s} = \frac{2NKV_{DD}f_s}{C_{int}} \tag{5.5}$$

Based on this equation, the sensitivity is proportional to the number of integration cycles. Hence searching for optimum clock pulses is very crucial to achieve the best circuit perfor-

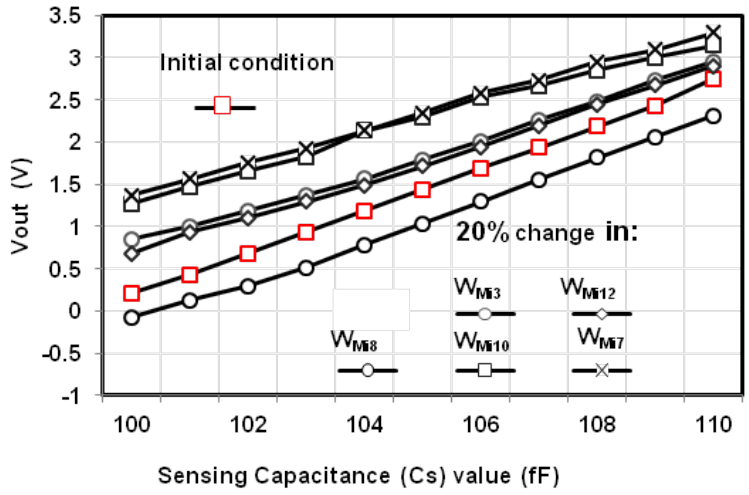


Figure 5.11: Simulation results showing the effect of mismatch error on sensitivity and dynamic range of the capacitive readout circuit.

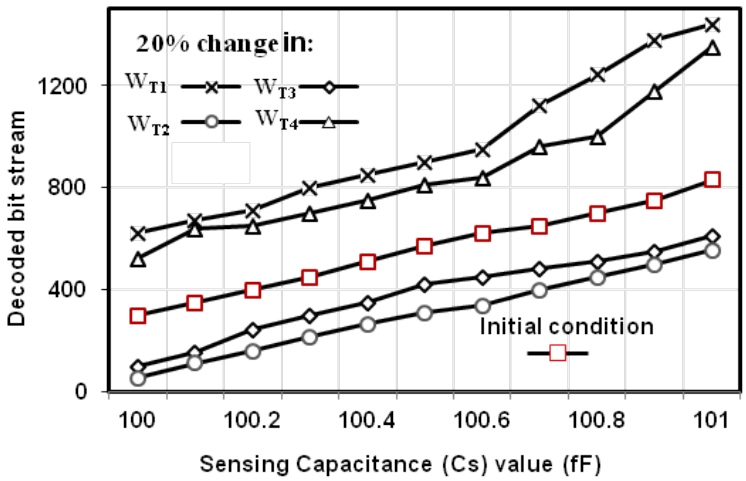


Figure 5.12: Simulation results showing the effect of comparator non idealities on the performance of $\Sigma\Delta$ modulator.

mance in terms of sensitivity and linearity. Figure 5.13 shows the circuit sensitivity and power consumption for different values of N. As it is shown, by increasing N, power consumption does not change considerably, but $f_s$ affects the power consumption significantly. On the other hand, according to Eq. (5.4), by increasing N, the output voltage and hence the sensitivity of the circuit will increase. However, the simulation results show a limitation in the increase of N factor as the output voltage reaches a saturation after certain period of time. Figure 5.14 shows the maximum value of N for various $C_S$ and three different values of $C_{int+}$

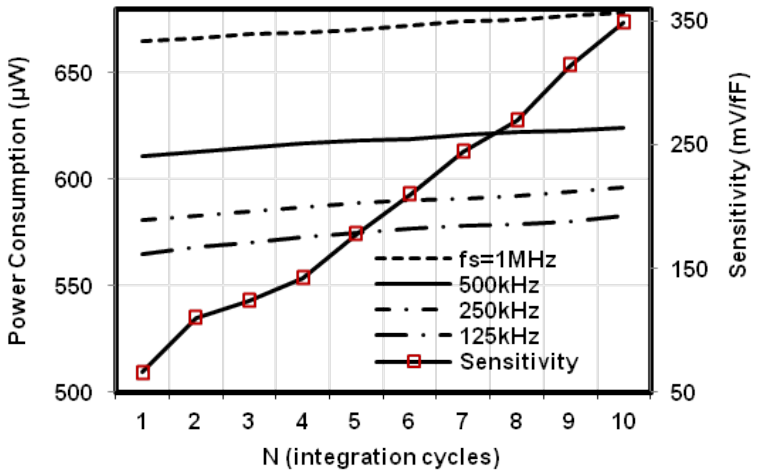


Figure 5.13: Sensitivity variation and power consumption for different values of N.

and $C_{int-}$. Referring to Eq. (5.4), the increase in integrating capacitance ($C_{int+}$ and $C_{int-}$) will increase the limit of N.

Based on the maximum estimated capacitance change and designed integrating capacitance value one can determine the best value of N in order to reach the optimum circuit sensitivity. The dynamic range and also linearity of the circuit change with different values of N. As shown in Figure 5.15, the increase in the value of N results in an increase in the sensitivity of the circuit. As a result, the sensor will have smaller dynamic range and the linearity is progressively deteriorated when N is increased. Based on the application and estimated variation range of capacitance, N can be determined to achieve the optimum results and best circuit performance.

### 5.2.6 Experimental results

The proposed capacitive sensor is fabricated using TSMC 0.35 $\mu m$ standard CMOS process. The die image is shown in Figure 5.16a. The SEM micrograph of interdigitated electrodes and their dimensions are shown in Figure 5.16b. The area occupied by CBCM and $\Sigma\Delta$ modulator is 100 $\mu m$ x 100 $\mu m$ and the area occupied by sensing and reference electrodes is 200 $\mu m$ x 100 $\mu m$, each. Based on the application, the electrode dimension can be further decreased to save the chip's area. Additionally, we have developed a low complexity fluidic package to expose the chip to chemical solvent as shown in Figure 5.16c. To test the circuit with different organic solvents, first we need to completely encapsulate and insulate any electrical connection including bonding wires and pads. For this purpose, a low viscosity epoxy resin

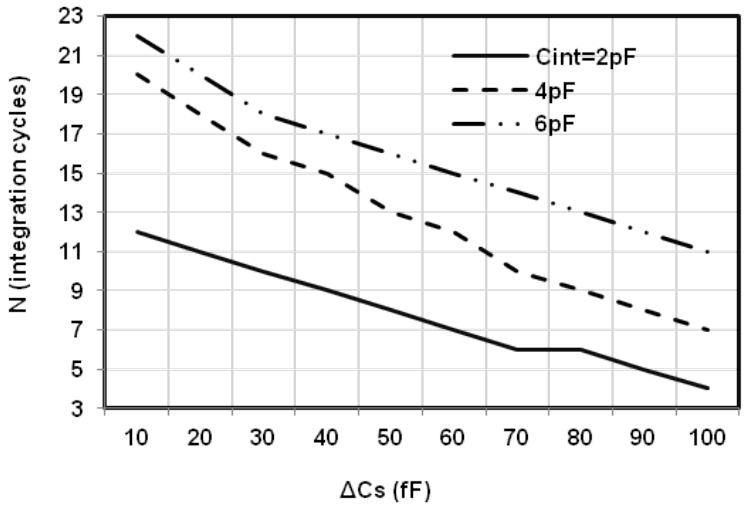


Figure 5.14: The maximum number of N for different integrating capacitance ($C_{int}$) value.

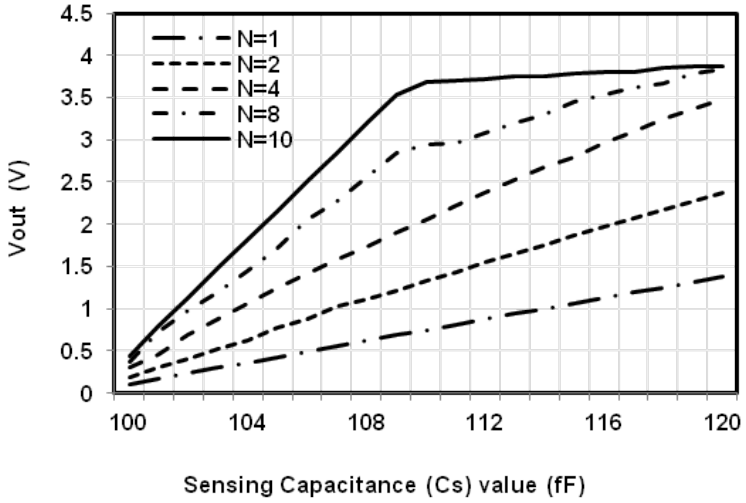


Figure 5.15: Effect of N on linearity and dynamic range of the sensor, (Cint=2pF).

(H70E, EPOTEK) has been used. The epoxy covered chip is then baked on a hot plate for 15 min until the epoxy is completely cured. The final encapsulated chip is shown in Figure 5.16c. In order to provide a well for solutions, a centrifuge tube is cut and fixed on the chip package using general-purpose epoxy glue. To evaluate the circuit functionality, two different experimental setups were prepared. First, a microprobe is used to verify the functionality of sensor by approaching a material to sensor and demonstrating the capacitance change. Then, various organic solvents with different dielectric constants were used to measure the sensitivity.

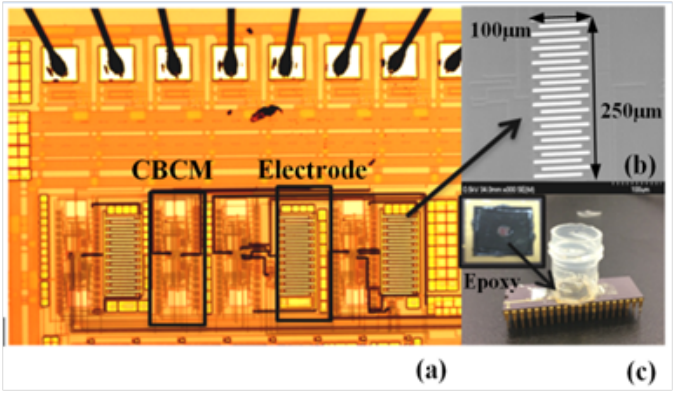


Figure 5.16: Die image and test setup : (a) Die micro photograph, (b) Capacitive electrodes, (c) Test fixture.

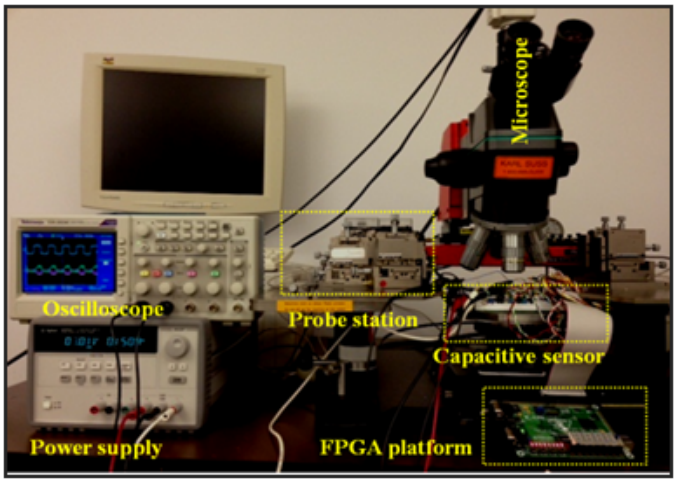


Figure 5.17: Experimental set-up : FPGA platform (clock generator and decoder), oscilloscope and Power supply, microprobe on top of the CMOS chip, and microscope.

### Experimental set-up

As shown in Figure 5.17, using a probe station, a microprobe covered with a dielectric material is moved down close to the surface of the capacitive electrodes. Herein, an epoxy resin with a dielectric constant equal to 3.6 was used. As the probe moves down to the capacitive electrodes, the dielectric constant of the surrounding environment changes from air to epoxy and the electrical field distribution changes which result in an increase in $C_S$ value. As shown in Figure 5.16c, the fluidic encapsulation is performed to prevent direct contact of solution with electrodes. This simple procedure is performed to directly expose the solvent to the device and measure the concentration of various chemical solvents. The FPGA platform and other instrumentation for the test of sensors are shown in Figure 5.17.

**Preliminary experimental results with micro-probe**

The waveforms in Figure 5.18a-c show the variations of the $V_{out+}$ and $V_{out-}$ and also the differential output voltage for three different states, (a) when no probe is above electrodes, (b) when the probe is kept in close proximity of electrodes and (c) when probe is attached to the surface. There is a 800 mV difference in output voltage before and after probe contact. The reason that we have a decrease in the output voltage is that $V_{out}$ is proportional to $(C_R - C_S)$ and as the sensing capacitance value increases the value of output voltage decrease. Figure 5.18d-f show the output bit stream generated for three different value of sensing capacitance before and after probe contacts. The generated bit stream is shown for one period of $\Phi 3$ clock pulse. It should also be mentioned that the needle shaped pulses are $\Phi 4$ clock pulse which it is generated by FPGA platform.

**Chemical Test Using Organic Solvent**

To evaluate the response of the sensor to organic solvents, we exposed the device to polar chemical solvents with different dielectric constants, namely : Acetone, Methanol, Ethanol and Dichloromethane. Prior to the addition of each solution, the sensor was cleaned by distilled water and then was dried on a hot plate to avoid any residues of previous analyte material. The real-time response of sensor, for empty well and also after exposure to 200 $\mu l$ of Methanol, Acetone and distilled water at room temperature are shown in Figures 5.19a-d

It shows that sensor's response, characterized by the amplitude of the output voltages, is different for each solvent compared to the empty well due to the changes in dielectric constant of solution on top of the interdigitated electrodes. As the dielectric constant of the solvent increases, the amplitude of the output voltage will increase due to the capacitance change. Figure 5.20 shows the average of output voltage variation for different organic solutions with different dielectric constants.

Three different dies have been encapsulated and tested ; moreover each experiment has been repeated twice on each die to ensure the repeatability of the results. As the dielectric constant increases, the sensing capacitance value also increases which leads to a change in output voltage value (Figure 5.20). The sensor was exposed to different concentrations of Ethanol as well. The average values for output voltage changes are reported in Figure 5.21. As shown, the sensor has generated different amplitudes of output voltage based on the concentration of Ethanol. It should be mentioned that in order to avoid Ethanol evaporation and to reduce the measurement error, after each run, the tube cap is completely closed and the results are recorded in a short period of time (less than 5 min). The summary of circuit specifications

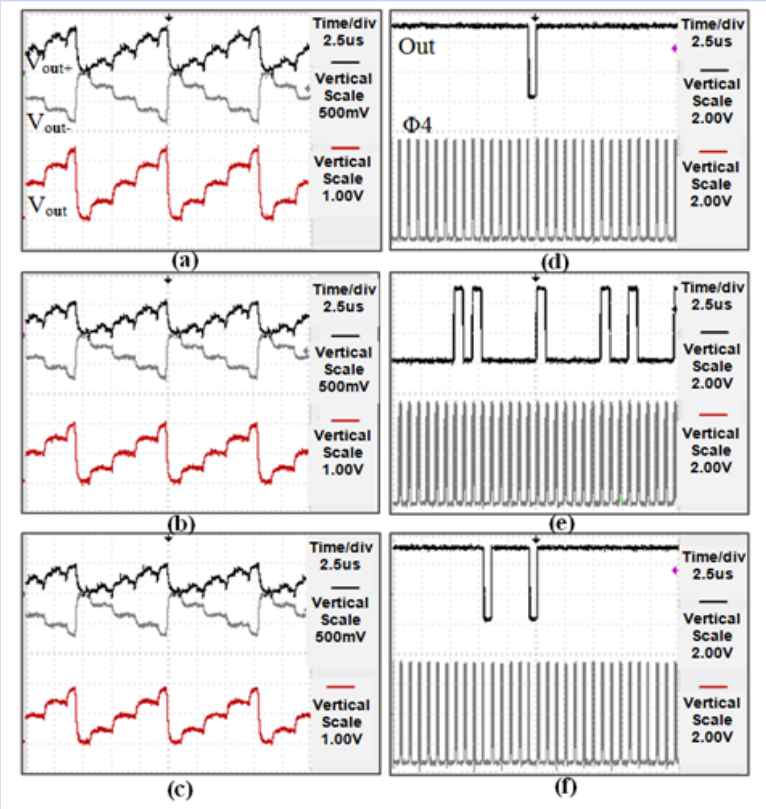


Figure 5.18: Probe test results, output voltage variation where (a) no probe, (b) probe is in close proximity of electrode, (c) probe is attached to the electrodes, output bitstream generated by ΣΔ modulator when : (d) no probe is on the surface, (e) probe is in close proximity of electrode, (f) probe is attached to the electrodes, (N=4).

and the comparison with other state-of-the-art CBCM circuitries are provided in Table 5.2.

### 5.2.7 Conclusion

In this paper, we described the design and implementation of a high sensitivity core-CBCM capacitive sensor. A new DC-input differential ΣΔ modulator is also presented to convert the capacitance changes to digital. Due to the inherent low frequency of the biological signals and required high resolution, the proposed modulator is suitable to be incorporated with biosensor readout interfaces. To verify the chip functionality and device detection capability, various organic solutions including Methanol, Ethanol, Acetone and Dichloromethane were examined.

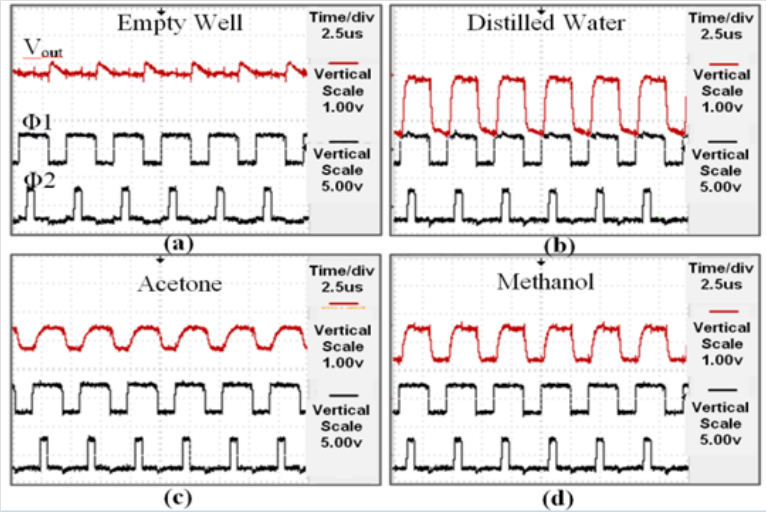


Figure 5.19: Output voltage for different organic solutions : (a) no solution, (b) distilled water (dielectric constant : 80), (c) Acetone (dielectric constant : 20.7), (d) Methanol (dielectric constant : 33.4), (N=1).

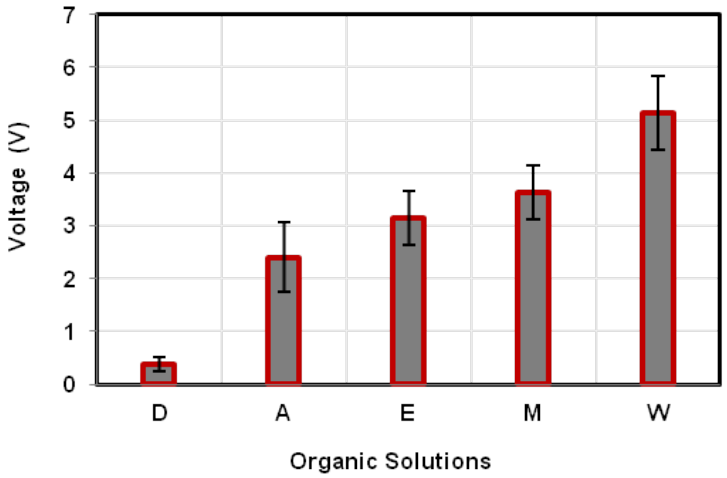


Figure 5.20: Measured average differential output voltage changes for different chemical solvents : D (Dichloromethane), A (Acetone), E (Ethanol), M (Methanol), W (Water).

### 5.2.8 Acknowledgment

Authors would like to thank the support of Canada Research Chair on Smart Medical Devices, NSERC in Canada, CMC Microsystems, and National Research Foundation (NRF) in United Arab Emirates.

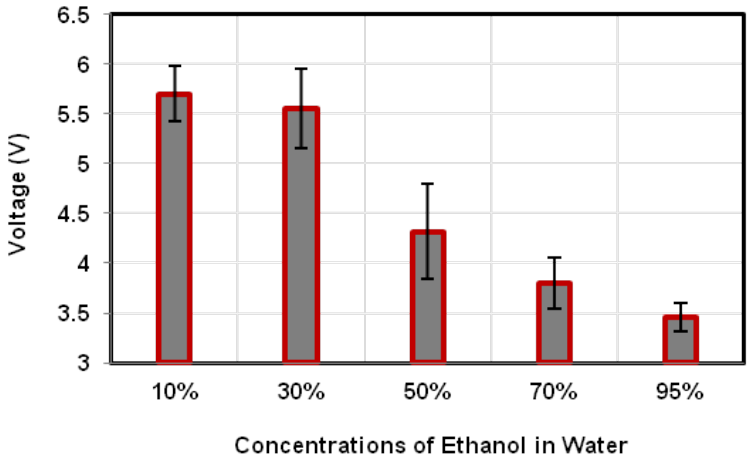


Figure 5.21: The average output voltage variation for different concentrations of Ethanol in Distilled water.

Table 5.2: Core-CBCM Chip specifications and comparison with other work

| Reference | [65] | [32] | [89] | This work |
|---|---|---|---|---|
| Chip Technology ($\mu m$) | 0.18 | 0.18 | 0.18 | 0.35 |
| Sensitivity (mV/fF) | 250 | 200 | 42 | 350 |
| Dynamic range | NA | 10fF | NA | 10fF |
| Supply voltage (V) | +1.8 | ±1.8 | +1.8 | ±3.3 |
| Output Voltage | Single | Differential | Single | Differential |
| Resolution (af) | 10 | 15 | 10 | 10 |
| Power Consumption ($\mu W$) | 0.7 @10kHz | 0.3 @1kHz | NA | 0.3 @1kHz |

# CHAPTER 6 HIGH THROUGHPUT CMOS CAPACITIVE READOUT SYSTEM

## 6.1 Overview

In previous chapter we introduced a fully differential capacitive readout interface based on charge measurement. The superior performance of the proposed circuit over state of the art of capacitive readout circuits motivates to further improve the design and expand it into a 8x8 sensor array. In this chapter we will present this capacitive sensor array and we also the validate its performance through several chemical and biological experiments. The following sections are the reproduction of a accepted article in IEEE Transactions on Biomedical Circuit and systems.

— G.Nabovati, E.Ghafarzadeh, A.Letournea, and M.Sawan, "Towards High Throughput Cell Growth Screening : A New CMOS 8x8 Biosensor Array for Life Science Applications", IEEE Transactions on Biomedical Circuits and Systems, Accepted for publication.

## 6.2 Article 2 : Towards high throughput cell growth screening : A new CMOS 8x8 biosensor array for life science applications

### 6.2.1 Abstract

In this paper we present a CMOS capacitive sensor array as a compact and low-cost platform for high-throughput cell growth monitoring. The proposed biosensor, consists of an array of 8x8 CMOS fully differential charge-based capacitive measurement sensors. A DC-input $\Sigma\Delta$ modulator is used to convert the sensors' signals to digital values for reading out the biological/chemical data and further signal processing. To compensate the mismatch variations between the current mirror transistors, a calibration circuitry is proposed which removes the output voltage offset with less than 11.2% error. We validate the chip functionality using various organic solvents with different dielectric constants. Moreover, we show the response of the chip to different concentrations of Polystyrene beads that have the same electrical properties as the living cells. The experimental results show that the chip allows the detection of a wide range of polystyrene beads concentrations from as low as 10 beads/ml to 100 k beads/ml. In addition, we present the experimental results from H1299 (human lung carcinoma) cell line where we show that the chip successfully allows the detection of cell attachment and growth over capacitive electrodes in a 30 h measurement period and the

results are in consistency with the standard cell-based assays. The capability of proposed device for label-free and real-time detection of cell growth with very high sensitivity opens up the important opportunity for utilizing the device in rapid screening of living cells.

*Index terms : CMOS, Cell Growth Monitoring, Capacitive Sensor Array, High-Throughput Screening*

### 6.2.2 Introduction

CMOS capacitive sensors have recently attracted the attentions for a variety of life science applications such as genetic analysis, infectious disease detection, and cellular studies [99–101]. A capacitive sensor consists of an interface circuit connected to capacitive electrodes realized in the top most metal layer in CMOS process. Among various interface circuit topologies, charge based capacitive measurement (CBCM) technique has demonstrated great advantages as highly accurate technique for sensing applications [63, 102]. CBCM was initially proposed for the measurement of cross talk capacitance in between the conductors in CMOS chips using off-chip DC ammeter [88]. Ghafar-Zadeh *et al.* took this technique to another level by developing an integrated single-ended $\Sigma\Delta$ charge to digital converter for Lab-on-Chip applications [103]. In another effort, Nabovati *et al.* reported a fully differential core-CBCM interface circuit for chemical solvent monitoring [104]. As a follow-up to that work, we used the same chip for cellular growth monitoring (Figure 6.1a and b). This figure shows the attachment of H1299 cells on the surface of CMOS chip. Following a standard cell culture procedure, the cells were prepared and introduced to the CMOS sensor. All tests were performed in triplicates to demonstrate the chips functionality. As seen in Figure 6.1c, the sensor can detect two phases of adhesion and growth in the cell culture followed by trypsinization process which leads to cell detachment from the sensing electrodes. These promising results, shown in Figure 6.1, have inspired the idea of developing an array of large number of capacitive micro-sensors integrated on the same chip for high throughput screening. In this paper, we take the first step toward this goal by developing an array of 8x8 interdigitated electrodes interconnected to fully differential $\Sigma\Delta$ charge to digital converters.

High throughput cell culture screening is the key challenge for a variety of life science applications including drug discovery and cytotoxicity monitoring [105, 106]. To date, several efforts have been made to develop microfluidic devices featuring arrays of micro-chambers for cell culture screening using optical microscopic techniques [107, 108]. However less attention have been paid on developing integrated sensors incorporated with cell culture micro-wells for monitoring cellular activities such as tumor cell proliferation and cytotoxicity monitoring using capacitive or ion-sensitive field effect transistors (ISFETs) [109, 110]. Among these,

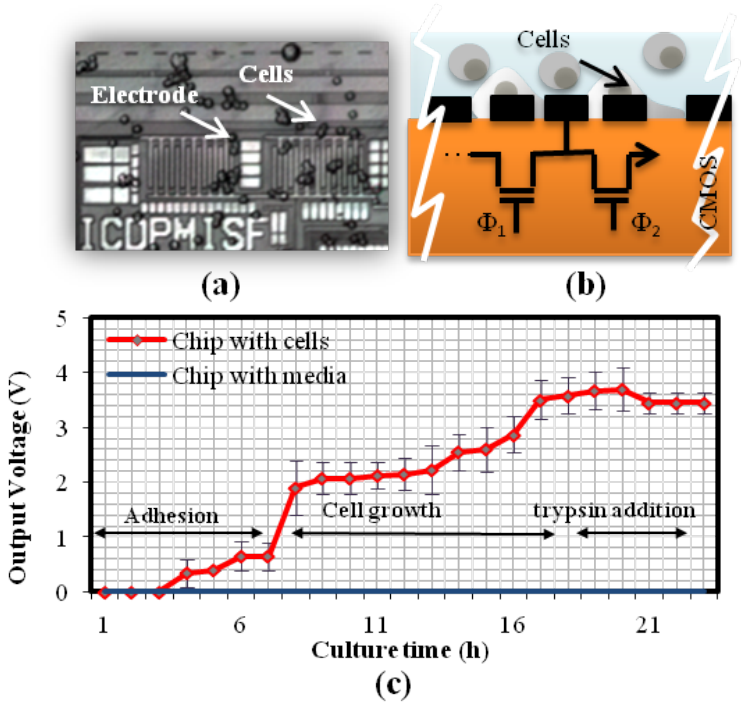


Figure 6.1: Illustration of recently proposed capacitive sensor for cellular analysis. (a) Cells attached on the interdigitated electrodes. (b) Simple illustration of CBCM circuitry. (c) Response of the chip to adherent H1299 cells.

capacitive techniques by offering low complexity platform have significantly attracted attentions as a mean to study cell-surface interaction that can be important for a variety of biological studies [66, 111]. Despite these great advances, still the development of a large number of capacitive micro-sensors for high-throughput screening is a challenge. These challenges can appear both in circuit design level or integration level. In circuit design process, due to the large array of sensing electrodes, the effect of parasitic and cross talk could be considerable, hence choosing the right electrode structure and dimension is very important. It is proved that choosing the electrode features close to the test analytes, can optimize the sensor performance. However, in cell-based applications, due to the small capacitance of the sensor, the detection sensitivity are limited by noise resulted from large parasitic capacitance that is many orders of magnitude greater than the sensor capacitance. Besides, the electronic noise from the readout circuit also affects the measured accuracy. Therefore, they should be considered for the development of sensitive and accurate sensing devices. On the other hand, the inclusion of CMOS technology in the applications that necessitates the direct contact of sensing or actuation electrodes with the chemical/biological solutions complicates the packaging and encapsulation process. The packages not only should protect the device from the

solutions but also it should be robust enough against several cleaning procedures and long-term experiments such as cell culture monitoring that can last up to 1 week. In this paper we address these challenges by developing a CMOS sensor array consisting of 64 capacitive electrodes.

### 6.2.3 Fully differential capacitive sensor array design and implementation

The proposed CMOS cell-based biosensor consists of a capacitive sensor system as shown in Figure 6.2a. In this section, we put forward the details of this system including 64 capacitive sensors ($C_S$), eight decoders, eight $\Sigma\Delta$ ADCs, and eight reference electrodes along with calibration circuitries. A FPGA system is also used to generate clocks ($\Phi_1, \Phi_2, \Phi_3$, and $\Phi_4$) in order to activate CBCM structure and DC-input $\Sigma\Delta$ modulators and finally readout the data from capacitive electrodes ($C_S$s). Also this FPGA controls the decoder and calibration circuits accordingly.

### 6.2.4 Differential charge to voltage converter

The fully differential charge to voltage converter consists of a CBCM structure ($M_1$-$M_4$), integrating capacitors ($C_{int+}$, $C_{int-}$) and several current mirrors as was previously described in [104]. As shown in Figure 6.2b, the sensing current $I_S^{i,j}$ which is charging the capacitive sensing electrodes ($C_S^{i,j}$) is described by

$$I_S^{i,j} = C_S^{i,j}\frac{dV_{SE}}{dt} = \beta(V_{DD} - V_{SE} - V_{thp})^2 \tag{6.1}$$

where $V_{DD}$ is a power supply voltage, $V_{SE}$ is the voltage dropped on sensing capacitor, $V_{thp}$ is the pMOS threshold voltage,$V_{DD} - V_{SE}$ is $M_2$ gate-source voltage, $0 < i, j \leq 8$, and $\beta$ is transistors parameter and is equal to $\mu_n C_{ox} W/L$ where $\mu_n$ is the surface mobility of charge carrier in MOS device, $C_{ox}$ is the gate insulator capacitance and $W/L$ is MOS transistor's aspect ratio.

By solving the above differential equation and by assuming that the sensing and reference electrodes are fully discharged at t=0, then the transient value of voltage on sensing electrode is given by

$$V_{SE} = \frac{C_S(V_{DD} - V_{thp})}{\beta(V_{DD} - V_{thp})t + C_S} + V_{DD} - V_{thp} \tag{6.2}$$

The transient current, that charges the integrating capacitor can be calculated as

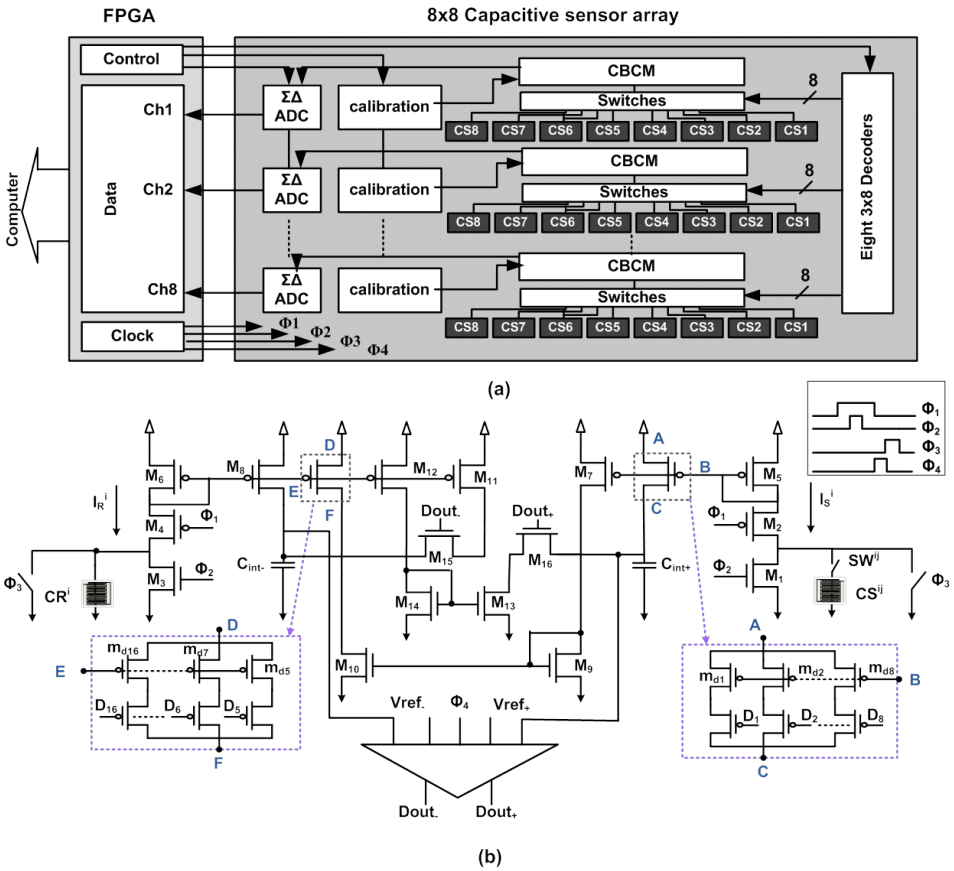


Figure 6.2: (a) System level block diagram of proposed cell-based capacitive sensor, CSs blocks refer to interdigitated sensing electrodes, and CBCM refers to charge based capacitive measurement circuit block. (b) Circuit implementation of capacitive readout interface.

$$I_S^{i,j} = \frac{K_1 {C_S^{i,j}}^2 (V_{DD} - Vthp)^2}{(\beta(V_{DD} - Vthp)t + C_S^{i,j})^2} - \frac{K_2 K_3 C_R^2 (V - DD - Vthp)^2}{(\beta(V_{DD} - Vthp)t + C_R^i)^2} \tag{6.3}$$

where $K_1$, $K_2$, and $K_3$ are the first ($M_5$, $M_7$), second ($M_6, M_8$) and third ($M_9, M_{10}$) current mirrors' amplification factors. The final value of current that is charging the integrating capacitor is calculated by the following equation.

$$I_S^{i,j} = f_s(K_1 C_S^{i,j} - K_2 K_3 C_R^i)(V_{DD} - Vthp) \tag{6.4}$$

We assume that in each $\Phi_2$ clock pulse period the capacitances are fully charged to approximately $V_{DD}$ and we also assume that $K_1 = K_2 K_3 = K$. Due to the circuit symmetry, the same equations exist for both currents charging $C_{int+}$ and $C_{int-}$ but with a negative sign for

the latter. The output voltage is obtained by

$$V_{out}^{i,j} = \frac{2K\Delta C^{i,j} V_{DD} f_{int}}{C_{int} f_s} = \frac{2K\Delta C^{i,j} V_{DD} N}{C_{int}} \tag{6.5}$$

where $\Delta C^{i,j} = C_S^{i,j} - C_R^i$ and $f_s$ is the frequency of $\Phi_2$, $C_{int} = C_{int+} = C_{int-}$ is the integrating capacitance, and $f_{int}$ is the frequency of $\Phi_3$. As it is seen from (7.2), as the number of integration cycles (N) increases, the output gain also increases. In other words, the sensitivity of the circuit can be adjusted by changing the ratio of $f_{int}$ and $f_s$. We will use this feature to control the sensitivity and dynamic range of the CBCM circuit.

**DC-input $\Sigma\Delta$ modulator**

The proposed $\Sigma\Delta$ modulator is realized by adding a voltage comparator, and a digital to analog converter to the described readout structures as shown in Figure 6.2b. Considering the differential architecture, two DACs, one with the negative current ($M_{13}$) and one with positive current ($M_{11}$) are added to the core-CBCM interface circuit. To implement the quantizer block, a 4-input comparator is adapted from [112] and modified for use in the CBCM circuit. Eight $\Sigma\Delta$ modulators are implemented in the array and the output bit-stream is collected and decoded using custom-made Labview data-acquisition system through an averaging routine that will be described later.

**Sensing electrodes array**

A complete capacitive sensor array is realized by integrating switches $SW^{i,j}$ , $0 < i, j \leq 8$ and 3x8 decoders as seen in Figure 6.3. The capacitive sensing electrodes, fabricated on topmost metal layer of CMOS chip play the important role of interfacing between readout circuitry and test solution. Each pixel in the array is composed of a pair of interdigitated electrodes which is patterned in M4 metal layer in TSMC 0.35 $\mu m$ CMOS technology. The dimensions of the electrode are specifically designed to fit the area constraints of CMOS chip and maximising the sensing sensitivity. The interdigitated electrode size is 50x50 $\mu m^2$, comprising four fingers with 5 $\mu m$ spacing. In order to make a direct contact with analyte solutions, the passivation layer in CMOS technology was removed in foundry process using etching techniques and the aluminum layer is used as the sensing layer. During the biological experiments, in order to protect the aluminium from direct exposure to cell culture solutions and also to provide a better electrode bio-compatibility, a thick layer of Polydimethylsiloxane (PDMS) is deposited on the electrodes serving as the passivation layer. More details about the PDMS deposition process are provided in section 5.2.6.

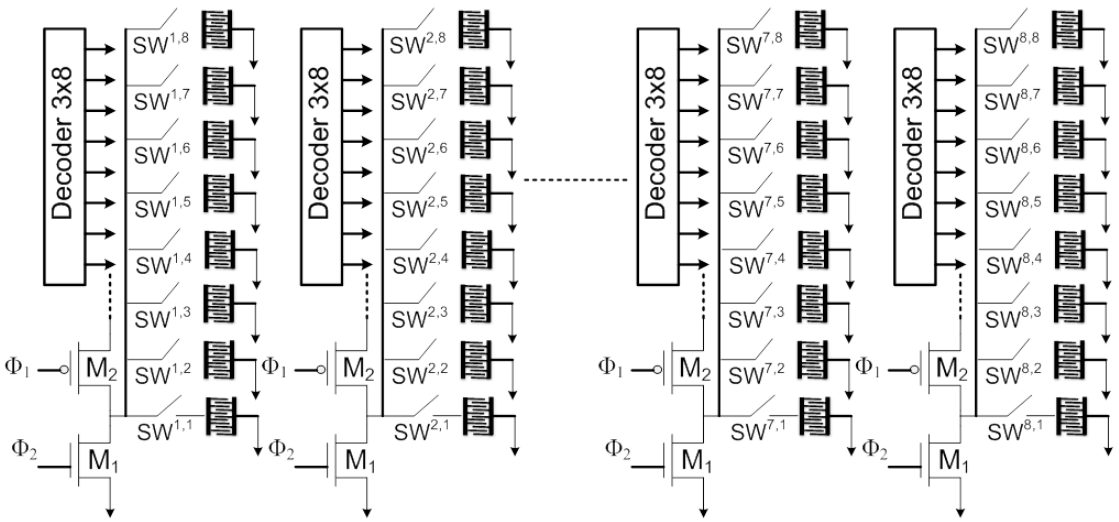


Figure 6.3: Capacitive sensor array and corresponding addressing circuit. SW switches are controlled by 3x8 decoders and they are connecting the sensing electrodes to core-CBCM circuits.

### Calibration circuitry

The dynamic range of the capacitive sensor can be significantly affected by the initial value of $C_S$ capacitors. Although the initial value is partially cancelled by the differential architecture, due to the circuit non-idealities and current mirrors mismatch, an offset value always exists at the output voltage. To cancel this offset value, we propose a novel auto-calibration method, shown in Figure 6.4a that can be applied for each individual pixel in the array. In each comparator's clock period, $V_{out}$ is compared with two threshold voltages ($V_{th-l}$ and $V_{th-h}$) that determine the upper and lower limits of output voltage, respectively. If $V_{out}$ is smaller than $V_{th-l}$, the comparator produces a digital value '1', which leads to a '1' in shift register's first output bit. The shift register's outputs are connected to a latched DAC (Figure 6.4b), once a switch is activated, a current will be added to the total current charging $C_{int+}$ at the output node. This process will continue until $V_{out}$ reaches the higher threshold value, where there will be no changes in the current sources and the total charging current will be fixed until the end of calibration phase. In an opposite scenario, if $V_{out}$ becomes higher than the upper threshold voltage ($V_{th-h}$) the discharging current will be added to the output node using latched DAC. This process repeats for all 8 channels in a single row and the calibration circuit is attached to each pixel by a 3x8 decoder. At the end of calibration phase, the calibration circuit is separated from the core circuit and the states of current mirrors is stored on the corresponding shift registers connected to each individual pixel. Figure 6.5 shows the performance of calibration circuit while adjusting the output voltage offset. In

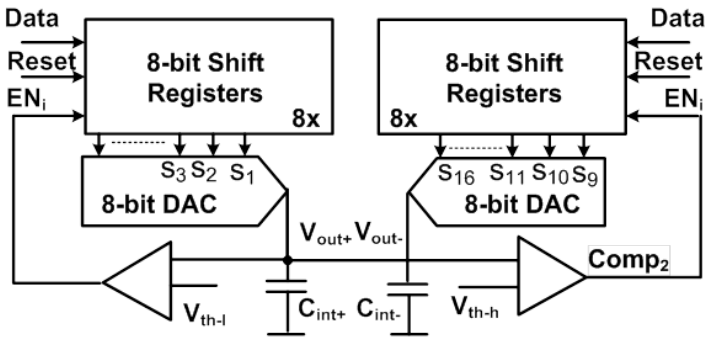


(a)

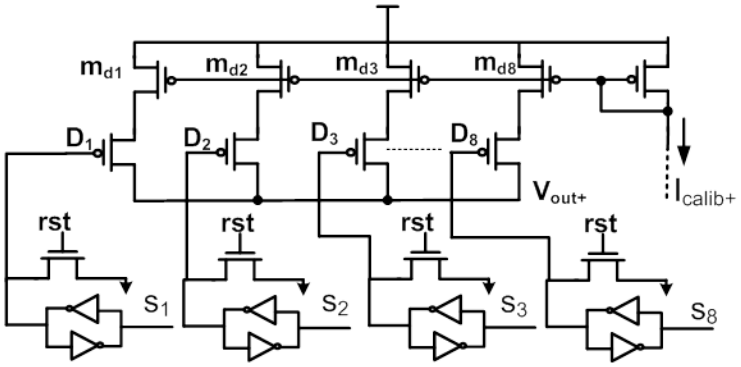


(b)

Figure 6.4: (a) Simplified block diagram of calibration circuitry. (b) Latched DAC with reset input. In each calibration clock, the output voltage is compared with the reference voltage, based on the difference with the reference voltage, the 4-bit DACs currents charging the integrating capacitors are adjusted.

this simulation, we made a 50% mismatch between the current mirror transistors ($M_6$ and $M_8$), and the value of $C_R$ and $C_S$ were selected as 50 fF. Although there is no capacitance difference, due to the mismatch, there is a 1 v offset at the output. During the calibration phase, $V_{out}$ is compared to $V_{th-l}$ and the discharging current varies accordingly and results in a lower $V_{out}$. At the end of calibration, the output voltage reaches to $V_{th-l}$ value. To find the optimum number of stages for calibration circuit, we designed three different calibration circuitries with 2, 4 and 6 stages. Thereafter the aspect ratios of current mirrors in CBCM circuit was varied to create a mismatch between the transistors. The output voltage error compared to the initial point where there is no mismatch is calculated for all three calibration circuits as well as the state where no calibration circuit attached to the CBCM. The results are shown in Figure 6.6 As seen, the 4 and 6 stages calibrations provide an output voltage with less than 11% error. Considering the area and power consumption, we have selected the calibration circuit design with 4-stage to compromise between accuracy and area.

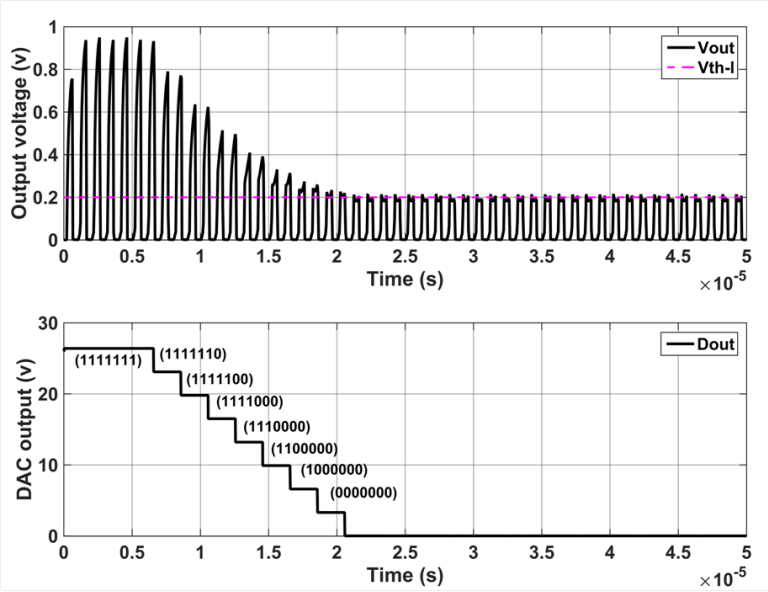


Figure 6.5: Simulation results showing the calibration circuit performance.

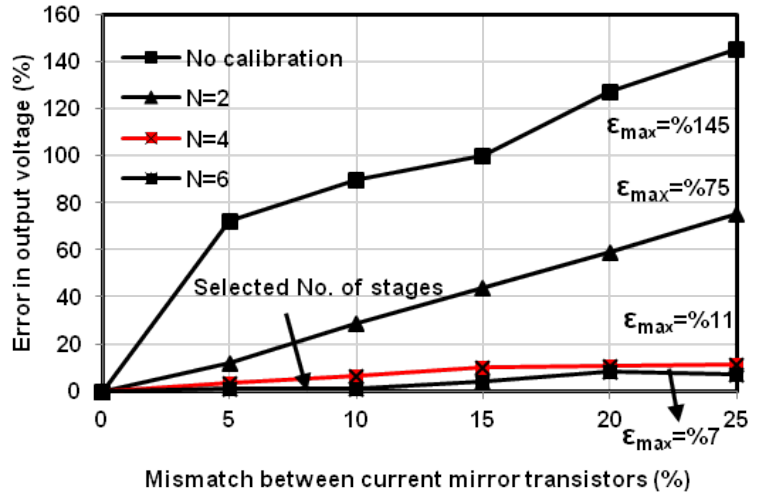


Figure 6.6: Simulation results showing the effect of number of calibration stages on the total error in output voltage caused by mismatch between current mirror transistors in CBCM circuit

### 6.2.5 ΣΔ Modulator design optimization

As previously described, by decoding the output bit-stream of ADC, the capacitance variations can be extracted. In order to study the effect of circuit's non-idealites on the overall system performance, parametric simulations can be done in circuit-level and then further decoded using an algorithm that runs in Matlab or is implemented in a FPGA platform. In

order to generate a single data for the decoder algorithm, one should run the simulations for about 100 times by changing each parameters (e.g. aspect ratio of transistors or capacitances) with 1% increment or decrement. Therefore, in order to study the effect of several parameters, the required time is very significant. Additionally the required decoding time depends on the number of bits in each stream that is a function of N (number of integration cycles). Considering above mentioned issues, in order to optimize the circuit parameters, we propose a circuit behavioral model in Matlab as discussed as follows. The proposed model has the advantage of being simpler and potentially running faster compared to Spectre simulations, allowing to run multiple parametric simulations at the same time. The fundamental equation for $\Sigma\Delta$ modulator relating y(n) to y(n-1) can be described as

$$Y(n) = Y(n-1) + X(n) - Q(n) \tag{6.6}$$

where y(n) is the output of summing node ($V_{out+}$ and $V_{out-}$), x(n) is the constant input (the output voltage variations which results in from $I_{sen+}$ and $I_{sen-}$), and Q(n) is the output of the quantizer for nth input sample ($D_{out+}$ and $D_{out-}$). The simplified block diagram of the Matlab algorithm which is developed to describe circuit behavior is shown in Figure 7.1. TQ is the sampling period ($\Phi_4$ clock pulse) and $T_{fin}$ is the final time of modulator operation (the number of generated bits for an input is equal to $\frac{T_{fin}}{TQ}$. According to the input value, different bit streams will be generated at the output of $\Sigma\Delta$ modulator. Based on this discussion, let us derive the equation for the modulator's output using the total charging current X(n).

$$X(n) = K\Delta C\frac{\Delta V}{\Delta t} = K\Delta C V_{dd} f_s \tag{6.7}$$

Assuming the digital value for X(n), is represented by Q(n), we have

$$Q(n) = K\Delta C\frac{\Delta V}{\Delta t} = K\Delta C V_{dd} f_s \tag{6.8}$$

$$Q(n) = \left\{ \begin{array}{cc} \mathrm{KC}_R V_{DD} f_s & \mathrm{Y(n\text{-}1)} > \mathrm{V}_{ref+} - V_{ref-} \\ 0 & \mathrm{Y(n\text{-}1)} \leq V_{ref+} - V_{ref-} \end{array} \right\} \tag{6.9}$$

Finally, Y(n) can be described as

$$Y(n) = Y(n-1) + \frac{TQ}{C_{int}}[K\Delta C V_{DD} f_s - Q(n)] \tag{6.10}$$

The above equation is used for building up our model. In order to optimize the performance

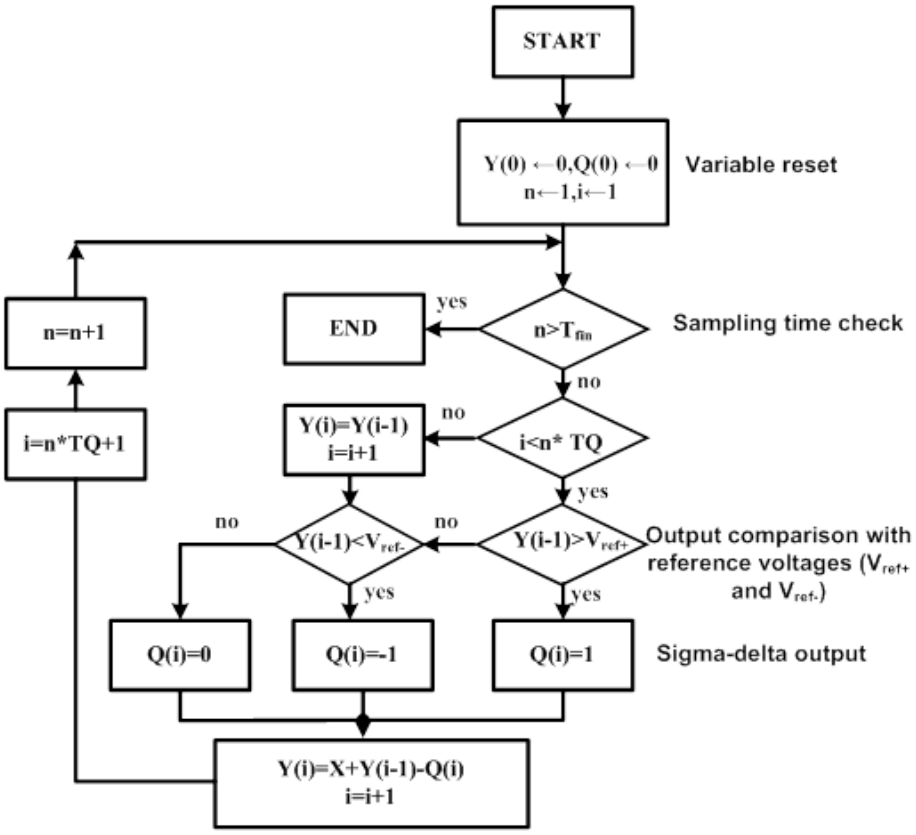


Figure 6.7: Behavioral model algorithm developed in Matlab.Y(n) is the output voltage, X is the constant input coming from sensing electrodes, Q(n) is the output of the quantizer for nth input sample, TQ is the sampling period, and $T_{fin}$ is total sampling time.

of the proposed modulator, we investigate the effect of critical circuit parameters variations on the performance of the $\Sigma\Delta$ modulator. These simulations help to find the relationship between maximum number of generated codes (resolution) and modulator parameters, including variations in integrating capacitor ($C_{int}$), the total sampling time for a fixed comparators clock frequency ($T_{fin}$), the gain of the digital to analog convertor ($G_{dac}$), and the gain of input signal ($G_{in}$). Each parameter is varied between -75% to +75%. In each run, the number of generated codes is calculated using a Matlab algorithm. The resulting curve showing of parameters is shown in Figure 6.8 and the effect of these variation is elaborated as follows.

— ***The total sampling time ($T_{fin}$)***

As shown in Figure 6.8, the resolution of the modulator strongly depends on the total sampling time. The oversampling ratio (N) is calculated as the ratio of total sampling time to comparators clock ($\frac{T_{fin}}{TQ}$). As the simulation time and hence the number of generated bits for a constant input increases, the resolution will also increase.

— ***The input gain ($A_{in}$)***

According to Eq. (6.4) and Eq. (6.5), the analog sensitivity has a linear relationship with the current mirror gain ; as the gain of the circuit increases, the variation of the output voltage for a specific charge value will increase. Although the increase in gain improves the sensitivity, but it decreases the dynamic range of modulator. For a 75% change in gain (K=16) it can be seen that the number of generated codes decreases. It is due to the fact that for a high value of the input gain, the input voltage will soon reach to $V_{DD}$ saturation voltage hence the dynamic range will be limited.

— ***The DAC gain ($A_{dac}$)***

Changes in DAC gain do not have significant effect on the number of generated codes. The only consideration is that the value of the DAC current that will be subtracted from the total input current should be larger than the input current, otherwise the modulator will not operate properly.

— ***The integrating capacitor ($C_{int}$)***

Referring to Figure 6.8, as the value of the capacitance decreases the number of generated codes increases. The analog output sensitivity has an inverse linear relationship with the value of capacitance and reducing the value of the capacitor will increase sensitivity of the circuit and hence the resolution of the modulator. It should be mentioned that the minimum value of the capacitor is limited by the total parasitic capacitances at the output node. After optimizing the circuit performance using Matlab model, the parameters are used to re-design the circuit.

After optimization procedure, we performed noise-analyses on the DC-input modulator to determine the effective number of bits (ENOB) and resolution. Theoretically, The signal to noise ratio for an oversampled ADC is obtained by [113] :

$$SNDR = 3.01 - n(2L + 1) - 9.36L - 2.76. \tag{6.11}$$

where $OSR = 2^n$ and L is modulator's order. Using above formula, the maximum value for SNDR for a 1st order $\Sigma\Delta$ modulator with OSR=128 is 51 dB which is equal to 8.25 bits resolution. The post layout SNDR measurement results for proposed $\Sigma\Delta$ modulator is shown in Figure 6.9. In this figure the modulator is measured as an standalone block and it is detached from the CBCM part. A sinusoidal waveform with a very low frequency of 10 Hz (close to DC value) is used as the input. Figure 6.9 shows the 4096-point FFT spectrum of a 10 Hz input signal with 1 kHz sampling frequency. The measurement bandwidth is 20 Hz and the oversampling ratio (OSR) is chosen as 128. The -20 dB/dec noise shaping can be seen in the FFT spectrum of output bitstream which confirms the performance of the 1st-order

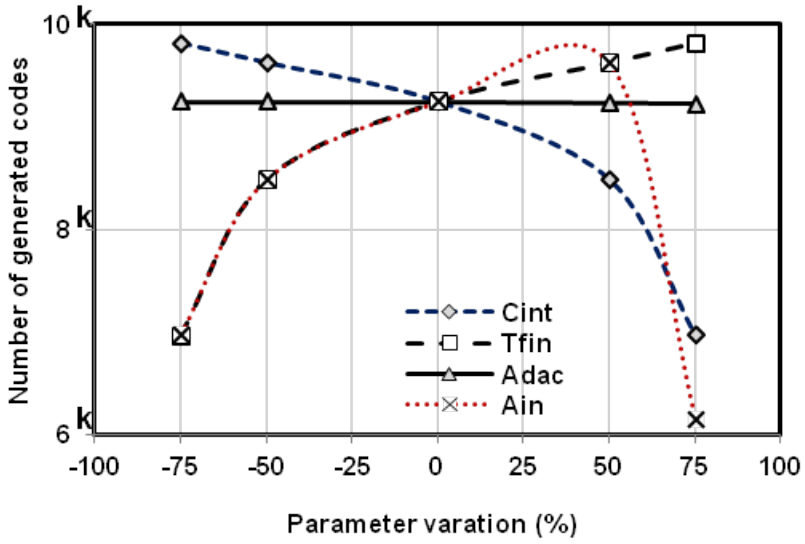


Figure 6.8: Search for optimal parameter using behavioral model. Cint is integrating capacitor at CBCM output, Ain is input signal amplification factor (the gain of CBCM current mirrors), Tfin is the total sampling time that reflects the number of stored bits and Adac is the amplification factor of DAC in modulator loop.

$\Sigma\Delta$ modulator. The peak SNDR with a -3 dBFS input is 46.2 dB which equals to ENOB of 7.4 bits. To investigate the effect of input variations on the noise shaping performance, the measurements are done for two input signals with 0 and 0.5 Hz frequencies and with amplitudes varying from $V_{FS}$ (full-scale voltage) to -60 dB below full scale input. The results are plotted in Figure 6.9. After validating $\Sigma\Delta$ performance as a standalone block, modulator is connected back to the CBCM and the SNDR measurements are done with varying the sensing capacitance's value as the input signal. The input capacitance is changed between 1 to 10 aF and the output bit stream was sampled at 1 kHz for 4096 points. The measured SNDR in this case is 45 dB which corresponds to the resolution of 7.2. bits. Considering the Full scale supply voltage, the minimum detectable output voltage variation with 7.2 bits is 22 mV. Since the sensitivity of CBCM circuitry is designed at 320 mV/fF, for 10 aF variations, we have 32 mV changes in the output voltage, which is more than the minimum detectable value by $\Sigma\Delta$ modulator. In other words the capcaitance variations less than 10 aF can be detected with the modulator. To validate the resolution of proposed circuit, post-layout simulations were performed where the input capacitance is varied between 0 to 6 fF and between 0 to 100 aF. The analog output coming from CBCM and digital output of $\Sigma\Delta$ modulator are plotted in Figure 6.10. As shown in this figure, the readout circuitry allows the detection of small capacitance values of as low as 10 aF.

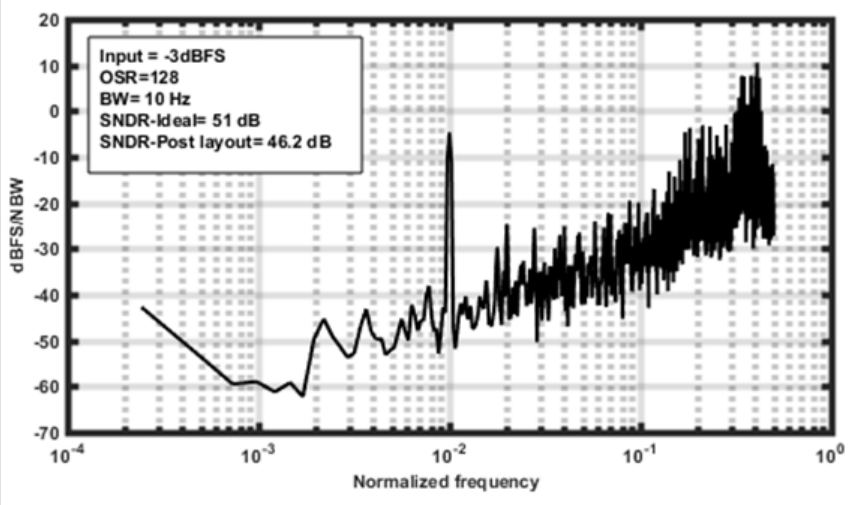


Figure 6.9: Post layout results : FFT waveform for the DC-input modulator with OSR=128 and sampling frequency of 1 kHz.

### 6.2.6 Experimental results

This section demonstrate and discuses the chip fabrication and packaging, test setup and results. We show the experimental results of the fabricated chip and validate its functionality using three approaches. At the first step, we show the chip characterisation results in response to various organic solvent and then we expose the chip to different concentration of polystyrene beads with the same dielectric properties as the living cells. Finally we show the response of the chip to the adherent H1299 cell lines.

#### Chip fabrication and measurement setup

The proposed integrated biosensor array is fabricated using a commercial CMOS process, TSMC (Taiwan Semiconductor Manufacturing Company, Hsinchu, Taiwan) that has a minimum feature size of 0.35 $\mu m$ and operates at a nominal power-supply voltage of 3.3 V. The overall system architecture and chip photograph are shown in Figure 6.12. The 3 x 3 $mm^2$ chip is comprised of a 8 x 8 array of sensing pixels. Each pixel contains a interdigitated capacitive electrode which is connected to a readout interface via switches controlled by digital control circuitry. As seen in Figure 6.12a, the chip is packaged and mounted on a slave PCB and the then it is connected to the main PCB where control signals are provided and output signals are recorded through a data acquisition system. There are eight analog outputs from the chip and eight digital outputs coming from the eight $\Sigma\Delta$ modulators. An FPGA platform is programmed through Labview FPGA module for data acquisition.

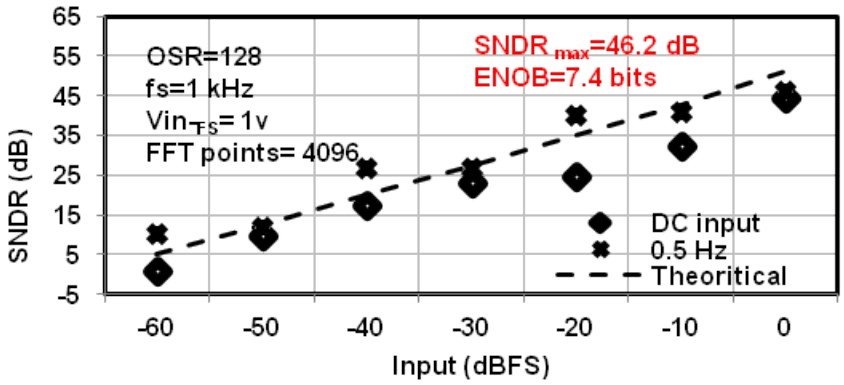


(a)

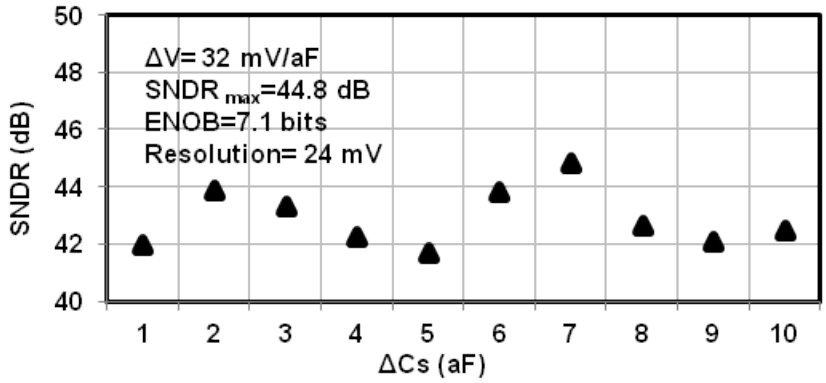


(b)

Figure 6.10: Post layout simulations : (a) SNDR for two inputs with DC and 0.5 Hz frequencies and for amplitudes varying between 0 to -60 dBFS. (b) SNDR measurement for input capacitance values between 1 to 10 aF.

### Data acquisition and ΣΔ modulator decoding

A data acquisition is implemented using a Virtex 5 FPGA system. To maximise the sampling frequency, three DMA (Direct Memory Access) FIFOs are used. The system allows to reach a maximum sampling frequency of 450 kHz for analog signals and 100 kHz for digital signals. The reading from the eight sensors in one column is performed simultaneously and recorded data is interlaced in the FIFOs. Signals are deinterlaced from the FIFOs, reconstructed and analysed using a specially designed standalone program made with LabView software. The amplitude measurement of each CBCM waveform is performed using a standard LabView Virtual Instrument using maximum and minimum values found in the 1 ms period. A 3-bit multiplexer is used to retrieve the digital data associated with eight different sensors in each column.

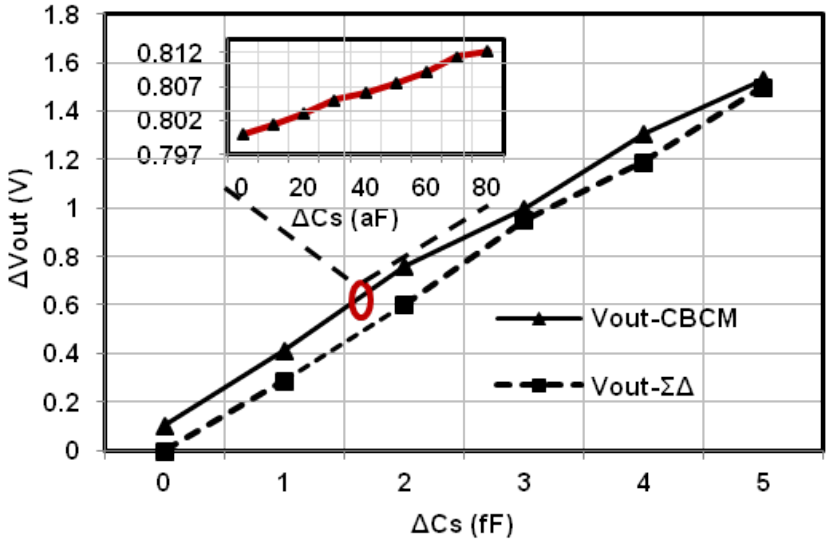


Figure 6.11: Post-layout simulations : output voltage for sensing capacitance variations between 0 to 6 fF and 0 to 100 aF.

### Chip protection and bio-compatible packaging

To protect the topmost metal layer (Al) from direct exposure to cells and biological side-effects, a very thin layer of the PDMS is spin-coated on top of the electrodes. This layer offers the advantages of biocompatibility, ease of processing, and chemical inertness. To avoid sensitivity reduction, the PDMS membrane should be as thin as possible. The final thickness of PDMS membrane depends mainly on spin coating speed, spinning duration and the ratio of PDMS parts. To reach the maximum sensitivity of the sensor, we chose PDMS thickness of less than 1 $\mu m$ for our application. The two parts of PDMS are mixed in 10 :1 ratio and the mixture is steered by hand for 5 minutes. Thereafter the mixture is placed under the vacuumed desiccators until all the bubbles are gone and the PDMS mixture is completely degassed. In the next step we took a very small droplet of mixture using a micropipette and pour it above the CMOS chip. Using tapes, the chip was fixed on a Petri dish as a container and it was spin-coated at the speed of 3000 rpm for 20 minutes. Finally, the fixture is placed in the oven at 80 °C to cure the PDMS membrane. The required spinning time and speed to reach the desired thickness was extracted from the data provided in [114]. Following PDMS deposition, a bio-compatible, high temperature epoxy resin (EPOTEK-353) was used to protect the the bonding wires and electrical connections from biological solutions. A small plastic ring is adhered on top of the packaged chip, as a micro-well, for containing the cell culture medium. To test the bio-compatibility of epoxy resin, a simple test was done where several cell culture dishes were coated with the epoxy and the cell viability

was optically observed for 2 days. The results confirmed the bio-compatibility of the selected epoxy. It was essential to clean and sterilize the CMOS chip, before culturing the cells on the electrode surface. The chips were first washed with Isopropanol (IPA) for 15 min to dissolve any possible contamination. Thereafter, they were washed with sterile distilled water and then were exposed to Ethanol for 15 min. In order to activate the surface of electrodes, they were treated in plasma cleaner for 3 min followed by 5 min UV-cleaning for sterilization. Treatment of the electrodes with plasma helps cells to attach better to the bottom of the wells. After UV sterilization all the future steps were done under the biological hood and in sterile condition.

### Chip calibration

To validate the calibration circuit performance, we changed the reference voltage (the input of calibration circuit) from 0 to 2V and the response of the 64-pixels was measured at the end of calibration phase. Figure 6.13 shows the calibration results were the average error in output voltage (which means the difference between final output voltage and determined reference voltages) is reported. For the sake of comparison, the post-layout simulation results and ideal curve are shown in this plot as well. The measurement confirm that the final average error for the calibration circuitry is less than 15.1%.

### Sensor response to organic solutions

To evaluate the response of the sensor to organic solvents, we introduced polar chemical solvents with different dielectric constants, namely : Isopropanol, Methanol, DI water and cell culture media which is an extremely ionic solution. Prior to test, the sensor was cleaned using DI water and then was dried on a hot plate to avoid residues remaining from the former tests. The real-time response of sensor to 200 $\mu l$ of these solutions at room temperature is shown in Figure6.14a. For the sake of comparison, the output of analog channels and also the decoded $\Sigma\Delta$ modulator bit streams are shown in the same figure. As seen, for the higher dielectric constant, the higher output voltage is achieved at the sensor's output. Although DI water and culture media have the same dielectric constants, the culture media is extremely ionic and that is why there is a noticeable variation in their responses. To show the capacitive sensor sensitivity, various dilution rates of Methanol in DI water was prepared and the real-time response of the sensor at different working frequencies was measured. The results are shown in Figure 6.14b. As the frequency increases, the output voltage variations get smaller and sensitivity decreases, leading to a higher dynamic range. This means that by having a tunable working frequency, one would be able to compromise between the sensitivity and

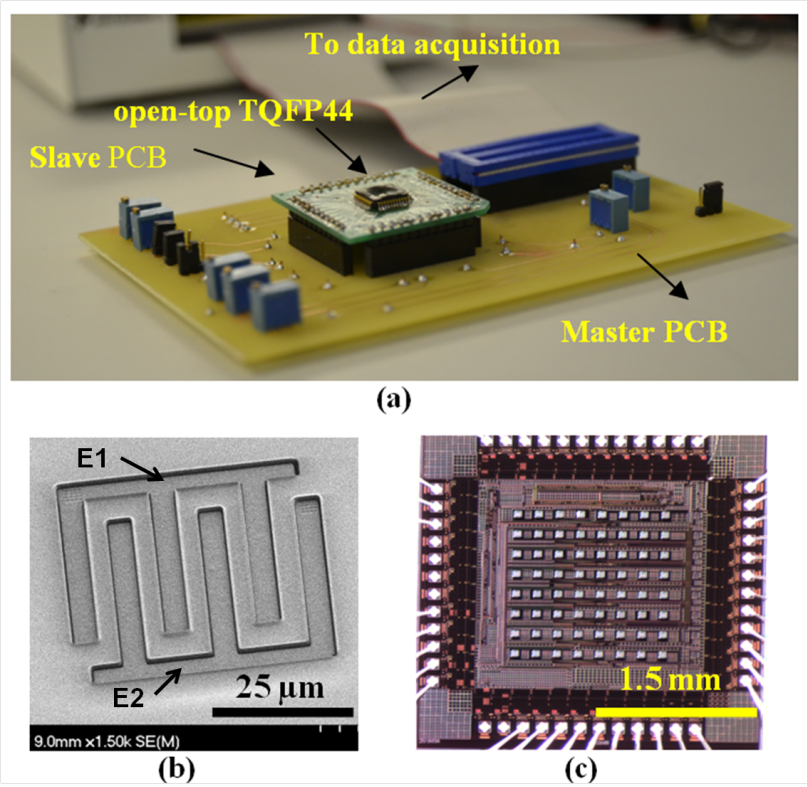


Figure 6.12: Test setup and die images. (a) Assembled devices on PCB. (b) SEM image of interdigitated electrodes, two pairs of interdigitated electrodes are shown as E1 and E2. (c) Die microphotograph.

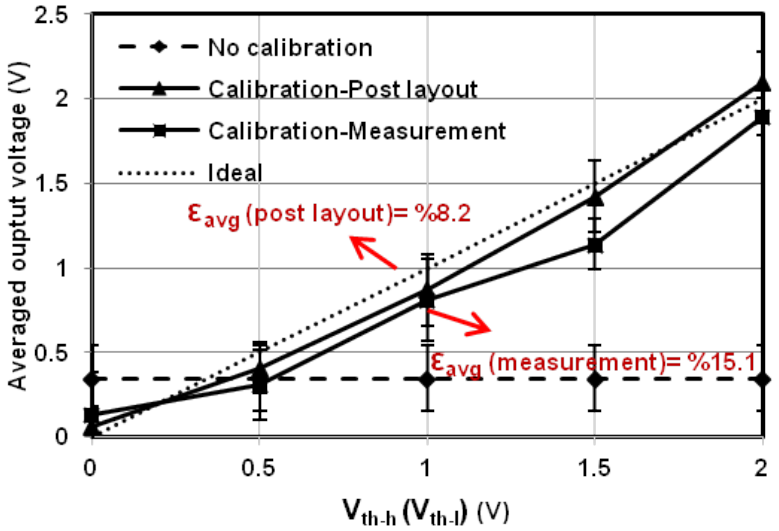


Figure 6.13: Measurement results showing the performance of the calibration circuit.

detection range for a particular application and the properties of the solution that is under the tests. This features makes the device capable of detecting cells with different concentrations. The results shown in Figure 6.14 prove the functionality of the propose device. As expected, for the high dielectric constant values, the higher output voltage is observed. For this reason, in Figure 6.14a, using DI water rather than Dichloromethane results in the higher average output voltage. In the other hand, as seen in Figure 6.14b, the higher percentage of Methanol, results in a lower dielectric properties in comparison with the dielectric constant of DI water, and consequently a lower output voltage is observed.

### Polystyrene beads response

In the next step, we exposed the chip to the various concentrations of Polystyrene beads diluted in DI water. Polystyrene microparticles are negative charge stabilized colloidal particles with approximately the same electrical properties as living cells [115]. The average diameter of the beads were 10 $\mu m$. Various samples with different dilution rates were prepared ranging from 10 beads/ml to 10k beads/ml and the response of the chip to each solution was monitored for 20 min. At the beginning of the experiment, the particles were suspended in the water but as the time passed by, more number of beads were deposited on the electrodes which resulted in an increase in the output voltage of the sensors. The response of the individual pixels to the 1k beads/ml concentration is shown in Figure 6.15.

The average output of device with 64 pixels using four different dilutions is shown in Figure 6.16. At the end of 20 min no significant change was further seen and the system reached to an stability. It is worth mentioning that after each step, the chip surface was thoroughly rinsed with DI water and sodium dodecyl sulfate surfactant (SDS) to remove the remaining residues of the beads over electrodes. These residues could potentially lead to an measurement error. All the experiments were carried out in the triplicates and the average values are reported. Figure 6.16 shows the functionality of all 64 sensors. Each color approximately represent the number of beads on the electrode. This is due to the fact that the higher number of beads, results in a higher dielectric constant in the proximity of the sensors. As the beads randomly distribute over the chip, any set of colors can be expected. This low complexity test not only show the functionality of the proposed system, but also it might be used in other applications such as microfluidics and dynamic studies of the beads in liquids.

### Cell culture results

A human lung carcinoma cell line, namely H1299, was chosen for the growth monitoring. The cells were first grown to confluent in RPMI medium. After two days the cell layers were

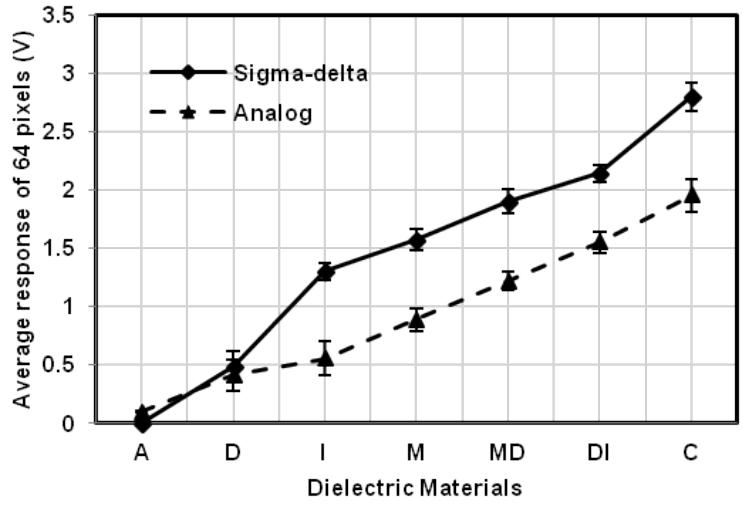


(a)

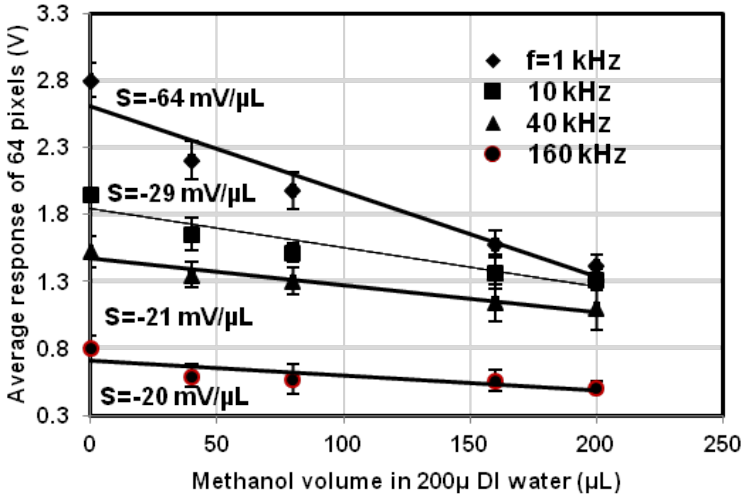


(b)

Figure 6.14: Sensor response to organic solvents, (a) the average response of the 64 pixel array to various chemicals including : A : Air, D : Dischlromethane, I : Isopropanol, M : Methanol, MD : Methanol dilution, DI : Deionized water, C : Culture media. "Sigma-delta" shows the decoded value of bit-streams coming from the output of $\Sigma\Delta$ modulator and "Analog" refers to the analog output voltage at integrating capacitor's node. (b) Sensor response to the dilutions of Methanol in DI water at different working frequencies (S refers to the slope of curves).

rinsed with phosphate-buffered saline (PBS) with pH 7.4 (Sigma Aldrich). Then, Trypsin-EDTA solution (0.25% Trypsin and 1 mM EDTA ; Sigma Aldrich) was used to detach the cells and RPMI Medium with 10% fetal bovine serum (FBS) was supplemented to the dispersed cell layer. The cell cultures were maintained at 37° C under 5% $CO_2$ in incubator. Based on the well size on the CMOS chip, appropriate aliquots of the cell suspension were diluted to the

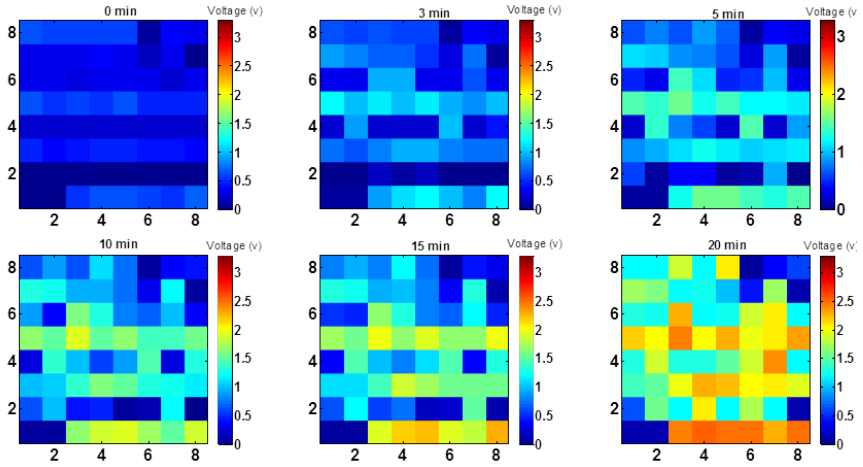


Figure 6.15: Response of the chip to Polystyrene beads diluted in DI water, 1 k beads/ml concentration is shown.

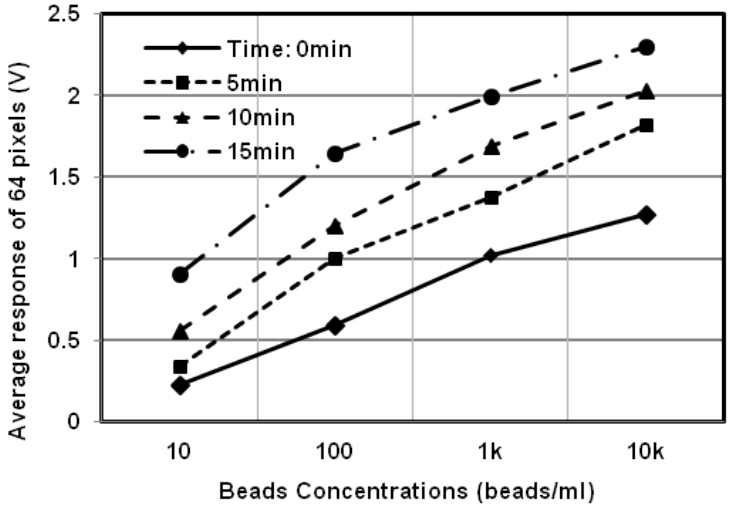


Figure 6.16: Response of the chip to Polystyrene beads diluted in DI water, from 10k beads/ml to 10 beads/ml dilutions are shown.

concentration of 100 kcells/ml. Then 200 $\mu l$ of cell suspension in the media was transferred to the well on top of the CMOS chips. The cell number was counted using Scepter$^{TM}$ 2.0 Digital Cell Counter (Milipore). To avoid contamination, the readout platform and associated interface circuit was placed under the biological hood during the measurements. Four CMOS chips were tested and each CMOS chip was monitored for 24 hours, and the data were sampled every 2 hour.

Figure 6.17 shows the response of the chip to the 100 k cells/ml dilution over 12 hours. As demonstrated in this figure, in first 4 hours before cell adhesion to the electrodes, there is

Table 6.1: Comparison of the proposed capacitive biosensor array with the state-of-art

| Ref. | Application | Method | Tech. ($\mu m$) | No.Electrodes | Sensing layer | ADC | Resolution |
|---|---|---|---|---|---|---|---|
| [101] | Cell proliferation monitoring | Charge-sharing | 0.35 | 16 | Si3N4 | No | 200mv/fF |
| [103] | Bacteria growth monitoring | CBCM | 0.18 | 3 | Aluminum | Sigma-delta | 250 mV/fF (6bits) |
| [115] | Cell manipulation | Electrophoresis | 0.35 | 32x32 | Gold | No | NA |
| [69] | Neurotransmitter dopamine | Capacitance to frequency conversion | 0.35 | 5x5 | Sio2 | No | 1 fM |
| [116] | Bacteria detection | Capacitance to frequency conversion | 0.25 | 16x16 | Al2O3 | No | 55 mv/fF (37 dB) |
| **This work** | Cell growth monitoring | CBCM | 0.35 | 64 | Aluminum +PDMS | Sigma-delta (8-channel) | 350 mV/fF (46 dB) |

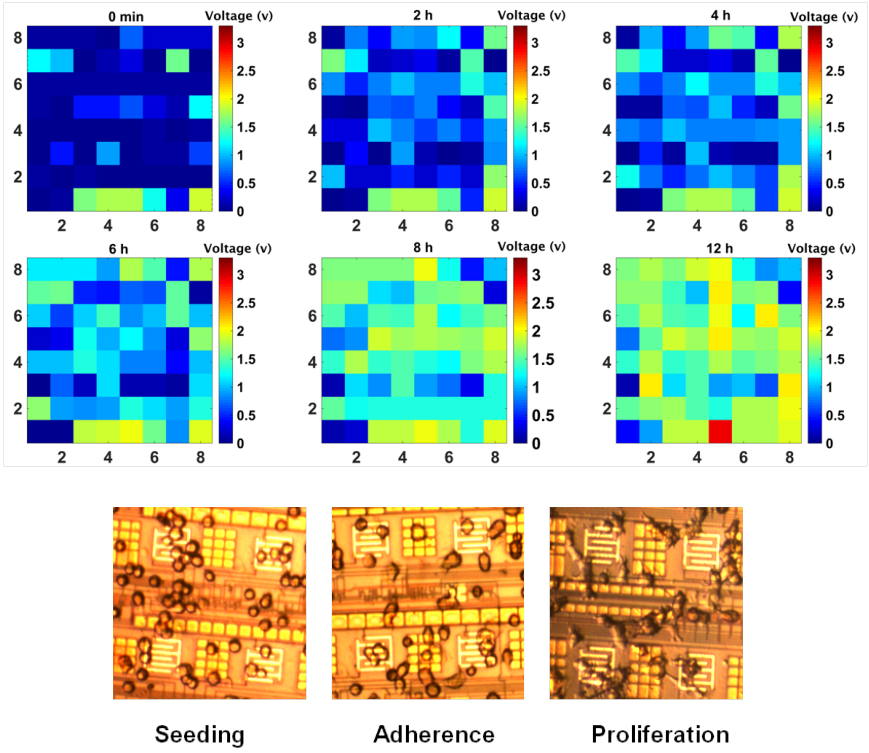


Figure 6.17: CMOS chip response to 100 k cells/ml for 12 h.

a small increase in the value of output voltage. As cells attach to the electrode, and start spreading over the electrode surface, the output voltage increases accordingly. Since the partial evaporation of media can affect the measurement accuracy, a loose cap was used on top of the well which provides gas exchange between cells and incubator environment and at the same time protects the media from evaporation. Moreover, due to the high humidity of incubator, the effect of evaporation is negligible and can be discounted in the measurements. To validate the chip results with a standard cell assay, Alamarblue was used. Alamarblue is a fluorometric/colorimetric growth assay that is based on the metabolic activity of the cells. The oxidation-reduction indicator in the assay fluoresces and changes color in response to the chemical reduction of growth medium resulting from cell growth. To measure the cell

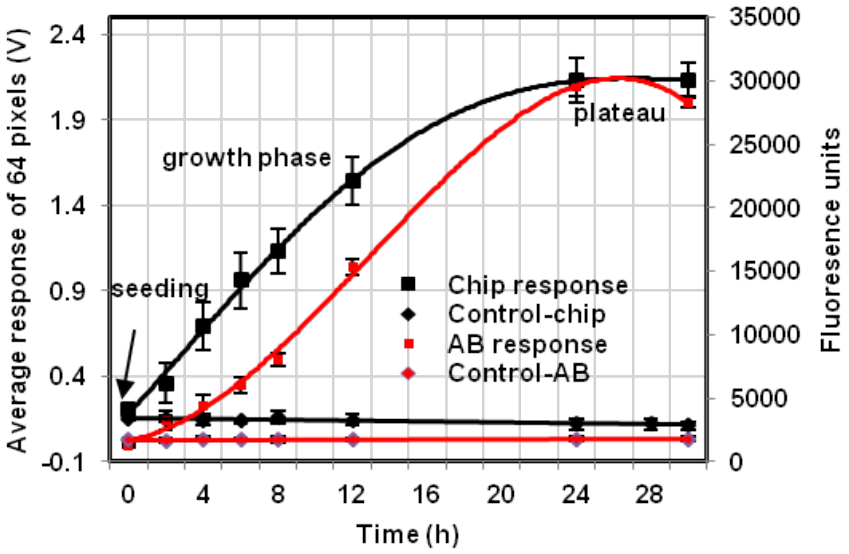


Figure 6.18: Comparison of the CMOS chip results and Alamarblue results for the same concentration of the cells.

growth rate using Alamarblue, the cells were harvested in the log phase and then diluted to the desirable concentration (100 k cells/ml). Thereafter, 200 $\mu l$ of the cell suspensions and 10 $\mu l$ of Alamarblue were added to the 96-well plates. The wells were kept in incubator and the fluorescence was measured by using a spectrophotometer, every 2h, for 24 hours. The fluorescence measurements were performed with excitation wavelength at 570 nm and emission wavelength at 600 nm. The CMOS chip results and Alamarblue readings are illustrated in a same graph in Figure 6.18. It is seen that after 8 hours the cells in the chip and in the wells have entered the log (exponential) phase and there is a noticeable increase in the slope of both curves. The graph shows a consistency between two results and the chip could successfully detect two phases (lag and log) in cell growth curve. Comparing these results with the results of our first prototype, shown in Figure 6.1c, confirm the success of the new capacitive sensor array in cell growth detection and cell screening application. As the continuation of this work, we are working towards the implementation of a high-throughput microfluidic structure to study the cells in micro-wells individually. A summary of proposed capacitive biosensor specifications as well as its comparison with the state-of-art is provided in Table 6.1

### 6.2.7 Conclusion

In this paper we presented an 8x8 capacitive sensor array for cell growth monitoring. The proposed device consists of 64 interdigitated electrodes fabricated in topmost metal layer of

0.35 $\mu$m CMOS technology. Each row of eight electrodes is connected to a core-CBCM capacitance to voltage converter incorporated with a DC-input $\Sigma\Delta$ modulator. We demonstrated the device functionality using various organic solvents with different dielectric constants. Moreover, the response of the sensing chip to polystyrene beads which have the same dimension and electrical properties as living cells are shown. Thanks to the high sensitivity of readout interface, the chip is able to detect the presence of single beads on the electrodes. Due to the design simplicity and compactness, the platform can be used as an efficient tool for cell monitoring purposes. The experimental results including the cell culture results on each single electrode of 64-electrodes array demonstrate the applicability of the proposed device for high-throughput screening of cellular activities suitable for a variety of life science applications such as drug discovery.

### 6.2.8 Acknowledgment

The authors would like to thank Laurent Mouden for chip packaging and wirebonding, Prof. Michael Buschmann for providing the cell lines, Prof. Marc Lavertu and Yuan Chang for technical support on cell culturing and Alamarblue experiments.

# CHAPTER 7 CHEMICAL INTERFACES TECHNIQUES AND MICROFLUIDIC PACKAGING

## 7.1 Overview

This chapter of the thesis mainly focuses on the cell analyses results and drug cytotoxicity monitoring. In this chapter a new functionalization technique employing polyelectrolyte multilayers (PEMs) is proposed. To allow high throughput measurements, a new approach for microwell fabrication and integration with microelectronic parts of the platform is proposed and its advantages and drawbacks are discussed. This chapter is the reproduction of an article submitted to IEEE Transactions on Biomedical Engineering.

— G. Nabovati, E. Ghafar-Zadeh, A. Letourneau, and M. Sawan, "A Fully Integrated Cell Imaging Platform for Real-Time Assessment of Living Cells", Submitted to IEEE Transactions on Biomedical Engineering (TBME).

## 7.2 Article 3 : A fully integrated cell imaging platform for real-time assessment of living cells

### 7.2.1 Abstract

We present in this paper a novel CMOS Based Smart Petri dish system for label-free monitoring of adherent mammalian cells activities. This system consists of an array of 8x8 capacitive sensors incorporated with a CMOS fully integrated readout circuit. The proposed re-configurable capacitive readout circuit with a wide dynamic range output allows the tracking of cellular activities using various initial cell concentrations ranging from 10 to 200 kcells/ml. For this purpose we developed a new polyelectrolyte encapsulation method for enhancing cell-CMOS biocompatibility. Given the fact that this encapsulation method improves the cell viability ; the proposed low-cost biosensor can measure the capacitance changes affected by cellular activities for more than three consecutive days using two different cell lines including Hek293 (human embryonic kidney cells) and H1299 (human lung carcinoma cells). In this work, we demonstrate the advantage of the proposed system for drug cytotoxicity as well as cellular growth monitoring purposes. In these experiments, standard Alamarblue cell-based assay is used as a control and Geneticin selective antibiotic (G418) is chosen as a cytotoxic drug introduced to non-resistant H1299 and resistant Hek293 cell lines. Furthermore, a new low complexity technique for microwell fabrication and integration is proposed

that allows the multiple assay monitoring. With the potential to perform label free cellular analysis, the proposed platform opens up an avenue to transit from traditional to smart cellular analysis techniques that can be applied in a variety of biological applications.

*Index Terms- CMOS, Cell-based Sensor, Cell Growth, Capacitance, Cytotoxicity, High Throughput Screening.*

### 7.2.2 Introduction

Recent advances in micro- and nano-technologies have enabled the development of High-Throughput Screening (HTS) techniques for various applications including drug discovery [117]. Owing to the seminal advances in micro-fabrication technologies, HTS is moving towards massively parallel, miniaturized, and label free platforms. The state-of-the-art DNA sequencing platform featuring millions of Ion-Selective Field Effect Transistors (ISFETs) has convincingly demonstrated the advantage of using standard microelectronic technologies such as Complementary Metal Oxide Semiconductor (CMOS) process in HTS applications [118]. Similarly, many researchers addressed the challenge of developing HTS Systems for monitoring cellular activities on a single chip. Due to the significant advantages of CMOS-based biosensors, such as non-invasive long term recordings, fast response and label free process, they have been widely applied in many biological and medical fields concerning the studying of the living-cell samples such as neural cell recording and stimulation [119–121], monitoring metabolic activity [122], cell manipulation [115, 123], and extracellular pH monitoring [124, 125].

Another important application of cell-based biosensors is the study of cell viability, proliferation and morphology. In this regard, CMOS-based impedance and capacitance based techniques are proposed that operate based on adhesion of the cells and measuring the capacitive coupling strength between the cells and sensing electrodes [117, 126, 127]. In this direction, Ghafar-Zadeh *et al.* proposed a capacitive sensor for real-time bacteria growth monitoring in which by using a CMOS capacitive sensor incorporated with a micro-channel, the growth of E. coli bacteria in an LB medium can be detected [65]. In another work in [57] a capacitive sensor based on the charge sharing principle is proposed which enables the proliferation detection of various cell types including bovine aortic smooth muscle cells and breast cancer cells. A summary of integrated Lab-on-Chips for various cell-based applications and selected publications is mentioned in Table 7.1.

The advantage of all mentioned standard microelectronic technologies, particularly CMOS, is the fact that they allow a monolithic integration of large numbers of micro-sensors along with their associated electronic circuitry for creating a single device capable of replacing an entire

chain of classical bioanalysis devices present in contemporary labs. Despite great advances of CMOS based HTS systems for monitoring the cellular activities, a few researchers have reported the design and implementation of CMOS HTS systems for cytotoxicity monitoring [128–132].

Table 7.1: A summary of integrated cell-based platforms

| **Application** | **Technique** | **CMOS Technology** | **Array Size** | Ref. |
|---|---|---|---|---|
| Recording | MEA | 0.5um | 64x64 | [120] |
| | MEA | 0.18um | 455 | [121] |
| Manipulation | Dielectrophoresis | 0.35um | 10k | [115] |
| | Magnetic | 0.18um | 8x8 | [123] |
| Acidification | ISFET | 1um | 40 | [124] |
| | ISFET | 0.5um | 16x16 | [125] |
| Adhesion | Capacitive | 0.35um | 12 | [57] |
| Cytotoxicity | Optical | CMOS/LED | 4 | [131] |
| | ECIS/Optical | 0.13um | 16 | [132] |

In all aforementioned research works using CMOS for monitoring cellular activities, particularly for cytotoxicity monitoring and drug screening, the researchers aim to develop a kind of fully automated high throughput CMOS systems or so called Smart Petri dishes.

Despite great efforts, Smart Petri dish technology is in early stage of development and there are several challenges that should be investigated. Herein we take a step towards this technology by developing a cell-based CMOS capacitive sensor array. The proposed system consists of integrated CMOS sensors working based on a fully differential charge-based measurement technique and is fabricated using TSMC 0.35 $\mu m$ standard CMOS technology.

Figure 7.1 shows the processing steps to prepare the fabricated chip for cellular analysis. For this purpose, we propose a new surface modification for the CMOS chip to increase cell adhesion property, which is based on alternate adsorption of oppositely charged polyelectrolytes. This paper reports the advantage of the proposed sensor for cellular analysis including cell viability studies, growth measurement, and drug cytotoxicity. The proposed device can successfully track the response of Hek293 and H1299 cell lines to Geneticin selective antibiotic. As for control experiments, we use Alamarblue viability reagent as a conventional method [133, 134] to validate the results. It is noteworthy that Alamarblue, Trypanblue, Microtitration (MTT) and other fluorescence techniques are widely used for cellular analysis and metabolism studies [135, 136]. However these conventional methods are time consuming, and they require labeling/preparation steps and off-chip optical setups. On the contrary, the proposed platform requires no additional steps, provides continuous measurements with unprecedented levels of accuracy and leads to an exceptional reduction in costs per each biological experiment.

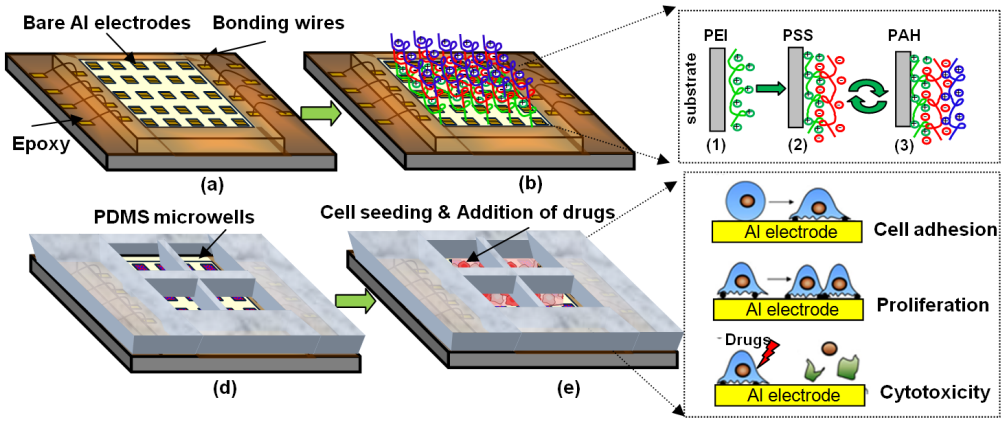


Figure 7.1: Simplified illustration of proposed cell-based biosensor and the preparation steps : (a) Packaging and wirebonding, (b) Layer-by-layer (LBL) coating, (c) Microwell implementation (d) Cell seeding, incubation, and monitoring.

### 7.2.3 Capacitive sensor design and fabrication

#### Cell-based capacitive sensing, operation principle

Figure 7.2 shows the proposed custom-designed CMOS capacitive sensor for cell monitoring. This sensor consists of sensing electrodes interconnected to underneath charged based interface circuit. The top most metal layer forms these sensing electrodes. Let us assume a single cell is attached on the top of electrodes and exposed to a low frequency electric field. The attached cells on the surface can vary the double layer capacitance which is formed between the electrode-electrolyte interface ($C_{bond}$). The presence rather than absence of the cells results in a minute capacitance change $\Delta C$ in between two electrodes. Despite the fact that $\Delta C$ is very low, a high precision capacitive readout circuit can be efficiently used for this purpose. It is noteworthy that $\Delta C$ depends on the cell morphology and cell position as well as cell-surface binding [137]. Among these, the cell-surface binding is influenced by various biomolecules coated on the surface of electrodes as well as the drug molecules in the cell culture medium. The healthier the cells are, the stronger bond exists between the electrodes and the cells. Therefore it results in a higher dielectric change. On contrary, introducing certain drugs or toxic substances that may damage the cell-surface binding or the cell membrane, results in a poor capacitive coupling. Additionally, an ionic polarization occurs around the cell membrane in the presence of an electric field as seen in Figure 7.2b. This ionic polarization leads to creation of an extra capacitance $C_{cell}$ [138]. A seen in Figure 7.2b, there is another capacitance ($C_{med}$) arisen from the coupling between cell growth solution and the other existing conductors excluding the sensing capacitors. Since this capacitance

has a constant value and does not change with the cell adhesion, it can be neglected in the calculations. It is worth mentioning that in this analysis, only the total capacitance resulted from cell-surface adhesion is of interest, thus we have neglected the resistance models for the sake of simplicity.

**High throughput capacitive sensor array**

For cellular studies, it is important to have a high throughput platform that allows monitoring of a large number of cells with different conditions at the same time. To meet this requirement, we have developed an array of 8x8 capacitive sensors implemented in 0.35 $\mu m$ technology for cell viability and proliferation detection. The simplified system block diagram of the proposed sensor is depicted in Figure 7.2a. The capacitive sensor array is composed of five parts including row /column decoders, sensing electrodes, capacitance to voltage converter, analog to digital converter and calibration circuitry. The supply voltage is fixed at 3.3. V. The sensing electrodes are implanted by miniaturized interdigitated microelectrode built on the topmost metal layer of CMOS chip in 0.35 $\mu m$ technology (Metal-4). The dimensions of the electrode are specifically designed to fit the area constraints of CMOS chip and to maximize the sensitivity. The pixel size is 50x50 $\mu m^2$ comprising 4 fingers. Each finger has 50 $\mu m$ width and 50 $\mu m$ length and the gap between the fingers is 5 $\mu m$. To enhance the sensitivity, the passivation layer on the electrodes was removed in the foundry process using dry-etch technique. Later on to improve the cell adhesion and extracellular matrix formation, a thin layer of polyelectrolyte membrane was deposited. The system is composed of 8x8 array of capacitive sensing electrodes as well as 8 reference electrodes which is shared between the pixels in a row. Each row of electrodes is connected to a readout interface, which works based on the charge based capacitive measurement technique (CBCM) which was previously proposed by our group in [104]. The readout interface is shown in Figure 7.2b. The capacitive electrodes are connected to two charging and discharging transistors. The current charging the capacitive electrode is described as

$$I_S^{i,j} = C_S^{i,j} \frac{dV_{SE}}{dt} = \beta(V_{DD} - V_{SE} - V_{thp})^2 \tag{7.1}$$

where $V_{DD}$ is a power supply voltage, $V_{SE}$ is the voltage drop on sensing capacitor, $V_{thp}$ is the pMOS threshold voltage, $V_{DD} - V_{SE}$ is $M_2$ gate-source voltage, $0 < i, j \leq 8$, and $\beta$ is transistors parameter and is equal to $\mu_n C_{ox} W/L$ where $\mu_n$ is the surface mobility of charge carrier in MOS device, $C_{ox}$ is the gate insulator capacitance and $W/L$ is MOS transistor's aspect ratio. This current is then amplified by a programmable gain current mirror. The variable gain current mirror helps to remove any offset voltage resulted from the fabrication

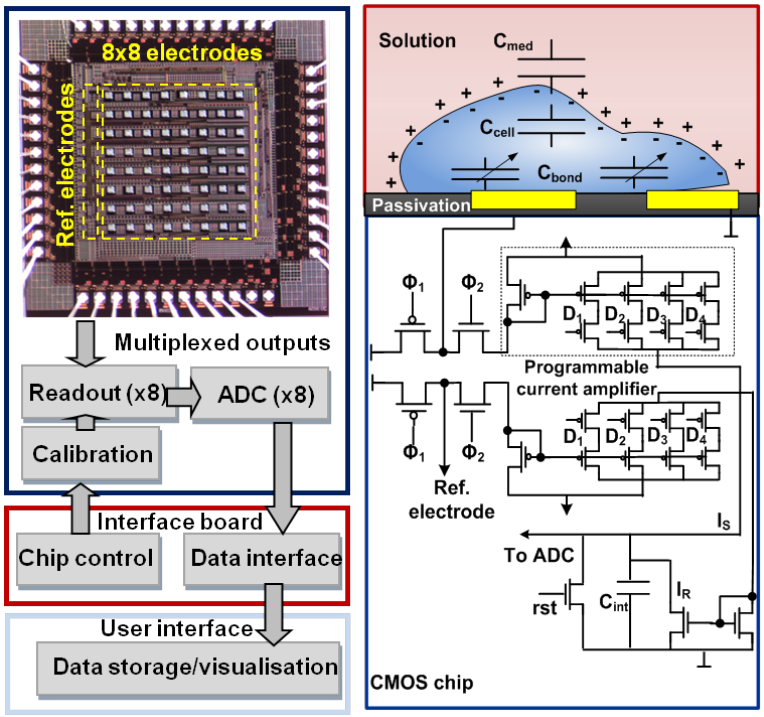


Figure 7.2: (a) System-level block diagram of proposed cell analysis chip. (b) Circuit implementation and cell-electrode capacitance model.

process and transistors' mismatch. Using the current equation, the output voltage at the integrating capacitor's node can be obtained as

$$V_{out}^{i,j} = \frac{2K\Delta C^{i,j} V_{DD} f_{int}}{C_{int} f_s} = \frac{2K\Delta C^{i,j} V_{DD} N}{C_{int}} \tag{7.2}$$

where $\Delta C^{i,j} = C_S^{i,j} - C_R^i$ and $f_s$ is the frequency of $\Phi_2$, $C_{int} = C_{int+} = C_{int-}$ is the integrating capacitance, and $f_{int}$ is the frequency of *rst* clock signal. The sensitivity and dynamic range of the proposed circuit can be adjusted by changing the ratio of integration frequency ($f_{int}$) to sampling frequency ($f_s$). The output voltage from CBCM circuitry enters an 8-bit $\Sigma\Delta$ modulator for analog to digital conversion which is described in details in [104].

### Chip fabrication and packaging

The chip is fabricated using standard CMOS 0.35 $\mu m$ TSMC technology. On return from the foundry, the loose dies were wirebonded on a TQFP44 open top package. The chips are bonded and packaged in a two-step process. A biocompatible epoxy (EPOTEK 353-ND) is first used to stabilize the bonds on the chip and the package and to cover any electrical

connections. Thereafter, Polydimethylsiloxane (PDMS) is used to form a well, isolating the bonding wires from the cells and containing the cell growth solution (Figure 7.1). The sensor readout is controlled by digital signals coming from FPGA platform which is controlled by LabVIEW and provides various working frequency from 1 to up to 100 kHz. This variable working frequency allows reaching the maximum detection limit and sensitivity based on the analyte type or cell concentration.

### 7.2.4 Integrated capacitive electrodes : protection and functionalization

Although CMOS process has several advantages such as the possibility to integrate the readout circuitry and sensing electrode and substantial increase in the electrodes density, it suffers from a main drawback for biosensing application, which is the use of aluminum alloys as the metal layers. Due to its limited stability and poor biocompatibility the aluminum electrodes are not suitable for biological and chemical applications. Therefore, a coating procedure is essential to protect the electrodes from being in direct contact with biological solutions and to promote a better cell-electrode adhesion. Among various techniques that exist for metal electrodes functionalization, the build-up of polyelectrolyte multilayer (PEM) films is one of the well-established and efficient techniques [139, 140]. Due to strong electrostatic interaction between PEMs of opposite charges, PEM coating has long-term stability and more importantly the thickness of the coating can be carefully controlled by varying the number of PEM layers or their chemical properties such as pH and salt concentration. Although this method is widely used for different materials such as gold and PDMS, no attention have been paid on using the PEMs on the aluminum electrodes in CMOS technology. Our team reported the coating of CMOS chip using polyelectrolyte in order to quantify the accuracy of integrated capacitive sensors for the detection of ultra thin polyelectrolyte layers [93]. Herein for the first time we explore the possibility of using this method as a means to coat integrated aluminium electrodes for improving their biocompatibility.

The ultra thin multilayers of charged molecules are performed through alternatively introducing the dilute aqueous solutions of positively and negatively charged PEMs to the aluminum electrodes (Figure 7.1b). The first layer is positively charged polyethyleneimine (PEI) layer which is formed on the surface of the CMOS chip as precursor base layer to initiate the sequential adsorption of the weak PEMs. This layer is followed by polystyrene sulfonate (PSS) and polyallylamine hydrochloride (PAH) layers. The electrodes layer-by-layer coating procedure was first preceded by a cleaning step in which the CMOS chips were washed with Isopropanol for 10 min followed by rinsing with ultrapure water. In first stage of deposition, the chips were incubated with pre-curser film, PEI (5mg/ml, Sigma Aldrich), for 20 min.

After this period, the chips were extensively rinsed by distilled water water. Thereafter The polyanion (PSS) (5mg/ml, Sigma Aldrich), and polycation (PAH) (5mg/ml, Sigma Aldrich), layer were alternatively adsorbed forming 5 polyelectrolyte bi-layers PEI-(PSS-PAH)5. For each layer formation, the chip was incubated for 10 min followed by extensive distilled water rinsing. In this work, 5 bi-layers are stacked up. Studies show that the thickness of polyelectrolyte membranes strongly depends on several parameters such as pH, salt concentration, and temperature [141]. It is also proved that the use of NaCl in polyelectrolyte solutions, leads the formation of thicker layers. To make sure that the cells are not in any contacts with the possibly toxic PEI layer, salty solutions of the PEMs (with 0.5 M NaCl) were prepared to ensure the full coverage of PEI layer by consequent PSS/PAH layers. In section 7.2.7, we put forward the detailed procedure to study the the toxicity effect of PEI on cells. We will also examine the optimum number of polyelectrolyte layers for achieving the best aluminum biocompatibility.

### 7.2.5 Microfluidic packaging and microwell fabrication

Significant advances have been made in combining cell culture and microtechnology insights to develop emerging biological instruments. Microtechnologies such as hybrid microfluidic and CMOS microelectronic technologies offer great advantage of low sample consumption, automation by running multiple biological protocols a and real-time monitoring of living cells over a long period of time. Despite significant advances, there are several practical challenges to develop hybrid microfluidic CMOS platforms. These challenges are the post-CMOS processing and packaging of hybrid microfluidics and CMOS chip [142].

Herein we propose a new alternative microfluidic packaging solution. Our solution relies on the use of flip-chip bonder for alignment and attachment of microfluidic fabricated structure on the sensing device. To enable the device for potential high throughput cell screening, we have fabricated a 4-well PDMS-glass microfluidic structure that allows the monitoring of the cells at very small volumes (1 $\mu l$) (Figure 7.3a). The microfluidic structure is composed of three layers, PDMS, PDMS, and glass. To pattern the layers, a mask-less laser-based method was used. In this method, the microwells layout was created using Autocad software, thereafter the wells were directly patterned on PDMS and glass by using a laser machine. The profile of microwells strongly depends on the laser power, intensity distribution of the laser beam, cutting speed, and the number of cutting passes; the latter determines the depth of micro wells as well. The optimum parameters were extracted experimentally and by exploring various laser setting combinations. The details of fabrication steps are as follows (Figure 7.3b-f).

1. The PDMS was prepared with a 1 :10 ratio and then it was spin coated on a Petri dish to form a uniform layer with the thickness of around 0.5 mm. Thereafter the PDMS samples were cured on a hot-plate at 80 $^{\circ}C$ for 2 hours.
2. The PDMS sheets were patterned and cut using the charge-pump laser machine. The top glass layer with the thickness of 0.2 mm was also patterned and cut.
3. The layers were thoroughly rinsed and cleaned using Acetone, Isopropanol, and distilled water followed by drying using nitrogen gas.
4. The loose dies were packaged on open-top TQFP-44 packages and then placed and fixed by a tape on a vacuum plate.
5. Using the flip-chip bonder, the first PDMS layer was picked up by the vacuum nozzle and was placed on the die by careful alignment using two cameras on the device. The two other layer were also picked up and stacked on the first layer. Having two cameras mounted on the device makes it possible to see the die and PDMS position at the same time and to align them with a very high precision
6. Using the femto pick and place nozzle, the layers were pressed on the die with a 5 N force. While pressing the layers to remove any excess air between the layers, the hot-plate was turned on, and the epoxy resin was carefully poured around the layers by a syringe. The soft PDMS layer under the influence of applied 5 N force will create a temporary hermetic bonding with underneath substrate so that it prevents the leakage of epoxy resin underneath of PDMS layer
7. Epoxy was cured for 2 hours at 80 $^{\circ}C$. While the epoxy was curing, the nozzle was constantly pressing the layers.
8. After the epoxy was completely cured, the chip was removed from the hot-plate while gradually moving up the nozzle and removing the pressure.

### 7.2.6 On-chip cell culture protocol and cytotoxicity monitoring experiments

Hek293 and H1299 cells were grown to confluence in EMEM and RPMI medias, respectively. The cell layers were briefly rinsed with phosphate-buffered saline (PBS), then, Trypsin-EDTA solution (0.25% Trypsin and 1 mM EDTA) was used to detach the cells under standard trypsinization procedure, and the suspension was refreshed and diluted to a suitable extent by centrifuging/re-suspension procedures. Afterwards, EMEM and RPMI medias with 10% fetal bovine serum (FBS) and 1% antibiotic (Penicillin/ Streptomycin) were supplemented to the dispersed cell layer. Prior to cell culturing, the chips were cleaned with Isopropanol and Ethanol and then were rinsed with ultrapure water. The surface was dried under air flow

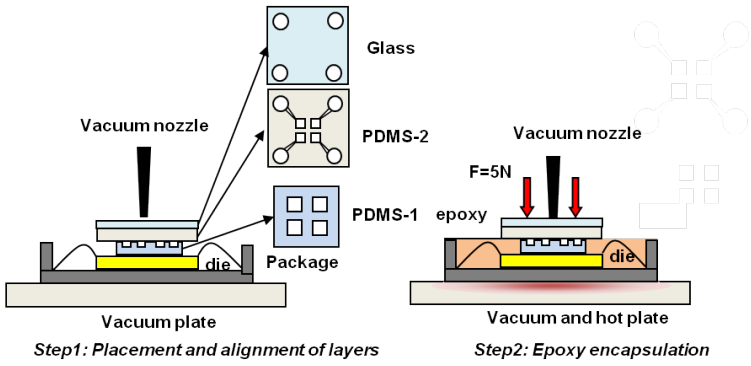


(a)

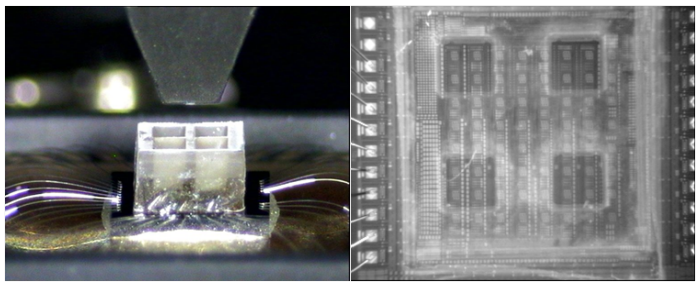

(b) (c)

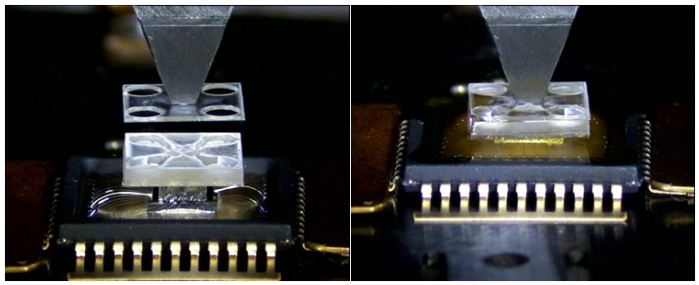

(d) (e)

Figure 7.3: (a) Schematic overview of microwell integration with CMOS chip. (b) Placing the first PDMS layer using the flip-chip bonder, (c) PDMS layer alignment on the sensors, (d) Top glass layer placement. (e) Pressing the layers and applying epoxy to cover the wire-bonds and to attach the layers while the chip is on a hot-plate.

and they were sterilized under UV radiation for 3 min. Then 200 $\mu l$ of the cell suspension were seeded into the chips. The chip were placed in the $CO_2$ incubator (37 $°C$, 5% $CO_2$) and the sensor's data were collected every 2 hours.

### Alamarblue assay

To validate the functionality of the proposed CMOS chip, Alamarblue was used as the control experiment. Alamarblue is a cell viability reagent that is used to asses cell viability and pro-

liferation. The active ingredient of Alamarblue is Resazurin which is a nontoxic naturally non-fluorescence blue compound. Upon entering the cell solution, Resazurin is reduced to Resorufin, which produces very bright red fluorescence. Viable cells continuously convert Resazurin to Resorufin, thereby generating a quantitative measure of viability and cytotoxicity [134]. Through all the experiments, Alamarblue was added as 10% of the sample volume (i.e., added 20 $\mu l$ Alamarblue reagent to 200 $\mu l$ sample), followed by a 1 to 2 hours incubation at 37°$C$. After incubation, the resulting fluorescence was measured on a fluorescence spectrophotometer. Fluorescence readings were made in triplicates using a Tecan plate-reader. Excitation and emission wavelength were set respectively to 570 and 600 nm and gain was fixed to 70.

### Cell concentration monitoring

One of the applications of proposed cell-based biosensor is cell concentration and viability monitoring. For this purpose, CMOS chips were first packaged and encapsulated following the same protocol in section II. Thereafter, the aluminum electrodes on the chip were functionalized by 5 polyelectrolyte bi-layers ($PEI(PSS/PAH)_5$) and a single PDMS microwell was attached to carry the cell growth solution. After following cleaning and sterilization process, The various concentrations of H1299 cell-line including 10 k, 50 k, 100 k and 200 k cells/ml were prepared by diluting the initial cell concentration in pre-warmed media. The cell concentration was first measured by a digital cell counter and thereafter 200 $\mu l$ of the cell suspension was transferred to the well and the response of the chip was monitored every 2 hours for the total time of 30 hours. The average capacitance variations for 64 pixels was measured in these experiments.

### Monitoring the effect of Geneticin Selective Antibiotic (G418, 50 mg/ml) on cell behaviour

Geneticin is an aminoglycoside known to block protein synthesis in both eukaryotic and procaryotic cells. Because many cellular activities such as adhesion, growth, and division require the production of proteins, this antibiotic interferes with the cell's normal life cycle. In genetic engineering, G418 is commonly used for selecting cells that have successfully uptaken a plasmid during a gene transfect process. Indeed, transfection plasmids often include a resistance gene to a specific antibiotic, such as Geneticin. The later addition of this antibiotic in the culture media can ensure that only effectively transfected cells can survive and divide thus providing an isogenic population. According to manufacturer protocol, selection doses usually range from 0.1 to 2 mg/ml for a 100 kcell/ml culture. At low concentration, cell di-

vision is slowed down and at intermediary dose, cells stop growing. At higher concentrations (above 2 mg/ml for cell lines used here), membrane damage becomes clearly visible, due to the lack of structural protein synthesis which leads to cell's death. This membrane deterioration changes the electrical properties of the cell, which can be detected by the sensors. While low doses can let non-resistant cells live for more than a week, high doses generally show significant effects in less than three days. The Hek293 cell line used in this study had already been transfected with Clontech EGFPLuc plasmid which leads to the production of green fluorescent protein along with resistance to Geneticin. H1299, however, were not resistant to this antibiotic. This genetic difference along with various concentration of Geneticin were used here to provoke different reactions and monitor them with both capacitive and biochemical/optical (Alamarblue) methods described as below.

**On-chip cytotoxicity test**

In the cytotoxicity experiment using the CMOS chip, cells in the stationary phase after plating were used. The initial concentration of cells seeded on the cell chip was 200 k cells/ml. Four CMOS chips were prepared in which two of them contained H1299 cells and the other two contained Hek293 cells. After 24 hours of cell seeding, two of the samples containing H1299 and Hek293 were treated with 5% dose of Geneticin and other two chips were remained untreated as a control sample. The response of the chip was recorded for three consecutive days and the condition of cells was also observed optically.

**Alamarblue cytotoxicity test**

In order to validate the CMOS chip results, the Alamarblue assay tests using the same toxicant concentrations were conducted. Cells were suspended in media at 100 kcells/ml concentrations and transferred on a 96-well plate (200 $\mu l$ per well). Alamarblue was added in wells one hour prior to measurement to allow the reduction reaction to occur. Fluorescence readings were made in triplicates using a micro-plate reader. Excitation and emission wavelength were set respectively to 570 and 600 nm and gain was fixed to 70. Cells were incubated for 24 hours and thereafter they were treated with Geneticin. For the sake of comparison, some control wells were prepared with the same cell concentration but without adding Geneticin.

**Aluminum biocompatibility experiment**

This experiment is performed to examine the biocompatibility induced by adding polyelectrolyte film on aluminium. For this, the confluency of cultured cell on bare and polyelectrolyte-

coated aluminium sheets was determined using ImageJ software. A cleaned aluminium tape was adhered at the bottom of conventional Petri dishes and half of the surface was then covered using scotch tape. In the next step, Layer-by-Layer (LBL) deposition was performed as described earlier and stopped at various steps to determine the best combination of anchor layer, number of bilayer, and the type of terminating layer for cell culture. Scotch tape was removed and dishes were sterilized using a UV sterilizer (3 min, 75% intensity) after which 3 ml of media containing 100 K Hek293 cells were added. At 24 and 48 hours marks, dishes were rinsed with sterile PBS to get rid of poorly attached cells and media was replaced. Pictures were taken after the second rinse using a fluorescence microscope and the the cells' confluency was measured in coated and no-coated aluminum layers.

### 7.2.7 Results and Discussions

#### Polyelectrolyte encapsulation

In this section we present the measurement results of CMOS chip coating by polyelectrolyte films. Prior to measuring the presence of ultra-thin layers on electrodes, a control experiment was performed to show the advantage of multiple ultrathin layers of polyelectrolyte materials for cell viability which was described earlier. Figure 7.4a shows a standard Petri dish and a two-sectioned aluminum tape. This simple device was used to culture 100 k cells/ml concentration of Hek293-GFP cells and to compare the cell confluency in both parts of aluminum sheet. As fluorescence imaging results show, the coated section of the aluminium sheet has a noticeably higher number of cells compared to the bare section. In this work, we coated the aluminum sheets with various combination of ultrathin layers including PEI only, PEI(PSS/PAH), PEI(PSS/PAH)PSS, PEI(PSS/PAH)3, PEI(PSS/PAH)3PSS, PEI(PSS/PAH)5, and PEI(PSS/PAH)5PSS. In total, seven different combinations of polyelectrolyte coatings were prepared and tested in triplicates. The cells were seeded on the standard Petri dishes and after 48 h the percentage of cell confluency on aluminum layers was measured using a fluorescence microscope. To account for the possible errors in the cell concentration, the relative cell confluency for each Petri dish was calculated by dividing the confluency of the coated aluminum half by the confluency of the bare aluminum half (Figure 7.4c). As reported in some studies [143], PEI is not a suitable coating for cell culture and the addition of this anchor layer leads to an decrease in cytocompatibility. Here, low number of layers also generally did not significantly change the biocompatibility of the surface. However, tests with 5 bilayers and PSS terminating layer showed a statistically significant (p-value under 0,05) increase in covered area, attesting that the surface modification performed here improves cell adhesion and growth. Comparison between coatings' parameters also revealed that for

a fixed number of bilayers, PSS terminating layers always leads to better results than PAH ones. The deposition of PEMs can therefore improve cytocompatibility of aluminium surface. Based on these experiments the optimum multilayer was chosen as $PEI(PASSPAH)_5PSS$.

To measure the thickness of the formed polyelectrolyte layer, usually AFM , ellipsometry or contact angel measurements are used. However, all this methods require complicated lab tools and procedures, Herein, we take advantage of our highly sensitive capacitive sensor to detect the formation of the polyelectrolyte films. The build up of PEMs was observed by changes in the sensors output voltage. The adsorption of oppositely charges polyelectrolytes results in a dielectric change above the capacitive electrodes which decreases with the number of adsorbed layers. During the adsorption process polyanion/polycation complexes are formed with the previously adsorbed polyelectrolyte layers leading to a charge reversal. Applying a capacitor model, the observed decrease can be quantitatively explained by assuming reduced electrostatic screening by mobile charges inside the PEMs compared to the bulk medium outside [144]. The adsorption of the negatively charged PSS to the positively charged electrodes, leads to an decrease of the surface potential whereas the subsequent adsorption of the positively charged PAH increases the surface potential. A slight signal decrease with increasing the number of layers is observed which is caused by the screening of the newly adsorbing charges by mobile ions inside the polyelectrolyte film [145]. Compared to conventional methods for detecting polyelectrolyte films formation and measuring the number of layers, the direct measurement of surface charge using highly sensitive capacitive sensor allows for the quantitative investigation of PEM formation and its properties. The response of the sensor varies based on the type and number of layers on the sensing electrodes. Figure 7.4d shows the measurement results for the average of 64 pixels and for three CMOS chips.

### Cell viability monitoring

In this section we show the cell concentration and viability monitoring using proposed capacitive sensor. We also demonstrate and discuss the measurement results of standard Alamarblue assay in comparison with the results of proposed device. We performed the same experiments in standard 96-well plates and the same concentrations of cells were seeded into the wells in triplicates. Figures 7.5a and 7.5b show the resulted data from both experiments. Based on the cell-electrode model described earlier, when cells adhere and proliferate on the surface of sensing electrodes, due to the capacitance coupling between the cell membrane and electrodes ($C_{bond}$) and also the polar capacitance in the cell structure ($C_{cell}$), the capacitance value across the electrodes changes. This theory confirms the results obtained from cell viability and cell concentration monitoring. For a larger number of cells attached on the electrodes,

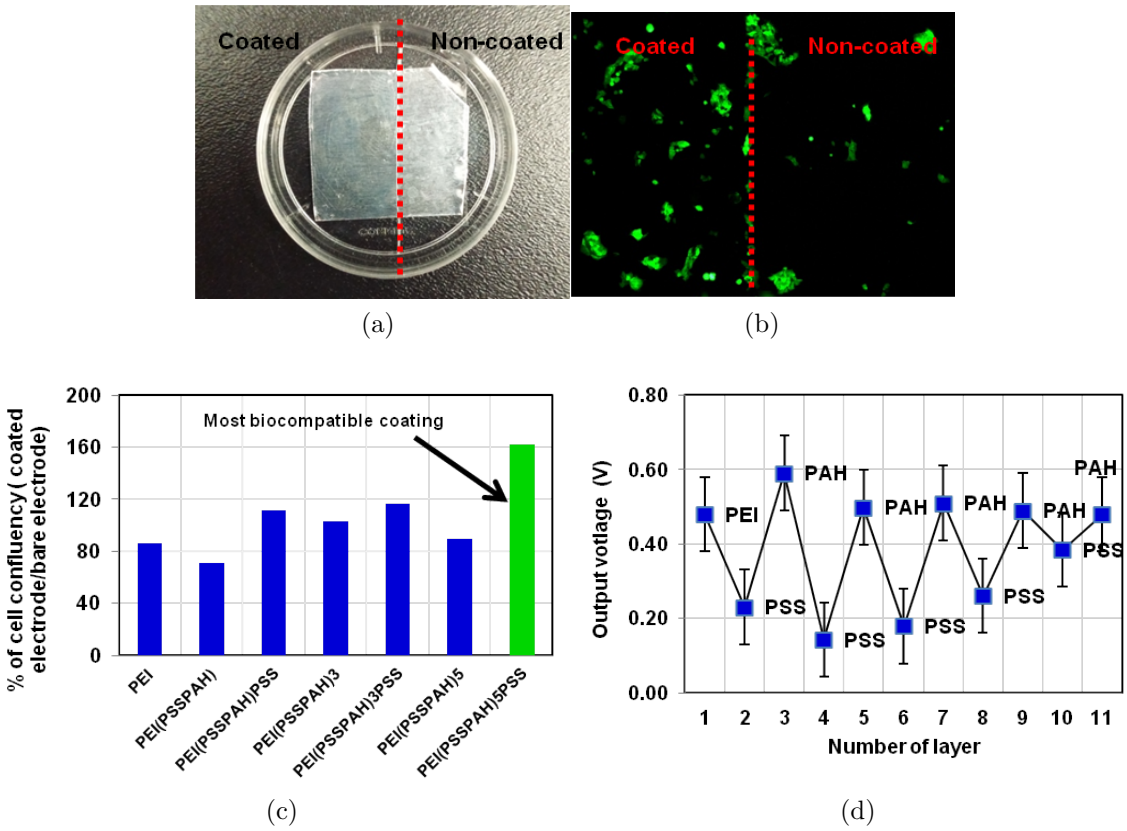


Figure 7.4: PEM bio-compatibility test on aluminium layers, (a) The aluminium sheet half-covered with the PEM, (b) Fluorescence image of GFP cells cultured on the surface. (c) The cell confluency measurements for various PEM coating combinations. (d) Detecting PEM formation on CMOS chip using capacitive sensor.

the higher capacitance change is observed. As more cell attachment becomes stronger, they start growing over the surface and the associated capacitance value become higher, until it reaches a plateau. Figure 7.5a shows the measurement result of the CMOS chip; as it is expected, for higher concentrations, the higher number of cells have covered the electrode surface resulting in a higher capacitance changes. Due to the random deposition of the cells on the electrodes, for 10k cells/ml only a few cells were placed on the electrodes, resulting in a very small capacitance changes. For higher concentrations, the capacitance changes can be easily distinguished between various concentrations of 50 k, 100 k and 200 k cells/ml. In fact, from the relationship between the capacitance change and cell number, it is possible to measure live or dead cells by measuring the output voltage variations.

The results of Alamarblue viability assay are shown in Figure 7.5b. Higher number of cells resulted in a higher reduction in Alamarblue and hence a higher fluorescence values over time.

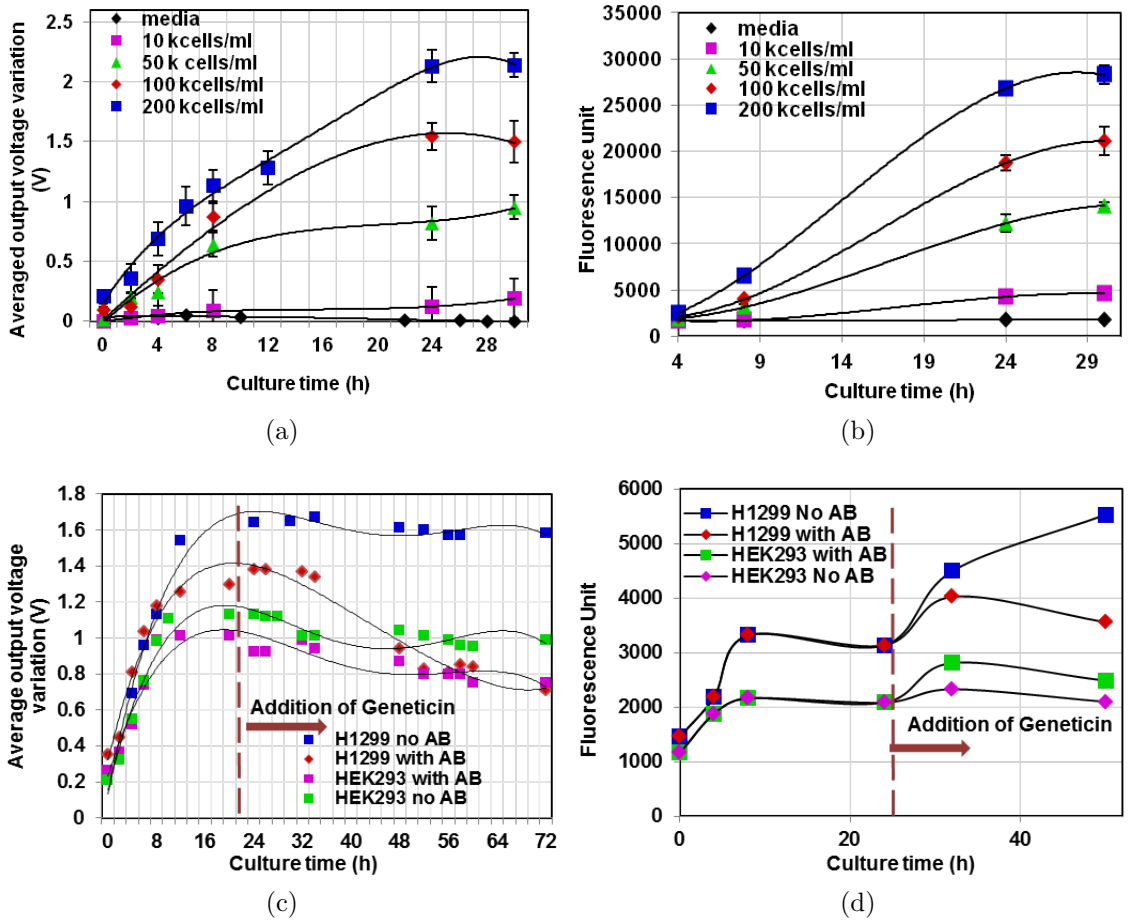


Figure 7.5: (a) CMOS chip results showing the response of capacitive sensors to various concentrations of H1299 cell lines, (b) Alamarblue results showing the cell concentrations, (c) CMOS chip results showing the effect of Geneticin on cell growth for resistant Hek-293GFP and non-resistant H1299 cell lines, (d) Alamarblue results showing the effect of Geneticin on cell growth for resistant Hek-293GFP and non-resistant H1299 cell lines.

### Cytotoxicity monitoring using Geneticin selective antibiotic

The Geneticin cytotoxicity test was performed using the protocol described earlier. Cells were allowed to grow to confluence and then they were treated with appropriate dosage of Geneticin. The samples were monitored for three consecutive days and as expected, Geneticin induced a large decrease in growth rate of H1299 cells but had no significant effect on Hek293 cells. In fact the damage in H1299 membrane caused by the Geneticin leads to a weaker bond between the cells and the electrodes, resulting in a drop in $C_{bond}$ values. On contrary, for untreated H1299 samples, the cells continued growing and proliferating over the capacitive electrodes, giving rise to the output voltage value. For Hek293 samples, as shown

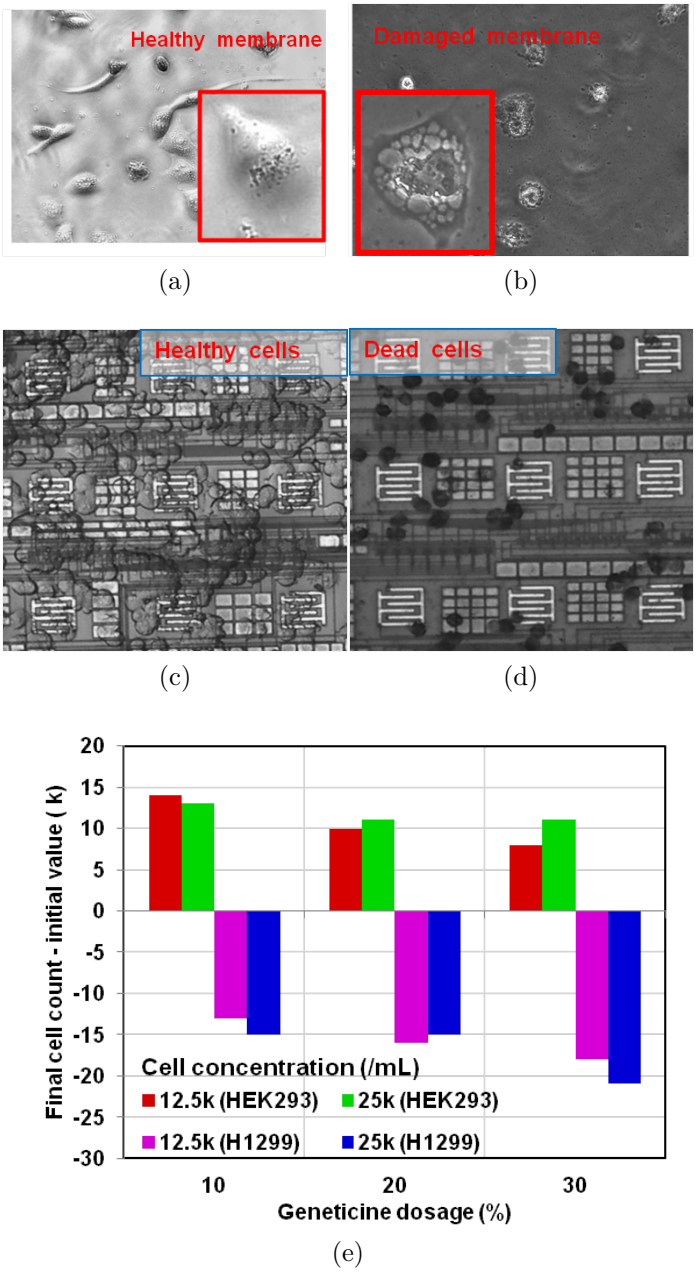


Figure 7.6: Optical observation of cells in (a) Standard Petri dish (before addition of Geneticin), (b) Standard Petri dish (24 hours after addition of Geneticin), (c) Smart Petri dish (before addition of Geneticin), (d) Smart Petri dish (24 hours after addition of Geneticin). (e) Cell counting results showing the effect of antibiotic on cell number after 48 hours.

in Figure 7.5c, no significant difference was observed between drug-treated and untreated samples which confirms their resistance to this type of antibiotic. This fact can be justified by cell-electrode capacitance model. Upon introducing the drug to the cells, it will start damaging the membrane which will consequently loosen the capacitive bond between the cells

and the electrodes and resulting a drop in the measured capacitance. On the other hand, since the drug inhibits the cells growth, smaller increment in the capacitance values is observed over time. The results obtained by Alamarblue assay confirms the CMOS chip results. As shown in Figures 7.5c and d , a consistency exist between the optical measurements obtained by spectrophotometer and the electrical measurements obtained from CMOS chip. This implies that the capacitance measured by the chip can produce results similar to those that the Alamarblue test produces while it does not require any additional preparation steps. As a control experiment, we performed several optical observations before and after adding the antibiotic reagent and while counting the number of viable cells before and after introducing antibiotic to cell growth medium. The results are shown in Figure 7.6a to d. As shown in these pictures, the introduction of Geneticin on H1299 cell has caused a membrane damage which has prevented their further attachment and proliferation on the capacitive electrodes. The results of cell counting for 48 hours after addition of Geneticin are shown in Figure 7.6e. As seen, for H1299 cell lines, the cell number has decreased comparing the initial number of the cells and for Hek293 this value has increased over time, showing a steady cell growth.

**High throughput CMOS-based assay**

The proposed CMOS chip with 4-microwell was tested for cell culture monitoring. The cells with concentration of 200 kcells/ml were prepared and seeded into the wells. Thereafter the sensor response was monitored for 12 hours. The results are shown in Figure 7.7. In first eight hours of cell seeding, a steady increase happened in the capacitance values. This increase has a direct effect on increasing the output voltage as shown in Figure 7.7. This figure shows individual pixels output voltage, the higher number of cells on the electrode and a stronger bond between the cells and the electrode, results in a higher capacitance value and therefore a higher output voltage. In fact, the sensor works like a 64 pixel camera in which the pixel color indicates the cell number and their viability on the specific sensing site. It is worth mentioning that some of the electrodes in the middle of the array are fully covered with PDMS (areas showing in blue in Figure 7.7) and no capacitance change was observed in this sensing sites. This fact, confirms that there is no leakage in the microwells walls and they are perfectly separated and sealed from adjacent wells.

After 8 hours from the start of cell seeding, due to the very small volume of the wells (1 $\mu l$), the media started to evaporate which resulted in an decrease in the cell viability. The cell death is observed by a gradual decrease in the capacitance values. In order to increase the wells volume and to prolong the media evaporation, an additional well can be attached on the top of the 4 microwells for providing a continuous cell growth medium supply to the wells.

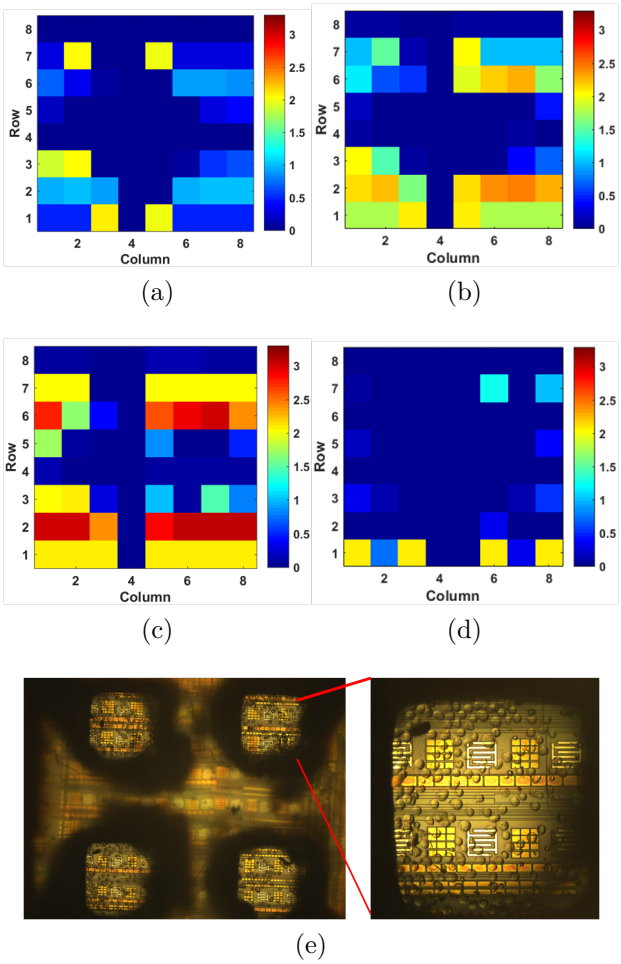


Figure 7.7: Cell culture monitoring using proposed 4-well microfluidic/microelectronic platform : (a) Right after seeding the cells. (b) 4 hours after cell seeding. (c) 8 hours after cell seeding (d) Media evaporation and cell death. (e) Chip scale microscopy showing the cultured cells in the microwells.

However, the aim of this experiment was mostly showing the bio-compatibility and stability of the fabricated microwells and it was performed as a short-term experiment for 12 hours. The proposed microfluidic packing technique is scalable and as the future steps of this work, higher density microwell arrays including 4x4 and 8x8 will be implemented. Due to the very small volumes of these fabricated wells, there are several concerns that need to be addressed for a long-term cell culture monitoring including : handling cell solution and inserting it into the small microwells, an effective method for cleaning the microwells and CMOS chip after each use, managing the leakage problem between the wells resulted from very thin walls and also the sealing techniques to avoid the evaporation of cell growth media.

### 7.2.8 Conclusion

A fully integrated cell chip was designed, implemented and characterized using capacitive measurement. The Hek293 and H1299 cell lines were used to perform several cell-based experiments including cell growth and cytotoxicity monitoring. A low-cost and low-complexity microfluidic fabrication method was proposed for high throughput cell culture monitoring. The results show that the cell chip provides inexpensive, quantitative, and real-time measurements for in- vitro drug cytotoxicity tests. Furthermore, this platform can potentially replace conventional biological experiments dealing with various types of mammalian adherent cells.

### 7.2.9 Acknowledgment

We thank Dr. Micheal Bouchman, Dr. Mark Levertu and Yuan Cheng for providing the cell lines. We also thank Laurent Mouden for chip wirebonding and technical assistance with biocompatible packaging. This research is supported by CMC Microsystems.

# CHAPTER 8 GENERAL DISCUSSION

The main statement of this thesis is that due to the capacitive behavior of the living cells, it is possible to detect their presence by the use of a capacitive sensor. Moreover we claimed that, since the drugs can alter the membrane integrity of the cells and can weaken their adherence properties and their ability to form extra-cellular matrix, it is possible to detect the effects of toxic drugs on cells by studying the cell surface interactions.

In this regard, we proposed two proof of concepts of a capacitive sensor with the sensing electrodes patterned on topmost metal layer of a CMOS chip. For proof of principle, several electrical, chemical, and biological experiments were conducted with the dielectric materials and living cell samples cultured on the CMOS chip.

As the second prototype we improved the design and extended it to an 8x8 array. We proposed the use of polyelectrolyte membranes to enhance the cell-electrode adherence. Instead of using conventional methods to detect the presence of PEMs, we used capacitive sensor as a mean to detect deposition of thin PEM films. Due to the charge presence in the PEMs structure, the surface charge density on the aluminum electrodes varies with each layer-by-layer deposition, resulting a change in the output capacitance values.

To validate the design, we exposed the chip to various concentrations of H1299 cell line. As was described earlier, the attachment of the cells on the electrodes give rise to the coupling capacitor which is formed above the electrode, resulting in an increase in the output voltage. Larger number of cells leads to a higher dielectric change above the electrodes. To show the device performance for cytotoxicity monitoring, Geneticin antibiotic was introduced to H1299 and Hek293 cell lines. As was discussed in chapter 6, the Hek23-gfp cell line resists to Geneticin. The results show that after 24 h, the H1299 cell lines stopped growing and due to the damage in their membrane, they started detaching from the sensors. This effect was seen as a decrease in the measured output voltage. However, the drug did not affect Hek293 cells and they continued growth over the electrodes. The correlation between the capacitance variation and cell viability was validated through visual observations and using Alamarblue viability dye.

To successfully perform these experiments several facts need to be considered in different aspects of circuit design, packaging, biointerface, and microfluidics :

1. As was discussed earlier, the CBCM suffers from mismatch non-ideality which can drastically change the measurement accuracy and limit the maximum capacitance detection range. This issue was noticed in the first prototype when the mismatch

caused a huge offset voltage in some chips, resulting in a very limited detection range. By proposing an auto calibration circuitry this non-ideality is partially mitigated. Careful layout was done for current mirror design to reduce the mismatch between the transistors.

2. To perform a long term cell monitoring, it was necessary to ensure that the chip package, microwell and the encapsulating material are all toxin free. For encapsulation we used biomedical epoxy and also the microwells were cut from standard plastic tubes or PDMS. The sterilization of chip and test setup was also very important and several test were failed due to the bacterial contamination in the test setup. Careful washing steps using Ethanol and ultra-pure distilled water followed by UV radiation was performed to ensure the complete sterilization of the chip.
3. Another important issue in biological experiments was the quality of cell-chip interface. As the first test samples, we used bare aluminum electrodes and we noticed the poor adhesion of cells on the electrodes. Although cells seemed attached and growing over the electrodes, however due to the loose bonds, they were easily washed away with media change. We tried several methods including PDMS deposition, plasma activation and PEM deposition. Plasma activation was useful for the beginning of the experiments and for making the surface temporarily hydrophilic while introducing the cell suspension. PDMS deposition was helpful in increasing the biocompatibility of the surface, but it was difficult to manage a uniform surface through spin coating of the packaged chips. Moreover, in some samples, the spin coating of PDMS led to the breaking of bonding wires.

   Among all, PEM proved to be more robust and due to the very thin layers it did not reduce the chip sensitivity. Another advantage of PEMs is that they are not washed away through several cleaning procedures.
4. Media evaporation was also another challenge in the long-term monitoring of the cell cultures. Although the chips were kept in $CO_2$ incubator with 100% humidity during the monitoring period, it was necessary to seal the wells to avoid media evaporation while providing enough oxygen for cells respiration. For this purpose, we used standard cell culture flask caps to cover samples under the test. However for the 4-microwell system, the problem was more consistent and due to the very small volumes of the cell media the evaporation happened in less than 12 h. To improve the performance, a microfluidic system is required to supply fresh media to the microwells.

The proposed technique, employing CMOS capacitance array for cell proliferation detection, represents an important monitoring capability that enables the development of a fast, label-free and cost-effective cell-based miniaturized system. Moreover, the proposed approach can

be adapted in diverse application such as drug screening and biocompatibility characterization of materials.

# CHAPTER 9 CONCLUSION AND RECOMMENDATIONS

## 9.1 Conclusion

Information about cell viability, growth rate, and motility is important for various life science applications. In this thesis we proposed the design and fabrication of a CMOS-based cell analysis chip. This platform can be used as a low-complexity and efficient alternative to microscopy tools for cell monitoring and drug screening studies. The proposed biosensor platform, fabricated in CMOS TSMC 0.35 $\mu m$ technology, features an array of 64 capacitive electrodes incorporated with a high resolution readout interface. Using a charge-to-digital conversion scheme, the proposed capacitive interface reaches the sensitivity of 350 mv/fF and the resolution of 10 aF. In order to protect the electrodes and to improve cell-electrode adhesion, we proposed, for the first time, the use of polyelectrolyte membranes for coating the aluminum electrodes. A low-cost, rapid prototyping technique is also proposed for microwell implementation and integration with the CMOS chip. In this method, we used diode charge pump laser to pattern the microwells on PDMS and glass and thereafter we utilized the flip-chip bonder to align and integrate the PDMS and glass layers on capacitive electrodes.

To prove the capability of the device for on-chip capacitance sensing, several biological experiments, mainly focused on cell viability and concentration monitoring, were conducted. To investigate the potential use of proposed device for drug screening application and cytotoxicity monitoring, we used Geneticin as a toxic reagent to H1299 cell line. As a control experiment, we also exposed the Geneticin to genetically modified Hek293-GFP cells. All steps in biological experiments were validated by performing parallel control experiments using Alamarblue viability reagent as well as the visual inspection of the cells on chip. The results obtained by the CMOS chip showed a good consistency with standard Alamarblue assay results. We have also shown a proof of concept of proposed microwell fabrication technique by a 4-well structure. Employing this structure, we conducted a a short-term cell culture monitoring experiment by seeding the H1299 cell line (200 k cells/ml) into fabricated microwells.

Based on the results obtained from this work, we believe that it is possible to fabricate high throughput CMOS-only assays for cell study and drug screening applications. The capacitance measurement reveals important information about various aspects of cell health and their growth properties. Thus, it can be used as an attractive tool in life science applications specially in cancer cell studies where the growth rate of cells and their response to anticancer drugs are of interest.

It is worth mentioning that although capacitive sensing technique has shown outstanding performance in cell growth studies, it is not the only possible solution for all biological experiments. In fact, optical methods have been more developed and have some unique advantages compared to fully-integrated electronic platforms. However, with the recent advancement in microfabrication technology and fabrication of highly integrated platforms with a very low cost and high yield, the use of microelectronics in biology can be extremely beneficial to reduce labor work, time, and cost of experiments.

## 9.2 Research contributions

The main contribution of this research involves fully integrated capacitive sensor arrays for on chip and real-time cell analysis. By measuring the capacitive coupling between the living cells and the interdigitated electrodes, built on top-most metal layer of CMOS technology, the cell culture parameters including cell viability, concentration, growth rate, and response to cytotoxic drugs can be quantified. The detailed contributions are as follows :

1. **Design, simulation, and implementation of an integrated capacitive sensor based on the fully differential charge-based capacitive measurement technique and a fully differential charge-input $\Sigma\Delta$ modulator.**

   The proof of concept for the integrated capacitance sensing approach is established through the design of single electrode sensors that operates based on the charge detection principle. A fully differential charged-based capacitive measurement readout circuit with the sensitivity of 350 mv/fF has been developed. Furthermore, a new DC-input first order $\Sigma\Delta$ modulator is proposed with the resolution of as low as 10 aF and signal to noise ratio (SNR) of 46.5 dB (7.7 bits).

2. **The optimization and improvement of the proposed biosensor by implementing an array of 8x8 capacitive sensor in TSMC 0.35 $\mu m$ CMOS technology.**

   The differential sensor achieves improved performance by compensating for parasitic capacitances, suppressing correlated noise and providing a higher output dynamic range. The differential output offset cancellation was achieved by a novel calibration circuitry based on the reconfigurable current mirror architecture. The sensors were tested on-bench and characterized with living cells cultured on the chip surface. The sensors were used to track the cell adhesion and proliferation. Promising correlation was observed between the variations in sensed capacitance and changes in cell viability. The proof of concept of the proposed biosensor platform was successfully fabricated and tested by chemical solutions, polystyrene beads, and H1299 cell line.

3. **Proposing a new bio-functionalization approach using polyelectrolyte membranes.**

   A surface coating method based on a layer-by-layer deposition technique is proposed. By alternating deposition of polyanions and polycations from aqueous solutions, multilayered films are formed on the bare CMOS-based aluminum electrodes. The cell culture results show a considerable improvement in cell-electrode adhesion properties.

4. **Proposing a new method for drug cytotoxicity monitoring using the capacitive sensor array.**

   According to the described cell-electrode capacitive model, the damages in the membrane caused by the toxic drugs result in a weaker capacitive bonding. By employing the proposed capacitive sensor array, this effect is studied with a real-time and continuous measurement of sensor capacitance variations.

5. **Design and implementation of a novel low-complexity microwell platform integrated with CMOS chip.**

   To provide multiple sensing sites for high throughput cell studies, a novel maskless technique based on direct patterning of PDMS and glass layers is proposed. A fast and low-complexity technique for direct alignment of microfluidic structures on CMOS chip is also proposed.

## 9.3 Recommendations for future work

A fully electronic cell-based assay was reported in this thesis with a higher sensitivity compared to the conventional cell analyses techniques. However more work can be done to enhance the proposed platform performance. These improvements can be overtaken from different aspects which are discussed as follows.

1. The size of the array is an important factor in high throughput cell study application. In this work we validated the design of an 8x8 fully integrated capacitive sensor array, to evaluate its reliability and its application for *in-vitro* cell monitoring. The higher number of sensing sites, allows monitoring the cell samples at single cell level and also gives a better statistical information about cell condition. Specifically, in cell proliferation monitoring, a high density array can give more accurate data about cell migration and spreading above the electrodes. This design can be extended to higher density structures such as 32x32, 64x64, and 128x128 sensor arrays. All functions such as signal processing, filtering, and analog to digital conversion can be integrated in one single CMOS chip using the latest System-on-Chip (SoC) design techniques to

achieve the needed miniaturized platform for micro-scale high-count sensing arrays. It is important to mention that in this design the electrodes pitch was chosen as 100 $\mu m$ considering the possibility to integrate the microwells on the electrodes and required spacing between the wells ensuring a good silage. If the microwell fabrication is not a concern, arrays with smaller pitch size and higher density can be fabricated.

2. For high throughput applications such as drug screening, it is necessary to have a high density array of microwells integrated on the sensing sites. In this work we showed the proof of concept of our proposed microwell fabrication method with 4 wells. Higher number of microwells can be integrated on the sensors as the continuation of this work. However the important challenge is the bonding of PDMS to the CMOS chip and also sealing the walls of microwells to avoid solution leakage. For higher density arrays, microfabrication techniques might be required to directly implement microwells on the loose dies. It is worth mentioning that the small size of the dies poses clear problems in handling and microfabrication which needs to be carefully considered.
3. The commercially standard packaging methods enclose the die within a carrier and the electrical connections are provided through the pads and bonding wires thus limiting the flexibility of the fluidic testings. In this work, we used manual epoxy encapsulation to protect the fragile wires and bonding pads. Although this method was successful, it was very laborious and timely. In addition, it required several trials and errors to perfectly cover all the fragile wires while leaving the sensing electrodes uncovered. Moreover, the bubbles and the holes in the cured epoxy lead to the fluidic leakage in the package and short-circuiting of the wires. Alternative techniques based on the photolithography can be followed to cover the electrical connections in a more efficient way.
4. The proposed sensor is solely based on the capacitive technique, measuring the cell adhesion strength. Relying on capacitance information, can limit a complete understanding of cell behavior and metabolism activity. To meet this requirement, a multiparameter sensor array can be developed combining capacitive, and pH sensor arrays. By developing this platform several parameters can be measured such as cell adhesion and morphology, electrical activity of cells (for electrically active cells such as neurons) as well as metabolic activity. We have already shown the preliminary design and implementation of a hybrid ISFET/capacitive sensor in [146]. Further optimization of this prototype may result in a multiparameter sensor for simultaneous pH and capacitance monitoring.

# PUBLICATIONS

**Journal publications**

— G. Nabovati, E. Ghafar-Zadeh, M. Mirzaei, G. Ayala-Charca, F. Awwad, and M. Sawan, “A new fully differential CMOS capacitance to digital converter for lab-on-chip applications”, IEEE Transactions on Biomedical Circuits and Systems, vol. 9, no. 3, pp. 353–361, 2015.

— G. Nabovati, E. Ghafar-Zadeh, A. Letourneau, and M. Sawan, “Towards high-throughput cell growth screening : A new CMOS 8x8 biosensor array for life science applications”, IEEE Transactions on Biomedical Circuits and Systems, Accepted.

— G. Nabovati, E. Ghafar-Zadeh, A. Letourneau, and M. Sawan, “A fully integrated cell imaging platform for real-time assessment of living cells”, IEEE Transactions on Biomedical Engineering, Submitted.

**Conference papers**

— G. Nabovati, E. Ghafar-Zadeh, and M. Sawan, “Novel DC-input $\Sigma\Delta$ capacitance to digital converter for biosensor applications”, IEEE International New Circuits and Systems Conference (NEWCAS), pp. 89–92, 2014.

— G. Nabovati, E. Ghafar-Zadeh, M. Mirzaei, G. Ayala-Charca, F. Awwad, and M. Sawan, “Fully integrated CMOS capacitive sensor for lab-on-chip applications”, IEEE International Symposium on Circuits and Systems (ISCAS), pp. 233–236, 2014.

— G. Nabovati, E. Ghafar-Zadeh, and M.Sawan, ”A novel multifunctional integrated biosensor array for simultaneous monitoring of Cell growth and acidification rate”, CASFEST, pp. 2855-2858, 2016.

**Poster presentations**

— G. Nabovati, E.Ghafarzadeh, M. Sawan, "Towards implantable biosensor for tracking tumor growth", ACFAS, May 2013.

**Live demonstrations**

— G .Nabovati, E. Ghafarzadeh, M. Mirzaei, M. Sawan, "CMOS capacitive sensor for cellular studies", ReSMiQ innovation day, September 2014.

— G. Nabovati, E. Ghafarzadeh, M. Sawan, "Smart petri dish : fully integrated cell imaging platform for real-time assessment of living cells ", ReSMiQ innovation Day,

October 2015

— G. Nabovati, E. Ghafarzadeh, M. Sawan, "Smart petri dish : fully integrated cell imaging platform for real-time assessment of living cells ", CMC Texpo, October 2015.

— G. Nabovati, E. Ghafar-Zadeh, A. Letourneau, and M. Sawan, "Live demonstration : CMOS capacitive sensor array for real-time analyses of living cells", IEEE International Symposium on Circuits and Systems (ISCAS), pp. 2374-2374, 2016.

**Awards**

— Brian L. Barge Award for Excellence in Microsystems Integration, CMC Microsystems Texpo, September 2015.

# REFERENCES

[1] G. Fotakis and J. A. Timbrell, "In vitro cytotoxicity assays : comparison of ldh, neutral red, mtt and protein assay in hepatoma cell lines following exposure to cadmium chloride," *Toxicology letters*, vol. 160, no. 2, pp. 171–177, 2006.

[2] J. M. Sargent, "The use of the mtt assay to study drug resistance in fresh tumour samples," in *Chemosensitivity Testing in Oncology*, pp. 13–25, Springer, 2003.

[3] J. O'Brien, I. Wilson, T. Orton, and F. Pognan, "Investigation of the alamar blue (resazurin) fluorescent dye for the assessment of mammalian cell cytotoxicity," *European Journal of Biochemistry*, vol. 267, no. 17, pp. 5421–5426, 2000.

[4] J. Müller, M. Ballini, P. Livi, Y. Chen, M. Radivojevic, A. Shadmani, V. Viswam, I. L. Jones, M. Fiscella, R. Diggelmann, *et al.*, "High-resolution cmos mea platform to study neurons at subcellular, cellular, and network levels," *Lab on a Chip*, vol. 15, no. 13, pp. 2767–2780, 2015.

[5] W. Messina, M. Fitzgerald, and E. Moore, "Sem and ecis investigation of cells cultured on nanopillar modified interdigitated impedance electrodes for analysis of cell growth and cytotoxicity of potential anticancer drugs," *Electroanalysis*, 2016.

[6] C. Wu, J. Zhou, N. Hu, D. Ha, X. Miao, and P. Wang, "Cellular impedance sensing combined with laps as a new means for real-time monitoring cell growth and metabolism," *Sensors and Actuators A : Physical*, vol. 199, pp. 136–142, 2013.

[7] A. Weltin, K. Slotwinski, J. Kieninger, I. Moser, G. Jobst, M. Wego, R. Ehret, and G. A. Urban, "Cell culture monitoring for drug screening and cancer research : a transparent, microfluidic, multi-sensor microsystem," *Lab on a Chip*, vol. 14, no. 1, pp. 138–146, 2014.

[8] G. H. Markx and C. L. Davey, "The dielectric properties of biological cells at radiofrequencies : applications in biotechnology," *Enzyme and Microbial Technology*, vol. 25, no. 3, pp. 161–171, 1999.

[9] C. Prodan, F. Mayo, J. Claycomb, J. Miller Jr, and M. Benedik, "Low-frequency, low-field dielectric spectroscopy of living cell suspensions," *Journal of applied physics*, vol. 95, no. 7, pp. 3754–3756, 2004.

[10] S. B. Prakash and P. Abshire, "On-chip capacitance sensing for cell monitoring applications," *IEEE Sensors Journal*, vol. 7, no. 3, pp. 440–447, 2007.

[11] R. A. Yotter, L. A. Lee, and D. M. Wilson, "Sensor technologies for monitoring metabolic activity in single cells-part i : optical methods," *IEEE Sensors Journal*, vol. 4, no. 4, pp. 395–411, 2004.

[12] C.-C. Shieh, M. Coghlan, J. P. Sullivan, and M. Gopalakrishnan, "Potassium channels : molecular defects, diseases, and therapeutic opportunities," *Pharmacological reviews*, vol. 52, no. 4, pp. 557–594, 2000.

[13] Y. Fang, "Non-invasive optical biosensor for probing cell signaling," *Sensors*, vol. 7, no. 10, pp. 2316–2329, 2007.

[14] A. A. Khalili and M. R. Ahmad, "A review of cell adhesion studies for biomedical and biological applications," *International journal of molecular sciences*, vol. 16, no. 8, pp. 18149–18184, 2015.

[15] D. Huh, G. A. Hamilton, and D. E. Ingber, "From 3d cell culture to organs-on-chips," *Trends in cell biology*, vol. 21, no. 12, pp. 745–754, 2011.

[16] A. García and C. Reyes, "Bio-adhesive surfaces to promote osteoblast differentiation and bone formation," *Journal of Dental Research*, vol. 84, no. 5, pp. 407–413, 2005.

[17] S. M. Shamah and B. T. Cunningham, "Label-free cell-based assays using photonic crystal optical biosensors," *Analyst*, vol. 136, no. 6, pp. 1090–1102, 2011.

[18] E. C. Butcher and I. L. Weissman, "Direct fluorescent labeling of cells with fluorescein or rhodamine isothiocyanate. i. technical aspects," *Journal of immunological methods*, vol. 37, no. 2, pp. 97–108, 1980.

[19] D. A. Scudiero, R. H. Shoemaker, K. D. Paull, A. Monks, S. Tierney, T. H. Nofziger, M. J. Currens, D. Seniff, and M. R. Boyd, "Evaluation of a soluble tetrazolium/formazan assay for cell growth and drug sensitivity in culture using human and other tumor cell lines," *Cancer Research*, vol. 48, no. 17, pp. 4827–4833, 1988.

[20] T. L. Riss, R. A. Moravec, A. L. Niles, H. A. Benink, T. J. Worzella, and L. Minor, "Cell viability assays," 2015.

[21] R. D. Petty, L. A. Sutherland, E. M. Hunter, and I. A. Cree, "Comparison of mtt and atp-based assays for the measurement of viable cell number," *Journal of bioluminescence and chemiluminescence*, vol. 10, no. 1, pp. 29–34, 1995.

[22] S. N. Rampersad, "Multiple applications of alamar blue as an indicator of metabolic function and cellular health in cell viability bioassays," *Sensors*, vol. 12, no. 9, pp. 12347–12360, 2012.

[23] A. Manickam, A. Chevalier, M. McDermott, A. D. Ellington, and A. Hassibi, "A CMOS electrochemical impedance spectroscopy (eis) biosensor array," *IEEE Transactions on Biomedical Circuits and Systems*, vol. 4, no. 6, pp. 379–390, 2010.

[24] V. Tsouti, C. Boutopoulos, I. Zergioti, and S. Chatzandroulis, "Capacitive microsystems for biological sensing," *Biosensors and Bioelectronics*, vol. 27, no. 1, pp. 1–11, 2011.

[25] I. Giaever and C. R. Keese, "Micromotion of mammalian cells measured electrically," *Proceedings of the National Academy of Sciences*, vol. 88, no. 17, pp. 7896–7900, 1991.

[26] H. Jafari, L. Soleymani, and R. Genov, "16-channel CMOS impedance spectroscopy DNA analyzer with dual-slope multiplying ADCs," *IEEE Transactions on Biomedical Circuits and Systems*, vol. 6, no. 5, pp. 468–478, 2012.

[27] N. Manaresi, A. Romani, G. Medoro, L. Altomare, A. Leonardi, M. Tartagni, and R. Guerrier, "A CMOS chip for individual cell manipulation and detection," *IEEE Journal of Solid-State Circuits*, vol. 38, no. 12, pp. 2297–2305, 2003.

[28] O. Akar, T. Akin, and K. Najafi, "A wireless batch sealed absolute capacitive pressure sensor," *Sensors and Actuators A : Physical*, vol. 95, no. 1, pp. 29–38, 2001.

[29] B. V. Amini and F. Ayazi, "A 2.5-v 14-bit cmos soi capacitive accelerometer," *IEEE Journal of Solid-State Circuits*, vol. 39, no. 12, pp. 2467–2476, 2004.

[30] N. Lazarus, S. S. Bedair, C.-C. Lo, and G. K. Fedder, "Cmos-mems capacitive humidity sensor," *Journal of Microelectromechanical Systems*, vol. 19, no. 1, pp. 183–191, 2010.

[31] C. Stagni, C. Guiducci, L. Benini, B. Riccò, S. Carrara, B. Samorí, C. Paulus, M. Schienle, M. Augustyniak, and R. Thewes, "Cmos dna sensor array with integrated a/d conversion based on label-free capacitance measurement," *IEEE Journal of Solid-State Circuits*, vol. 41, no. 12, pp. 2956–2964, 2006.

[32] S. B. Prakash and P. Abshire, "A fully differential rail-to-rail cmos capacitance sensor with floating-gate trimming for mismatch compensation," *IEEE Transactions on Circuits and Systems I : Regular Papers*, vol. 56, no. 5, pp. 975–986, 2009.

[33] R. Pei, Z. Cheng, E. Wang, and X. Yang, "Amplification of antigen–antibody interactions based on biotin labeled protein–streptavidin network complex using impedance spectroscopy," *Biosensors and Bioelectronics*, vol. 16, no. 6, pp. 355–361, 2001.

[34] D. HAFEMAN, J. PARCE, H. MCCONNELL, *et al.*, "Light-addressable potentiometric sensor for biochemical systems," *Science*, vol. 240, no. 4856, pp. 1182–1185, 1988.

[35] G. Xu, X. Ye, L. Qin, Y. Xu, Y. Li, R. Li, and P. Wang, "Cell-based biosensors based on light-addressable potentiometric sensors for single cell monitoring," *Biosensors and Bioelectronics*, vol. 20, no. 9, pp. 1757–1763, 2005.

[36] Q. Liu, H. Huang, H. Cai, Y. Xu, Y. Li, R. Li, and P. Wang, "Embryonic stem cells as a novel cell source of cell-based biosensors," *Biosensors and Bioelectronics*, vol. 22, no. 6, pp. 810–815, 2007.

[37] Q. Liu, H. Cai, Y. Xu, Y. Li, R. Li, and P. Wang, "Olfactory cell-based biosensor : a first step towards a neurochip of bioelectronic nose," *Biosensors and Bioelectronics*, vol. 22, no. 2, pp. 318–322, 2006.

[38] Y.-H. Lin, A. Das, and C.-S. Lai, "A simple and convenient set-up of light addressable potentiometric sensors (laps) for chemical imaging using a commercially available projector as a light source," *Int. J. Electrochem. Sci*, vol. 8, no. 5, pp. 7062–74, 2013.

[39] Q.-j. Liu, W.-w. Ye, H. Yu, N. Hu, L.-p. Du, and P. Wang, "Neurochip based on light-addressable potentiometric sensor with wavelet transform de-noising," *Journal of Zhejiang University Science B*, vol. 11, no. 5, pp. 323–331, 2010.

[40] P. Bergveld, "Thirty years of isfetology : What happened in the past 30 years and what may happen in the next 30 years," *Sensors and Actuators B : Chemical*, vol. 88, no. 1, pp. 1–20, 2003.

[41] C. Jakobson, U. Dinnar, M. Feinsod, and Y. Nemirovsky, "Ion-sensitive field-effect transistors in standard cmos fabricated by post processing," *IEEE sensors journal*, vol. 2, no. 4, pp. 279–287, 2002.

[42] T. M. Abdolkader, A. G. Alahdal, A. Shaker, and W. Fikry, "Isfet ph-sensor sensitivity extraction using conventional mosfet simulation tools," *International Journal of Chemical Engineering and Applications*, vol. 6, no. 5, p. 346, 2015.

[43] N. Nikkhoo, P. G. Gulak, and K. Maxwell, "Rapid detection of e. coli bacteria using potassium-sensitive fets in cmos," *IEEE transactions on biomedical circuits and systems*, vol. 7, no. 5, pp. 621–630, 2013.

[44] M. Asif, O. Nur, M. Willander, and B. Danielsson, "Selective calcium ion detection with functionalized zno nanorods-extended gate mosfet," *Biosensors and Bioelectronics*, vol. 24, no. 11, pp. 3379–3382, 2009.

[45] P. A. Hammond, D. Ali, and D. R. Cumming, "Design of a single-chip ph sensor using a conventional 0.6-$\mu$m cmos process," *IEEE Sensors Journal*, vol. 4, no. 6, pp. 706–712, 2004.

[46] P. Georgiou and C. Toumazou, "Isfet threshold voltage programming in cmos using hot-electron injection," *Electronics letters*, vol. 45, no. 22, pp. 1112–1113, 2009.

[47] Q. Liu and P. Wang, *Cell-based biosensors : principles and applications*. Artech House, 2009.

[48] M. S. Lord, C. Modin, M. Foss, M. Duch, A. Simmons, F. S. Pedersen, F. Besenbacher, and B. K. Milthorpe, "Extracellular matrix remodelling during cell adhesion monitored by the quartz crystal microbalance," *Biomaterials*, vol. 29, no. 17, pp. 2581–2587, 2008.

[49] C. I. Cheng, Y.-P. Chang, and Y.-H. Chu, "Biomolecular interactions and tools for their recognition : focus on the quartz crystal microbalance and its diverse surface chemistries and applications," *Chemical Society Reviews*, vol. 41, no. 5, pp. 1947–1971, 2012.

[50] J. Xi, J. Chen, M. Garcia, and L. Penn, "Quartz crystal microbalance in cell biology studies," *J Biochip Tissue chip S*, vol. 5, pp. 2153–0777, 2013.

[51] H. Yu, H. Cai, W. Zhang, L. Xiao, Q. Liu, and P. Wang, "A novel design of multifunctional integrated cell-based biosensors for simultaneously detecting cell acidification and extracellular potential," *Biosensors and Bioelectronics*, vol. 24, no. 5, pp. 1462–1468, 2009.

[52] Q. Liu, C. Wu, H. Cai, N. Hu, J. Zhou, and P. Wang, "Cell-based biosensors and their application in biomedicine," *Chemical reviews*, vol. 114, no. 12, pp. 6423–6461, 2014.

[53] A. J. Tudos and R. B. Schasfoort, "Introduction to surface plasmon resonance," *Handbook of surface plasmon resonance*, pp. 1–14, 2008.

[54] R. Robelek, "Surface plasmon resonance sensors in cell biology : basics and application," *Bioanalytical Reviews*, vol. 1, no. 1, pp. 57–72, 2009.

[55] K.-T. Chang, Y.-J. Chang, C.-L. Chen, and Y.-N. Wang, "Multichannel lens-free cmos sensors for real-time monitoring of cell growth," *Electrophoresis*, vol. 36, no. 3, pp. 413–419, 2015.

[56] T. S. Pui, Y. Chen, C. C. Wong, R. Nadipalli, R. Weerasekera, S. K. Arya, H. Yu, and A. R. Rahman, "High density cmos electrode array for high-throughput and automated cell counting," *Sensors and Actuators B : Chemical*, vol. 181, pp. 842–849, 2013.

[57] S. B. Prakash and P. Abshire, "Tracking cancer cell proliferation on a cmos capacitance sensor chip," *Biosensors and Bioelectronics*, vol. 23, no. 10, pp. 1449–1457, 2008.

[58] S. Michaelis, J. Wegener, and R. Robelek, "Label-free monitoring of cell-based assays : Combining impedance analysis with spr for multiparametric cell profiling," *Biosensors and Bioelectronics*, vol. 49, pp. 63–70, 2013.

[59] N. Hu, J. Zhou, K. Su, D. Zhang, L. Xiao, T. Wang, and P. Wang, "An integrated label-free cell-based biosensor for simultaneously monitoring of cellular physiology multiparameter in vitro," *Biomedical microdevices*, vol. 15, no. 3, pp. 473–480, 2013.

[60] K. Su, J. Zhou, L. Zou, T. Wang, L. Zhuang, N. Hu, and P. Wang, "Integrated multifunctional cell-based biosensor system for monitoring extracellular acidification and cellular growth," *Sensors and Actuators A : Physical*, vol. 220, pp. 144–152, 2014.

[61] M. Varshney and Y. Li, "Interdigitated array microelectrodes based impedance biosensors for detection of bacterial cells," *Biosensors and Bioelectronics*, vol. 24, no. 10, pp. 2951–2960, 2009.

[62] S. MacKay, P. Hermansen, D. Wishart, and J. Chen, "Simulations of interdigitated electrode interactions with gold nanoparticles for impedance-based biosensing applications," *Sensors*, vol. 15, no. 9, pp. 22192–22208, 2015.

[63] E. Ghafar-Zadeh, M. Sawan, E. Ghafar-Zadeh, and M. Sawan, "CMOS capacitive sensors for lab-on-chip applications," *Book, Springer Editor*, 2010.

[64] A. H. Graham, C. R. Bowen, J. Taylor, and J. Robbins, "Neuronal cell biocompatibility and adhesion to modified cmos electrodes," *Biomedical microdevices*, vol. 11, no. 5, pp. 1091–1101, 2009.

[65] E. Ghafar-Zadeh, M. Sawan, V. P. Chodavarapu, and T. Hosseini-Nia, "Bacteria growth monitoring through a differential cmos capacitive sensor," *IEEE transactions on biomedical circuits and systems*, vol. 4, no. 4, pp. 232–238, 2010.

[66] N. Couniot, L. Francis, and D. Flandre, "A 16x16 CMOS capacitive biosensor array towards detection of single bacterial cell," 2015.

[67] L. Juhász, A. Vass-Vamai, V. Timár-Horváth, M. P. Desmulliez, and R. S. Dhariwal, "Porous alumina based capacitive mems rh sensor," in *Design, Test, Integration and Packaging of MEMS/MOEMS, 2008. MEMS/MOEMS 2008. Symposium on*, pp. 381–385, IEEE, 2008.

[68] L. Moreno-Hagelsieb, B. Foultier, G. Laurent, R. Pampin, J. Remacle, J.-P. Raskin, and D. Flandre, "Electrical detection of dna hybridization : three extraction techniques based on interdigitated al/al 2 o 3 capacitors," *Biosensors and bioelectronics*, vol. 22, no. 9, pp. 2199–2207, 2007.

[69] M. S.-C. Lu, Y.-C. Chen, and P.-C. Huang, "5× 5 CMOS capacitive sensor array for detection of the neurotransmitter dopamine," *Biosensors and Bioelectronics*, vol. 26, no. 3, pp. 1093–1097, 2010.

[70] K. Iniewski, *CMOS Biomicrosystems : Where Electronics Meet Biology*. John Wiley & Sons, 2011.

[71] M. Barbaro, A. Bonfiglio, L. Raffo, A. Alessandrini, P. Facci, and I. BarakBarak, "A cmos, fully integrated sensor for electronic detection of dna hybridization," *IEEE Electron Device Letters*, vol. 27, no. 7, pp. 595–597, 2006.

[72] J. W. Ko, H. C. Koo, D. W. Kim, S. M. Seo, T. J. Kang, Y. Kwon, J. L. Yoon, J. H. Cheon, Y. H. Kim, J. J. Kim, *et al.*, "Electroless gold plating on aluminum patterned chips for cmos-based sensor applications," *Journal of The Electrochemical Society*, vol. 157, no. 1, pp. D46–D49, 2010.

[73] A. Hierlemann, "Integrated chemical microsensor systems in cmos-technology," in *The 13th International Conference on Solid-State Sensors, Actuators and Microsystems, 2005. Digest of Technical Papers. TRANSDUCERS'05.*, vol. 2, pp. 1134–1137, IEEE, 2005.

[74] H. Watanabe and H. Honma, "Fabrication of nickel microbump on aluminum using electroless nickel plating," *Journal of the Electrochemical Society*, vol. 144, no. 2, pp. 471–476, 1997.

[75] G. O. Mallory and J. B. Hajdu, *Electroless plating : fundamentals and applications*. William Andrew, 1990.

[76] L. Berdondini, P. D. van der Wal, N. F. de Rooij, and M. Koudelka-Hep, "Development of an electroless post-processing technique for depositing gold as electrode material on cmos devices," *Sensors and Actuators B : Chemical*, vol. 99, no. 2, pp. 505–510, 2004.

[77] Y.-C. Liu, C.-M. Sun, L.-Y. Lin, M.-H. Tsai, and W. Fang, "A tunable range/sensitivity cmos-mems capacitive tactile sensor with polymer fill-in technique," in *TRANSDUCERS 2009-2009 International Solid-State Sensors, Actuators and Microsystems Conference*, pp. 2190–2193, IEEE, 2009.

[78] C.-T. Ko, J.-P. Wu, W.-C. Wang, C.-H. Huang, S.-H. Tseng, Y.-L. Chen, and M.-C. Lu, "A highly sensitive cmos-mems capacitive tactile sensor," in *19th IEEE International Conference on Micro Electro Mechanical Systems*, pp. 642–645, IEEE, 2006.

[79] M. Bruening and M. Adusumilli, "Polyelectrolyte-multilayer-films-and-membrane-functionalization," *Mater. Matters*, vol. 6, no. 3, pp. 76–81, 2011.

[80] D. Volodkin, R. Von Klitzing, and H. Moehwald, "Polyelectrolyte multilayers : towards single cell studies," *Polymers*, vol. 6, no. 5, pp. 1502–1527, 2014.

[81] J. Wu, G. K. Fedder, and L. R. Carley, "A low-noise low-offset capacitive sensing amplifier for a 50-$\mu$g/ hz monolithic cmos mems accelerometer," *IEEE Journal of Solid-State Circuits*, vol. 39, no. 5, pp. 722–730, 2004.

[82] N. Yazdi, H. Kulah, and K. Najafi, "Precision readout circuits for capacitive microaccelerometers," in *Sensors, 2004. Proceedings of IEEE*, pp. 28–31, IEEE, 2004.

[83] C. Hagleitner, A. Hierlemann, D. Lange, A. Kummer, N. Kerness, O. Brand, and H. Baltes, "Smart single-chip gas sensor microsystem," *Nature*, vol. 414, no. 6861, pp. 293–296, 2001.

[84] H. Kulah and K. Najafi, "A low noise switched-capacitor interface circuit for sub-micro gravity resolution micromachined accelerometers," in *Solid-State Circuits Conference, 2002. ESSCIRC 2002. Proceedings of the 28th European*, pp. 635–638, IEEE, 2002.

[85] D. A. Johns and K. Martin, *Analog integrated circuit design*. John Wiley & Sons, 2008.

[86] N. Couniot, D. Bol, O. Poncelet, L. A. Francis, and D. Flandre, "A capacitance-to-frequency converter with on-chip passivated microelectrodes for bacteria detection in saline buffers up to 575 mhz," *IEEE Transactions on Circuits and Systems II : Express Briefs*, vol. 62, no. 2, pp. 159–163, 2015.

[87] S. Xia, K. Makinwa, and S. Nihtianov, "A capacitance-to-digital converter for displacement sensing with 17b resolution and 20$\mu$s conversion time," in *2012 IEEE International Solid-State Circuits Conference*, pp. 198–200, IEEE, 2012.

[88] D. Sylvester, J. C. Chen, and C. Hu, "Investigation of interconnect capacitance characterization using charge-based capacitance measurement (cbcm) technique and three-dimensional simulation," *IEEE journal of solid-state circuits*, vol. 33, no. 3, pp. 449–453, 1998.

[89] I. Evans and T. York, "Microelectronic capacitance transducer for particle detection," *IEEE Sensors journal*, vol. 4, no. 3, pp. 364–372, 2004.

[90] K.-H. Lee, S. Choi, J. O. Lee, J.-B. Yoon, and G.-H. Cho, "Cmos capacitive biosensor with enhanced sensitivity for label-free dna detection," in *2012 IEEE International Solid-State Circuits Conference*, pp. 120–122, IEEE, 2012.

[91] D. Strle, B. Stefane, U. Nahtigal, E. Zupanic, F. Pozgan, I. Kvasic, M. Macek, J. Trontelj, and I. Musevic, "Surface-functionalized comb capacitive sensors and cmos electronics for vapor trace detection of explosives," *IEEE Sensors Journal*, vol. 12, no. 5, pp. 1048–1057, 2012.

[92] A. Balasubramanian, B. Bhuva, R. Mernaugh, and F. Haselton, "Si-based sensor for virus detection," in *Sensors, 2003. Proceedings of IEEE*, vol. 1, pp. 299–303, IEEE, 2003.

[93] E. Ghafar-Zadeh and M. Sawan, "A charge based sigma delta capacitive sensor for ultrathin polyelectrolyte layer detection," in *Northeast Workshop on Circuits and Systems (NEWCAS)*, 2008.

[94] E. Ghafar-Zadeh, S. F. Chowdhury, A. Aliakbar, V. Chodavarapu, R. Lambrose, L. Beital, M. Sawan, and M. Trifiro, "Handheld impedance biosensor system using engineered proteinaceous receptors," *Biomedical microdevices*, vol. 12, no. 6, pp. 967–975, 2010.

[95] T. E. Mlsna, S. Cemalovic, M. Warburton, S. T. Hobson, D. A. Mlsna, and S. V. Patel, "Chemicapacitive microsensors for chemical warfare agent and toxic industrial chemical detection," *Sensors and Actuators B : Chemical*, vol. 116, no. 1, pp. 192–201, 2006.

[96] J. Gardner, A. Pike, N. De Rooij, M. Koudelka-Hep, P. Clerc, A. Hierlemann, and W. Göpel, "Integrated array sensor for detecting organic solvents," *Sensors and Actuators B : Chemical*, vol. 26, no. 1, pp. 135–139, 1995.

[97] E. Ghafar-Zadeh and M. Sawan, "A hybrid microfluidic/cmos capacitive sensor dedicated to lab-on-chip applications," *IEEE transactions on biomedical circuits and systems*, vol. 1, no. 4, pp. 270–277, 2007.

[98] L. Sumanen, M. Waltari, V. Hakkarainen, and K. Halonen, "Cmos dynamic comparators for pipeline a/d converters," in *Circuits and Systems, 2002. ISCAS 2002. IEEE International Symposium on*, vol. 5, pp. V–157, IEEE, 2002.

[99] J. Musayev, Y. Adlguzel, H. Kulah, S. Eminoglu, and T. Akln, "Label-free DNA detection using a charge sensitive CMOS microarray sensor chip," *IEEE Sensors Journal*, vol. 14, no. 5, pp. 1608–1616, 2014.

[100] W.-A. Lai, C.-H. Lin, Y.-S. Yang, and M. S.-C. Lu, "Ultrasensitive and label-free detection of pathogenic avian influenza DNA by using CMOS impedimetric sensors," *Biosensors and Bioelectronics*, vol. 35, no. 1, pp. 456–460, 2012.

[101] S. B. Prakash and P. Abshire, "Tracking cancer cell proliferation on a CMOS capacitance sensor chip," *Biosensors and Bioelectronics*, vol. 23, no. 10, pp. 1449–1457, 2008.

[102] I. Evans and T. York, "Microelectronic capacitance transducer for particle detection," *IEEE Sensors Journal*, vol. 4, no. 3, pp. 364–372, 2004.

[103] E. Ghafar-Zadeh, M. Sawan, V. P. Chodavarapu, and T. Hosseini-Nia, "Bacteria growth monitoring through a differential CMOS capacitive sensor," *IEEE Transactions on Biomedical Circuits and Systems,*, vol. 4, no. 4, pp. 232–238, 2010.

[104] G. Nabovati, E. Ghafar-Zadeh, M. Mirzaei, G. Ayala-Charca, F. Awwad, and M. Sawan, "A new fully differential CMOS capacitance to digital converter for lab-on-chip applications," *IEEE Transactions on Biomedical Circuits and Systems*, vol. 9, no. 3, pp. 498–507, 2014.

[105] D. Li, R. Zang, S.-T. Yang, J. Wang, and X. Wang, "Cell-based high-throughput proliferation and cytotoxicity assays for screening traditional chinese herbal medicines," *Process Biochemistry*, vol. 48, no. 3, pp. 517–524, 2013.

[106] O. Kepp, L. Galluzzi, M. Lipinski, J. Yuan, and G. Kroemer, "Cell death assays for drug discovery," *Nature Reviews Drug Discovery*, vol. 10, no. 3, pp. 221–237, 2011.

[107] P. Y. Chiou, A. T. Ohta, and M. C. Wu, "Massively parallel manipulation of single cells and microparticles using optical images," *Nature*, vol. 436, no. 7049, pp. 370–372, 2005.

[108] A. K. White, M. VanInsberghe, I. Petriv, M. Hamidi, D. Sikorski, M. A. Marra, J. Piret, S. Aparicio, and C. L. Hansen, "High-throughput microfluidic single-cell rt-qpcr," *Proceedings of the National Academy of Sciences*, vol. 108, no. 34, pp. 13999–14004, 2011.

[109] G. Nabovati, E. Ghafar-Zadeh, and M. Sawan, "A 64 pixel ISFET-based biosensor for extracellular pH gradient monitoring," in *IEEE International Symposium on Circuits and Systems (ISCAS), 2015*, pp. 1762–1765.

[110] M. Brischwein, E. Motrescu, E. Cabala, A. Otto, H. Grothe, and B. Wolf, "Functional cellular assays with multiparametric silicon sensor chips," *Lab on a Chip*, vol. 3, no. 4, pp. 234–240, 2003.

[111] Y. Song, M. Li, J. Yang, J. Wang, X. Pan, Y. Sun, and D. Li, "Capacitive detection of living microalgae in a microfluidic chip," *Sensors and Actuators B : Chemical*, vol. 194, pp. 164–172, 2014.

[112] L. Sumanen, M. Waltari, V. Hakkarainen, and K. Halonen, "CMOS dynamic comparators for pipeline A/D converters," in *IEEE International Symposium on Circuits and Systems, 2002*, vol. 5, pp. 157–160.

[113] E. Janssen and A. van Roermund, "Basics of sigma-delta modulation," in *Look-Ahead Based Sigma-Delta Modulation*, pp. 5–28, Springer, 2011.

[114] J. H. Koschwanez, R. H. Carlson, and D. R. Meldrum, "Thin PDMS films using long spin times or tert-butyl alcohol as a solvent," *PLoS one*, vol. 4, no. 2, p. e4572, 2009.

[115] N. Manaresi, A. Romani, G. Medoro, L. Altomare, A. Leonardi, M. Tartagni, and R. Guerrier, "A cmos chip for individual cell manipulation and detection," *IEEE Journal of Solid-State Circuits*, vol. 38, no. 12, pp. 2297–2305, 2003.

[116] N. Couniot, L. A. Francis, and D. Flandre, "A 16×16 CMOS capacitive biosensor array towards detection of single bacterial cell," *IEEE Transactions on Biomedical Circuits and Systems*, vol. 10, no. 2, pp. 364–374, 2016.

[117] C. Laborde, F. Pittino, H. Verhoeven, S. Lemay, L. Selmi, M. Jongsma, and F. Widdershoven, "Real-time imaging of microparticles and living cells with cmos nanocapacitor arrays," *Nature nanotechnology*, 2015.

[118] J. M. Rothberg, W. Hinz, T. M. Rearick, J. Schultz, W. Mileski, M. Davey, J. H. Leamon, K. Johnson, M. J. Milgrew, and M. Edwards, "An integrated semiconductor

device enabling non-optical genome sequencing," *Nature*, vol. 475, no. 7356, pp. 348–352, 2011.

[119] B. Eversmann, M. Jenkner, F. Hofmann, C. Paulus, R. Brederlow, B. Holzapfl, P. Fromherz, M. Merz, M. Brenner, and M. Schreiter, "A 128 128 cmos biosensor array for extracellular recording of neural activity," *IEEE Journal of Solid-State Circuits*, vol. 38, no. 12, pp. 2306–2317, 2003.

[120] L. Berdondini, P. Van Der Wal, O. Guenat, N. F. de Rooij, M. Koudelka-Hep, P. Seitz, R. Kaufmann, P. Metzler, N. Blanc, and S. Rohr, "High-density electrode array for imaging in vitro electrophysiological activity," *Biosensors and bioelectronics*, vol. 21, no. 1, pp. 167–174, 2005.

[121] C. M. Lopez, A. Andrei, S. Mitra, M. Welkenhuysen, W. Eberle, C. Bartic, R. Puers, R. F. Yazicioglu, and G. G. Gielen, "An implantable 455-active-electrode 52-channel cmos neural probe," *IEEE Journal of Solid-State Circuits*, vol. 49, no. 1, pp. 248–261, 2014.

[122] M. Brischwein, E. Motrescu, E. Cabala, A. Otto, H. Grothe, and B. Wolf, "Functional cellular assays with multiparametric silicon sensor chips," *Lab on a Chip*, vol. 3, no. 4, pp. 234–240, 2003.

[123] H. Lee, Y. Liu, D. Ham, and R. M. Westervelt, "Integrated cell manipulation system—cmos/microfluidic hybrid," *Lab on a Chip*, vol. 7, no. 3, pp. 331–337, 2007.

[124] S. Martinoia, N. Rosso, M. Grattarola, L. Lorenzelli, B. Margesin, and M. Zen, "Development of isfet array-based microsystems for bioelectrochemical measurements of cell populations," *Biosensors and Bioelectronics*, vol. 16, no. 9, pp. 1043–1050, 2001.

[125] B. Stein, M. George, H. Gaub, J. Behrends, and W. Parak, "Spatially resolved monitoring of cellular metabolic activity with a semiconductor-based biosensor," *Biosensors and Bioelectronics*, vol. 18, no. 1, pp. 31–41, 2003.

[126] J. Hong, K. Kandasamy, M. Marimuthu, C. S. Choi, and S. Kim, "Electrical cell-substrate impedance sensing as a non-invasive tool for cancer cell study," *Analyst*, vol. 136, no. 2, pp. 237–245, 2011.

[127] H. E. Park, D. Kim, H. S. Koh, S. Cho, J.-S. Sung, and J. Y. Kim, "Real-time monitoring of neural differentiation of human mesenchymal stem cells by electric cell-substrate impedance sensing," *BioMed Research International*, vol. 2011, 2011.

[128] A.-Y. Chang and M. S.-C. Lu, "A cmos magnetic microbead-based capacitive biosensor array with on-chip electromagnetic manipulation," *Biosensors and Bioelectronics*, vol. 45, pp. 6–12, 2013.

[129] N. Halonen, T. Datta-Chaudhuri, A. Hassinen, S. Prakash, P. Möller, P. Abshire, E. Smela, S. Kellokumpu, and A. Lloyd Spetz, "Cell clinic ; cmos chip measuring capacitance as indication of cell adhesion applied in evaluating the cytotoxicity of nanomaterials," in *Eurosensors 2014, Brescia, Italy, September 7-10*.

[130] W. Li, T. Knoll, and H. Thielecke, "On-chip integrated lensless microscopy module for optical monitoring of adherent growing mammalian cells," in *2010 Annual International Conference of the IEEE Engineering in Medicine and Biology*, pp. 1012–1015, IEEE.

[131] Q. Liu, J. Yu, L. Xiao, J. C. O. Tang, Y. Zhang, P. Wang, and M. Yang, "Impedance studies of bio-behavior and chemosensitivity of cancer cells by micro-electrode arrays," *Biosensors and Bioelectronics*, vol. 24, no. 5, pp. 1305–1310, 2009.

[132] T. Chi, J. S. Park, J. C. Butts, T. A. Hookway, A. Su, C. Zhu, M. P. Styczynski, T. C. McDevitt, and H. Wang, "A multi-modality cmos sensor array for cell-based assay and drug screening," *IEEE transactions on biomedical circuits and systems*, vol. 9, no. 6, pp. 801–814, 2015.

[133] S. Al-Nasiry, N. Geusens, M. Hanssens, C. Luyten, and R. Pijnenborg, "The use of alamar blue assay for quantitative analysis of viability, migration and invasion of choriocarcinoma cells," *Human reproduction*, vol. 22, no. 5, pp. 1304–1309, 2007.

[134] J. O'Brien, I. Wilson, T. Orton, and F. Pognan, "Investigation of the alamar blue (resazurin) fluorescent dye for the assessment of mammalian cell cytotoxicity," *European Journal of Biochemistry*, vol. 267, no. 17, pp. 5421–5426, 2000.

[135] P. W. Sylvester, "Optimization of the tetrazolium dye (mtt) colorimetric assay for cellular growth and viability," *Drug Design and Discovery : Methods and Protocols*, pp. 157–168, 2011.

[136] T. Xia, N. Li, and X. Fang, "Single-molecule fluorescence imaging in living cells," *Annual review of physical chemistry*, vol. 64, pp. 459–480, 2013.

[137] S. Michaelis, R. Robelek, and J. Wegener, "Studying cell–surface interactions in vitro : A survey of experimental approaches and techniques," in *Tissue engineering III : cell-surface interactions for tissue culture*, pp. 33–66, Springer, 2011.

[138] S. B. Prakash and P. Abshire, "A cmos capacitance sensor that monitors cell viability," in *IEEE Sensors, 2005.*, p. 4 pp., IEEE.

[139] J. T. Wilson, W. Cui, V. Kozlovskaya, E. Kharlampieva, D. Pan, Z. Qu, V. R. Krishnamurthy, J. Mets, V. Kumar, J. Wen, *et al.*, "Cell surface engineering with polyelectrolyte multilayer thin films," *Journal of the American Chemical Society*, vol. 133, no. 18, pp. 7054–7064, 2011.

[140] V. Gribova, R. Auzely-Velty, and C. Picart, "Polyelectrolyte multilayer assemblies on materials surfaces : from cell adhesion to tissue engineering," *Chemistry of Materials*, vol. 24, no. 5, pp. 854–869, 2011.

[141] H. Lee, "Effects of temperature, salt concentration, and the protonation state on the dynamics and hydrogen-bond interactions of polyelectrolyte multilayers on lipid membranes," *Physical Chemistry Chemical Physics*, vol. 18, no. 9, pp. 6691–6700, 2016.

[142] T. Datta-Chaudhuri, P. Abshire, and E. Smela, "Packaging commercial cmos chips for lab on a chip integration," *Lab on a Chip*, vol. 14, no. 10, pp. 1753–1766, 2014.

[143] V. Moby, A. Kadi, N. de Isla, J. Stoltz, and P. Menu, "Polyelectrolyte multilayer films : effect of the initial anchoring layer on the cell growth," *Bio-medical materials and engineering*, vol. 18, no. 4-5, pp. 199–204, 2008.

[144] M. F. Durstock and M. F. Rubner, "Dielectric properties of polyelectrolyte multilayers," *Langmuir*, vol. 17, no. 25, pp. 7865–7872, 2001.

[145] P. A. Neff, B. K. Wunderlich, R. v. Klitzing, and A. R. Bausch, "Formation and dielectric properties of polyelectrolyte multilayers studied by a silicon-on-insulator based thin film resistor," *Langmuir*, vol. 23, no. 7, pp. 4048–4052, 2007.

[146] G. Nabovati, E. Ghafar-Zadeh, and M. Sawan, "A novel multifunctional integrated biosensor array for simultaneous monitoring of cell growth and acidification rate," in *2016 IEEE International Symposium on Circuits and Systems (ISCAS)*, pp. 2855–2858, IEEE, 2016.

# APPENDIX A BIOLOGICAL EXPERIMENTS : EQUIPMENTS AND PROTOCOLS

All biological experiments in this thesis are carried out in Biostim laboratory in Polytechnique Montreal. The cell lines are provided by the Biomaterials and Cartilage Laboratory at Polytechnique Montreal. The required chemical and biological materials are purchased from ATCC, Sigma Aldrich and Termofisher companies.The detailed on-chip cell culture protocol and the list of equipments are provided as follows.

**Cell culture equipments**

1) $CO_2$ incubator
2) Biological hood, Class II, Type A2.
3) Autoclave
4) Automated cell counter
5) Benchtop Centrifuge
6) Adjustable volume pipetters
7) Ultrapure water system
8) Water bath
9) UV Flood sterilizing system
10) Fluorescent upright microscope
11) Cell culture microscope
12) $-20°C$ , $-80°C$, and $-150°C$ freezers
13) $4°C$ refrigerator
14) Analytical balance

**CMOS chip cleaning steps**

1) Wash the chips with Isopropanol.
2) Rinse with Distilled water.
3) Wash with Ethanol for 5 min.
4) Rinse with sterilize ultra-pure distilled water.
5) Place under UV radiation for 5 min, 75% intensity.
6) Wash the chip surface with PBS and growth medium before seeding the cells.

**On-chip cell culture protocol**

*(Parts of the following protocol is taken from www.thermofisher.com and is modified based on*

*the application.)*

1) Remove the cell culture media from the culture flask.

2) Gently wash the cells with PBS.

3) Remove the washing solutions from the culture flask.

4) Add pre-warmed trypsin to detach the cells from the flask.

5) Incubate at room temperature for 4 minute.

5) Observe the cell detachment under the microscope.

6) Add pre-warmed media to the detached cell layer and disperse the medium by pipetting over the cell layer surface several times.

7) Transfer the cells to the centrifuge tubes and centrifuge them at 200 x g for 5 to 10 minutes.

8) Resuspend the cells in a minimal volume of pre-warmed growth medium.

9) Remove samples for cell counting.

10) Based on the desired concentration, dilute cell suspension to the recommended seeding density and transfer the suspension to the pre-cleaned CMOS chips.

11) Transfer the chips to the incubator.

# APPENDIX B CHIP PACKAGING EQUIPMENTS

CMOS chip wirebonding, packaging, and microwell fabrication are carried out in LASEM laboratory in Polytechnique Montreal. The equipments are listed as follows.

**1) Wirebonder**

To wirebond the loose dies to the packages, a wedge wirebonder machine was used. The wirebonder uses aluminum wires of 17.5 $\mu m$ diameter with the minimum pad pitch of 80 $\mu m$.

**2) Oxford Lasers, A-SERIES**

This laser is a micromachining system for etching, microdrilling, and microcutting different materials such as glass, metal, PMMA, and polymers. The laser power is 50 mW with 355 nm wavelength.

**3) Flip-chip bonder**

The Femto Flip-chip bonder is a hybrid module assembly system used in manufacturing operations for precision placement of electronics and microelectronics components. The resolution is 0.5 $\mu m$, and the bonding force varies between 0.2 and 10 N.

**4) Precision spin coater**

The spin coater is used for preparing the PDMS layers for microwell fabrication. The spinning speed of the machine varies between 0 to 6000 rpm. Different thicknesses can be obtained by changing the spinning speed and its duration.

**5) Standard lab oven**

To cure the PDMS samples, a standard oven with the temperature ranging from 50 to 225 degrees was used.